Enhanced Spectrum Sensing for Cognitive Cellular Systems

Von der Fakultät für Ingenieurwissenschaften,
Abteilung Elektrotechnik und Informationstechnik
der Universität Duisburg-Essen

zur Erlangung des akademischen Grades

Doktor der Ingenieurwissenschaften (Dr.-Ing.)

genehmigte Dissertation

von

Trung Thanh Nguyen

aus

Hanoi, Vietnam

Gutachter: Prof. Dr.-Ing. Thomas Kaiser
Gutachter: Prof. Dr.-Ing. Andreas Czylwik
Tag der mündlichen Prüfung: 04.02.2016

ACKNOWLEDGMENTS

The dissertation is written in the Institute of Digital Signal Processing (DSV) at the University of Duisburg-Essen, in Germany. It culminates from my Ph.D study over a span of years under the supervision of Prof. Dr.-Ing. Thomas Kaiser.

First of all, I would like to extend my sincere gratitude to Prof. Dr.-Ing. Thomas Kaiser for his extremely valuable guidance. He inspires me on the pursuit of scientific research, in general, as well as specifically on my dissertation topic. The success of my dissertation would not have been possible without his continuous support and encouragement. In the past of four years, he has provided me with useful insights in various areas, including methodologies of research and scientific activities. I am very thankful to have done this research topic under his supervision and have had the opportunity to be a part of his amazing team. Under his guidance, I have expanded my mind in order to continue making progress on research. I would like to thank Prof. Dr.-Ing. Andreas Czylwik (Department of Communication Systems, University of Duisburg-Essen, Germany) for having a keen interest in my work and being my co-supervisor.

In addition, I would like to thank Mr. Theo Kreul, an active leader of the Software Configurable Platforms and Prototyping Group in DSV. He has successfully led working packages, in which a cognitive cellular system has been developed.

I am also thankful to my DSV colleagues for their support and for our joint work and insightful discussions on research topics and experiments. Thanks to the extraordinary endeavors of my DSV colleagues, my work has been evaluated and improved. Being part of the DSV, I have had many memorable experiences in research activities, visiting trips and friendships. I would also like to thank other friends of mine who are not mentioned here. With their kind help, my time in Germany has been wonderful.

Moreover, I would like to express my deepest appreciation to my home country, Vietnam, for the initiative that has given me the opportunity to undertake my Ph.D study in Germany.

Last but not least, I would like to thank my parents for bringing me up and encouraging me to pursue my research interest. I would also like to thank my beloved wife, Thanh Nga, for her endless love and unconditional support. In particular, I am grateful for my beloved children: my daughter, Bao Khue, and my son, Bao Khanh, for always bringing me so much joy and impetus. To them, I dedicate this dissertation.

July 2016

Duisburg, Germany

Trung Thanh Nguyen

ABSTRACT

This dissertation aims at improving spectrum sensing algorithms in order to effectively apply them to cellular systems. In wireless communications, cellular systems occupy a significant part of the spectrum. The spectrum usage for cellular systems are rapidly expanding due to the increasing demand for wireless services in our society. This results in radio frequency spectrum scarcity. Cellular systems can effectively handle this issue through cognitive mechanisms for spectrum utilization. Spectrum sensing plays the first stage of cognitive cycles for the adaptation to radio environments.

This dissertation focuses on maximizing the reliability of spectrum sensing to satisfy regulation requirements with respect to high spectrum sensing performance and an acceptable error rate. To overcome these challenges, characteristics of noise and manmade signals are exploited for spectrum sensing. Moreover, this dissertation considers system constraints, the compatibility with the current and the trends of future generations. Newly proposed and existing algorithms were evaluated in simulations in the context of cellular systems. Based on a prototype of cognitive cellular systems (CCSs), the proposed algorithms were assessed in realistic scenarios. These algorithms can be applied to CCSs for the awareness of desired signals in licensed and unlicensed bands.

For orthogonal frequency-division multiplexing (OFDM) signals, this dissertation exploits the characteristics of pilot patterns and preambles for new algorithms. The new algorithms outperform the existing ones, which also utilize pilot patterns. Additionally, the new algorithms can work with short observation durations, which is not possible with the existing algorithms. The Digital Video Broadcasting - Terrestrial (DVB-T) standard is taken as an example application for the algorithms. The algorithms can also be developed for filter bank multicarrier (FBMC) signals, which are a potential candidate for multiplexing techniques in the next cellular generations. The experimental results give insights for the reliability of the algorithms, taking system constraints

into account. Another new sensing algorithm, based on a preamble, is proposed for the DVB-T2 standard, which is the second generation of of DVB system. DVB-T2 systems have been deployed in worldwide regions. This algorithm can detect DVB-T2 signals in a very short observation interval, which is helpful for the in-band sensing mode, to protect primary users (in nearly real-time) from the secondary transmission.

An enhanced spectrum sensing algorithm based on cyclostationary signatures is proposed to detect desired signals in very low signal-to-noise ratios (SNRs). This algorithm can be developed to detect the single-carrier frequency division multiple access (SC-FDMA) signal, which is adopted for the uplink of long-term evolution (LTE) systems. This detector substantially outperforms the existing detection algorithms with the marginal complexity of some scalar multiplications. The test statistics are explicitly formulated in mathematical formulas, which were not presented in the previous work. The formulas and simulation results provide a useful strategy for cyclostationarity-based detection with different modulation types.

For multiband spectrum sensing, an effective scheme is proposed not only to detect but also to classify LTE signals in multiple channels in a wide frequency range. To the best of our knowledge, no scheme had previously been described to perform the sensing tasks. The scheme is reliable and flexible for implementation, and there is almost no performance degradation caused by the scheme compared to single-channel spectrum sensing. The multiband sensing scheme was experimentally assessed in scenarios where the existing infrastructures are interrupted to provide mobile communications.

The proposed algorithms and scheme facilitate cognitive capabilities to be applied to real cellular communications. This enables the significantly improved spectrum utilization of CCSs.

ZUSAMMENFASSUNG

Die vorliegende Dissertation zielt auf die Verbesserung von Spektrum Sensing Algorithmen ab, die effektiv auf zellulare Funksysteme angewendet werden können. In der drahtlosen Kommunikation besetzen zellulare Funksysteme große Teile des verfügbaren Frequenzspektrums. Der Bedarf an Frequenzressourcen wächst stark mit der steigenden Nachfrage unserer Gesellschaft nach mobiler Kommunikation. Dies führt zu einer Verknappung des verfügbaren Funkfrequenzspektrums. In zellularen Funksystemem kann dieses Problem mit kognitiven Mechanismen zur Spektrumsnutzung entschärft werden. Das Spektrum Sensing zur Adaptierung an die Funkumgebung bildet hierbei die erste Stufe der kognitiven Zyklen. Sie ermöglicht die Implementierung kognitiver Fähigkeiten in zellulare Systeme.

Die vorliegende Dissertation konzentriert sich auf die Maximierung der Zuverlässigkeit des Spektrum Sensings zur Erfüllung der regulatorischen Anforderungen in Bezug auf eine hohe Leistungsfähigkeit des Spektrum Sensings bei einer akzeptablen Fehlerwahrscheinlichkeit. Um diese Anforderungen zu erfüllen werden Eigenschaften von Störsignalen und Nutzsignalen ausgenutzt. Weiterhin werden Systembeschränkungen und die Kompatibiltät mit aktuellen sowie Trends zukünftiger Systemgenerationen berücksichtigt. Die vorgeschlagenen und einige vorhandene Algorithmen wurden in Simulationen im Kontext der zellularen Systeme untersucht und ausgewertet. Mit Hilfe eines vorhandenen Prototyps eines kognitiven zellularen Funkssystems (CCSs) konnten einige der untersuchten Algorithmen in realistischen Szenarien überprüft und bewertet werden. Diese Algorithmen lassen sich in CCSs zur Erkennung von Nutzersignalen in lizenzierten oder nicht lizenzierten Frequenzbändern nutzen.

Zur Erkennung von Signalen des Orthogonalen Frequenzmultiplexverfahrens (OFDM) nutzen die entwickelten Algorithmen die Eigenschaften von Pilotsignalen und Präambeln. Die neuen Algorithmen übertreffen die bisher bekannten, die auch Pilotmusters nutzen. Weiterhin können die neuen Algorithmen auch bei Systembeschränkungen auf kurze Beobachtungsintervalle arbeiten, was bei den bekannten Algorithmen nicht möglich ist.

Als Anwendungsbeispiel wird der Digital-Video-Rundfunk - Terrestrisch (DVB-T) Standard betrachtet. Die Algorithmen können auch auf Filterbank-Multi-Carrier (FBMC) Signal entwickelt werden. FBMC ist ein potenzieller Kandidat für Multiplexverfahren für zukünftige zellulare Funksysteme. Die experimentelle Überprüfung der Algorithmen zeigt deren Zuverlässigkeit auch unter Systemeinschränkungen. Ein weiterer Spektrum Sensing Algorithmus wird für den DVB-T2-Standard vorgeschlagen, der auf einer Präambel basiert und die zweite Generation des DVB-Systems darstellt. Diese DVB-T2-Systeme werden weltweit in verschiedenen Regionen für DVB-Systeme eingesetzt. Der Algorithmus kann die DVB-T2-Signale in einer extrem kurzen Beobachtungszeit erfassen. Dies ist hilfreich beim In-Band-Sensing zum Schutz der Primärnutzer vor Störungen durch Sekundärnutzer in Echtzeit.

In dieser Arbeit wird ein verbesserter Spektrum Sensing Algorithmus vorgeschlagen, der auf der zyklisch-stationären Signatur basiert und die Erkennung gewünschter Signale unter sehr niedrigen Signal-zu-Rausch-Verhältnissen (SNR) erlaubt. Dieser neue Algorithmus für SC-FDMA (engl. single-carrier frequency division multiple access) Signale kann effektiv für die Detektion von Mobilstationen in aktuellen und zukünftigen LTE-Systemen genutzt werden. Er übertrifft vohandene Algorithmen wesentlich, bei einer nur marginalen Komplexität von einigen Skalarmuliplikationen. Die Teststatistiken für die untersuchten Algorithmen sind mathematisch formuliert. Dies war in früheren Arbeiten nicht enthalten. Die mathematische Beschreibung und die simulierten Ergebnisse geben eine nützliche Strategie für das zyklisch-stationär basierte Sensing bei verschiedenen Modulationsarten an.

Für das Mehrkanal Spektrum Sensing wird ein Schema vorgeschlagen, das nicht nur die Erkennung, sondern auch die Klassifizierung von LTE-Signalen erlaubt. Dies ist sehr wahrscheinlich eine Anforderung beim Betrieb zukünftiger Funksysteme. Nach aktuellem Kenntnisstand wurde hierfür noch kein Verfahren zum Spektrum Sensing veröffentlicht. Das vorgeschlagene Verfahren ist mit flexiblen Designs implementierbar. Es zeigt sich eine nur vernachlässigbar geringe Leistungseinbuße im Vergleich zum Sensing der Einzelkanäle. Das Mehrkanal-Sensing wurde in einem Szenario experimentell untersucht, bei dem die vorhandene Infrastruktur unterbrochen ist.

Die vorgelegte Arbeit zeigt, dass die vorgeschlagenen Algorithmen und Schemata für die Implementierung in realen zellularen Funksystemen geeignet sind. Auf dieser Grundlage kann die Zuweisung und Verwendung von Funkressourcen in CCSs erheblich verbessert werden.

Contents

List of Figures

List of Tables

LIST OF ACRONYMS

3GPP	The 3rd Generation Partnership Project
5G-PPP	The 5G Infrastructure Public Private Partnership
AGM	Arthimetic-to-Geometric
AIF	Antenna Interface
API	Application Programming Interface
AWGN	Additive White Gaussian Noise
B4G	Beyond the Fourth Generation
BPSK	Binary Phase-Shift Keying
CAF	Cyclic Autocorrelation Function
CCS	Cognitive Cellular Systems
CE	Cognitive Engine
CFAR	Constant False-Alarm Rate
CFO	Carrier Frequency Offset
CLT	Central Limit Theorem
CM	Cognitive Manager
CP	Cyclic Prefix
CPRI	Common Public Radio Interface
CR	Cognitive Radio
CRM	Cognitive Resource Manager
CRN	Cognitive Radio Network
CRS	Cognitive Radio System
CSD	Cyclic Spectrum Density
D2D	Device-to-Device
DFE	Digital Front End

DRAM	Dynamic Random-Access Memory
DSP	Digital Signal Processor
DVB-T	Digital Video Broadcasting - Terrestrial
DVB-T2	Digital Video Broadcasting - Second Generation Terrestrial
EC	Estimation-Correlator
ECC	Electronic Communications Committee
ED	Energy-based Detection
ETSI	European Telecommunications Standards Institute
eNB/eNodeB	Evolved Node B
EV	Eigenvalue-based detection
EVD	Eigenvalue Decomposition
FBMC	Filter Bank Multicarrier
FBSE	Filter Bank Spectral Estimator
FCC	Federal Communications Commission
FDD	Frequency Division Duplex
FE	Front-End
FFT	Fast Fourier Transform
FIR	Finite Impulse Response
G	Generation
GDB/GLDB	Geo-Location Database
GLRT	Generalized Likelihood Ratio Test
IDFT	Inverse Discrete Fourier Transform
IMT	International Mobile Telecommunications
IPC	Inter Process Communication
ITU	International Telecommunication Union
ITU-R	International Telecommunication Union - Radiocommunication Sector
KKT	Karush-Kuhn-Tucker
LLR	Likelihood Ratio
LTE	Long-Term Evolution
MAC	Medium Access Control
MCS	Monte Carlo Simulation

MFD	Matched Filter Detection
MicroTCA	Micro Telecommunications Computing Architecture
MIMO	Multiple-Input Multiple-Output
MISO	Multiple-Input Single-Output
MLE	Maximum Likelihood Estimation
MME	Maximum-Minimum Eigenvalue
MMSE	Minimum Mean Square Error
MRC	Maximum Ratio Combination
MTM	Multitaper Method
MTSE	Multi-Taper Spectral Estimator
NP	Neyman-Pearson theorem
NU	Noise Uncertainty
OFDM	Orthogonal Frequency-Division Multiplexing
OTA	Over The Air
PC	Personal Computer
PCC	Probability of Correct Classification
PDF	Probability Distribution Function
PedA	ITU Pedestrian A channel model
PHY	Physical Layer
PPA	Periodical Peaks of Autocorrelation
PS	Protocol Stack
PSD	Power Spectral Density
PSS	Primary Synchronization Signal
PU	Primary User
QAM	Quadrature Amplitude Modulation
QP	Quiet Period
QTI	Quadratic Time-Invariant
REM	Radio Environment Map
RF	Radio Frequency
RF-FE	Radio-Frequency Front-End
ROC	Receiver Operating Characteristic

SCF	Spectral Correlation Function
SC-FDMA	Single-Carrier Frequency Division Multiple Access
SDO	Standard Organizer
SDR	Software-Defined Radio
SISO	Single-Input Single-Output
SNR	Signal-to-Noise Ratio
SPI	Serial Peripheral Interface
SS	Spectrum Sensing
SSM	Spectrum Sensing Module
SSS	Secondary Synchronization Signal
TDD	Time Division Duplex
TDSC	Time-Domain Symbol Cross-correlation
TVWS	TV White-Space
WRAN	Wireless Regional Area Network
WRC	World Radiocommunication Conference
WS	White Space
TS	Technical Specification
IEEE	Institute of Electrical and Electronics Engineers
DySPAN	Dynamic Spectrum Access Networks
RSRQ	Reference Signal Receive Quality
RSRP	Reference Signal Receive Power
AGC	Automatic Gain Control
DRX	Discontinuous Reception command

NOTATION

x	Scalar
$\mathbf{x}$	Vector
$\mathbb{X}$	Matrice
$*$	Convolution
$\|\|.\|\|$	Norm
$\|.\|$	Absolute value
$\max_{\Theta}$	Maximization with respect to variable Θ
$\arg\max_{\Theta}$	Argument of the maximum
Re	Real part
x^*	Complex conjugate of x
$\sqrt{(.)}$	Squared root
$\widehat{(.)}$	Estimated scalars
$x \sim \mathbb{C}N\left(\mu, \sigma^2\right)$	Complex circular Gaussian random variable x with mean μ and variance σ^2
$E\left[.\right]$	Expectation
$\int_a^b$	Integral from a to b
$\sum$	Summation
$\lim$	Limitation
$\mathcal{O}(.)$	Computational complexity

1 INTRODUCTION

1.1 Motivations

The radio-frequency spectrum is now experiencing scarcity since the demand of high data rate in wireless communications is increasing rapidly. The current spectrum bands are crowded with many kinds of wireless services, while the radio spectrum is a limited resource. However, spectrum usage is being under-utilized, as shown by spectrum occupancy measurements in worldwide regions [5–10]. Most of the measurements show that the overall spectrum occupancy is low and the spectrums are fragmented with vacant or partially used spectrum parts. For example, for 30 MHz–3.0 GHz, the spectrum occupancy is about 14% [9] and 13% [10] in Chicago and Vienna, USA, respectively. Naturally, awareness of the spectrum parts is essential to improve spectrum utilization, allowing spectrum parts to be reused and spectrum bands to be intelligently farmed to reduce the fragmented spectrum. The spectrum awareness, now termed as *spectrum sensing*, is a stage in the cognitive cycle in the concept of *cognitive radio* (CR) [11, 12]. Spectrum sensing has been a research interest for about two decades, and much work has been done on it. A main challenge of spectrum sensing is to reliably protect incumbent users with a high probability of correction at an acceptable false-alarm level. Furthermore, spectrum sensing must be compatible with specific wireless communications.

In wireless communications, cellular systems consume large spectrum bands, as shown in measurements—for example, in [5]. Cellular communications are speedily developing. Therefore, the spectrum scarcity of cellular systems has received increasing attention. Spectrum sensing for cellular systems must satisfy the requirements from telecommunication regulators for the probability of correction/error at a sensing sensitivity and system constraints, such as sensing durations, in in-band and out-band sensing modes. In terms of spectrum access, spectrums can be categorized into licensed and unlicensed. Spectrum sensing requires detecting the signals

in the bands and need to classify the signals. This dissertation focuses on spectrum sensing techniques for CCSs, which are based on different signal standards.

1.2 Key Contributions

Aiming at improving spectrum sensing for CCSs, this dissertation gives the following contributions:

- **In the unlicensed spectrum: Pilot-added OFDM-based signals**
  This dissertation exploits the periodical autocorrelation of pilot-added OFDM signals to improve detection. Two new algorithms are proposed to improve existing algorithms. The algorithms take DVB-T signals, as an example, to calculate the detection performance. The simulation results show that the proposed algorithms have a higher performance than the existing algorithms based on pilot patterns such as time-domain symbol cross-correlation (TDSC) algorithms. Besides, the new algorithms can work with short observations, with which the existing algorithms cannot work. These contributions are published in [13]. This is one of the improvements made by the new algorithms for CCS operations which constrain the length of observation durations. These contributions are published in [13].

- **In the unlicensed spectrum: Preamble-added OFDM signals**
  A new, robust sensing algorithm based on the first preamble symbol of DVB-T2 signals is proposed. This algorithm overcomes the noise uncertainty and requires very short observation durations. The formulas for detection performance and false alarm are derived, and a scheme of the algorithm is introduced for CCSs. The algorithm is very effective for the in-band sensing mode, in which the primary signals are mostly detected in real-time after being transmitted. DVB bands are an unlicensed spectrum with the most potential to utilize the white-spaces. DVB-T2 is a next standard of DVB signals and has been deployed throughout the world. This shows that the new algorithm can be widely applied to detect white-spaces in unlicensed spectrum TV bands. These above contributions are published in [14].

- **In the licensed spectrum for uplink: SC-FDMA signals**

A new algorithm based on cyclostationary signatures is proposed. This algorithm significantly outperforms existing algorithms. Additionally, clues are provided (with respect to modulation schemes) when applying cyclostationarity-based spectrum sensing algorithms. This algorithm can be further developed for a detection of SC-FDMA signals, which are used for the uplink signal of cellular systems. These contributions are introduced in [15].

- **In the licensed spectrum for downlink: Multiband spectrum sensing**
  A multiband sensing scheme is proposed to detect and classify LTE signals in downlinks. The sensing scheme has a low computational complexity and can be feasibly implemented with a filter bank. The design and main configuration parameters of the scheme are introduced. The simulation results evaluate the performance of the scheme with observation durations in fading environments. These particular contributions are published in [4].

- **The experimental evaluation of spectrum sensing with a CCS for unlicensed spectrums**
  A productive system for cognitive LTE-Advanced has been designed and developed in the kogLTE project. This dissertation utilizes the system to evaluate the reliability of new algorithms, which are implemented in a SDR platform. The experimental results show an agreement with the simulation results. Besides, the experiments give important guidelines to deploy the algorithms in a real CCS in terms of system constraints such as observation time due to a limitation of memory capacity. These contributions are published in [16].

- **The experimental evaluation of spectrum sensing with a CCS for public safety communications**
  A cognitive LTE-Advanced system is developed for public safety communications when the existing infrastructure of mobile communications is destroyed or interrupted. The system is designed and developed in the ABSOLUTE project. Based on the system, this dissertation applies the multiband sensing scheme in a CR framework. The experimental results evaluate the reliability of the multiband sensing scheme. Additionally, this dissertation provides descriptions of the operations, which are evolved to spectrum sensing, to supply mobile communications in emergency situations. The descriptions are useful to deploy the kind of CCSs. These mentioned contributions are published in [17].

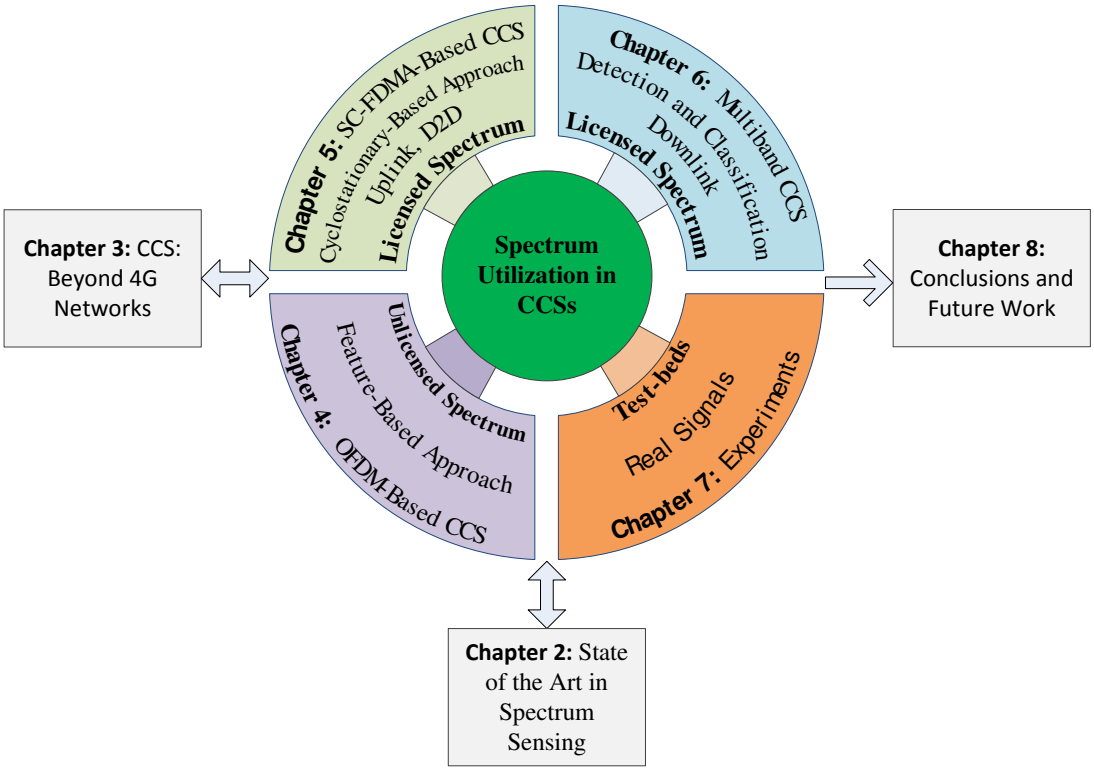

Fig. 1.1: Conceptual relation between the key contributions and organization of this dissertation.

1.3 Chapter Outline

For convenience, Fig. 1.1 describes the organization and key contributions of this dissertation in a conceptual relation. Chapter 2 presents a background on statistics and spectrum sensing such as fundamental concepts, general framework formulation, and basic approaches of spectrum sensing. Chapter 3 investigates spectrum sensing for cellular systems. The potential applications and positions of spectrum sensing in CCSs are presented. This chapter shows that spectrum sensing is an enabler to boost the system capacity of cellular systems. Chapter 4 introduces new spectrum sensing algorithms for OFDM-based signals. In particular, new algorithms for pilot-added OFDM signals are proposed. Additionally, an algorithm based on preamble is discovered for DVB-T2 signals. Chapter 5 presents a new algorithm based on cyclostationary signatures. This algorithm can be developed for a detection of SC-FDMA signals. In Chapter 6, a new multiband spectrum sensing scheme is proposed to detect and classify downlink signals in multiple channels. Next, experiments with CCSs are introduced in Chapter 7. The experimental results assessed the reliability of the algorithms for pilot-added OFDM signals and the reliability

of the multiband sensing scheme. Finally, Chapter 8 draws conclusions and mentions future work.

1.4 Publication Record

A collection of contributions for this dissertation has been compiled from the following publications:

- **T.T. Nguyen**, M. Hoffmann, T. Kreul, and T. Kaiser, "Experiment on multi-channel spectrum sensing with filter bank realization for cognitive LTE-A systems," Int. Conf. Advanced Technologies for Communications 2015 (ATC 2015), Hochiminh, Vietnam, Oct. 2015.

- **T.T. Nguyen**, A. Kabbani, S. Peethala, T. Kreul, and T. Kaiser, "Experiments on spectrum sensing algorithms of pilot-added OFDM signals with a cognitive LTE-A system," 20th IEEE International Workshop on Computer Aided Modelling and Design of Communication Links and Networks (IEEE CAMAD 2015), Guildford, UK, Sept. 2015.

- **T.T. Nguyen**, T. Kreul, and T. Kaiser, "An enhanced spectrum sensing algorithm with maximum ratio combination of spectral correlation," 23rd European Signal Processing Conference (EUSIPCO 2015), Nice, France, 31 Aug. –4 Sept. 2015.

- **T.T. Nguyen**, H. Cao, T. Kreul, and T. Kaiser, "A multi-channel spectrum sensing scheme with filter bank realization for LTE Signals," ***(Best Student Paper Award)*** 3rd IEEE Int. Workshop on Emerging COgnitive Radio Applications and aLgorithms (IEEE CORAL 2015), in conjunction with IEEE WoWMoM 2015, Boston, USA, June 2015.

- **T.T. Nguyen**, H. Cao, T. Kreul, and T. Kaiser, "Exploiting periodical peaks of autocorrelation of pilot-added OFDM signals for enhanced spectrum sensing algorithms," 18th Int. OFDM Workshop 2014 (InOWo'14), Essen, Germany, Aug. 2014.

- **T.T. Nguyen**, H. Cao, A.B. Güven, Y. Gao, A. Kabbani, T. Kreul, and T. Kaiser, "Robust spectrum sensing of DVB-T2 signal using the first preamble symbol," Int. Conf. Advanced Technologies for Communications 2013 (ATC 2013), Hochiminh, Vietnam, Oct. 2013.

Other related publications by the author of this dissertation:

- H. Cao, W. Jiang, T. Javornik, M. Wiemeler, **T.T. Nguyen**, and T. Kaiser, "Spectrum awareness scheme of the rapidly deployable eNodeB for unexpected and temporary events," 1st IEEE International Workshop on Emerging Technologies and Trends for Public Safety Communications (ETPSC 2013), co-located with IEEE CAMAD 2013, Berlin, Germany, Sept. 2013.

- H. Cao, W. Jiang, **T.T. Nguyen**, A.B. Güven, Y. Wang, Y. Gao, A. Kabbani, M. Wiemeler, T. Kreul, F. Zheng, and T. Kaiser, "The design of an LTE-A system enhanced with cognitive radio," 21st European Signal Processing Conference (EUSIPCO 2013), Marrakech, Morocco, Sept. 2013.

- W. Jiang, H. Cao, **T.T. Nguyen**, A.B. Güven, Y. Wang, Y. Gao, A. Kabbani, M. Wiemeler, T. Kreul, F. Zheng, and T. Kaiser, "Key issues towards beyond LTE-Advanced systems with cognitive radio," IEEE 14th Workshop on Signal Processing Advances in Wireless Communications (SPAWC), Darmstadt, Germany, June 2013.

- V.D. Nguyen, K.N. Quang, L.P. Van, **T.T. Nguyen**, D.T. Ha, and V.B. Pham, "Joint MAC and routing protocol for OFDMA-based adhoc networks," 4th Int. Conf. Communications and Electronics (ICCE 2012), Hue, Vietnam, Aug. 2012.

2 State of the Art in Spectrum Sensing

2.1 Statistical Theory

2.1.1 Fundamental Concepts

Mitola III and Maguire first proposed the concept of CR and pioneered the research, as in [11]. CR is described such that a radio node can detect *user communications needs* for the intelligent use of radio resources [12]. In the context of CR, the hardware of radio nodes can be flexibly controlled or supported by a kind of software platform, *software radio*, by which radio nodes are easily adaptable to the changes of the radio environment. The resources are, therefore, effectively utilized. It should be noted that the detection of user communications needs could be carried on any parameter underlying radio environments at the state *Observe* in the cognition cycle as in [11, 12].

CR has been a research interest for about two decades. A detection of user-needs on radio spectrum resources conduced the concept of *spectrum sensing* [18]. In a basic cognitive cycle, spectrum sensing is equivalent to the stage of radio-scene analysis [19]. Therefore, spectrum sensing is a core function of CR. A sensing radio node detects the presence of desired signals in a range of spectrum frequency. The spectrum part which is not occupied by a desired signal is termed a *white space* (WS). Spectrum sensing considers WSs in terms of frequency, time, and spatial direction (or geographical area) [20]. Hence, spectrum sensing is shown in these three dimensions. Alternatively, with spectrum sensing, spectrum awareness [20, 21] dwells on the ability to be aware of radio environments with respect to the detection of WSs and the classification/identification of signals or parameters physically underlying the environments.

To standardize CR-based products, the term *software-defined radio* (SDR) is also introduced by standard organizers (SDOs). For example, the International Telecommunication

Union–Radiocommunication Sector (ITU–R) defines SDR in [22] as a radio device that partially or fully realizes the capabilities of CR. Meanwhile, a whole radio-system employing CR technology is called a Cognitive Radio System (CRS) [22]. CRS can execute a cognitive cycle in order to obtain knowledge (by spectrum sensing), adapt its operation to radio environment, and learn from obtained results. The ITU-R has been provided with general guidelines for the development of CRS. In industry cooperation, SDR could be defined by different words. As in [23], SDR-Forum (now The Wireless Innovation Forum) defines the concept of SDR as "some or all of the physical layer functions are Software Defined."

This dissertation focuses on spectrum sensing for cellular systems. In the scope of this dissertation, spectrum sensing conveys both the abilities of detection and classification/identification. From a statistic point of view, these abilities are measured by the probabilities of random variables from noise, generated signals, and radio environments. Thus, spectrum sensing relies on the statistical characteristics of noise and desired signals. In communication, both noise and a generated signal could follow random processes. Statistical theory backs up the research of spectrum sensing. The relation between spectrum sensing and statistical theory will be introduced in the following sections.

2.1.2 Problem Description

Basically, the presence of a desired signal, which is depicted as "yes" or "no," depends on the probability of distribution of statistical parameters for the signals. When the probability exceeds a threshold, it is most likely that the desired signal exists, indicating "yes." The formula of the probability functions to make the decision is called the statistical criterion. There are two hypotheses denoted by H_1 and H_0 respectively to the presence and non-presence of the desired signal. These are *simple (binary) hypotheses*. There are *composite hypotheses* in the case where the number of hypotheses is more than two. For example, composite hypotheses are used to distinguish between the presences of different signals and noise only.

The detection problem has simple hypotheses by default. The probability of detection (or correction) corresponds to the case where the detector indicates "yes" and the desired signal really exists. Conversely, miss-detection is used to measure the ineffectiveness of the detector. The false alarm shows that the presence of the signal is determined by the detector; whereas, the

signal does not exist.

2.1.3 Background on Random Processes for Spectrum Sensing

Studying random processes provides the insights of spectrum sensing. In communications, the in-phase and quadrature components of noise follow a random process [24]. Components of signals (e.g., preambles, pilots, and synchronization sequences) are normally modeled as deterministic. Random variables can have different statistical characteristics such as mean, variance, and the shape of probability distribution functions (PDFs). The statistical characteristics are clues to distinguish between noise and signal and between types of signal. Besides, they can be utilized to estimate unknown parameters. Covariance examines a relation between random variables in dimensions. Meanwhile, correlation is a reduced version of covariance since it has no dimension. To simplify, this part mentions the relation of two random variables by correlation. Here, correlation is used to measure the dependency between two random variables. Hence, autocorrelation and cross-correlation are reviewed for random processes.

Two random processes are first mentioned: stationary and nonstationary. A random process is called (not strictly and wide-sense) stationary when the statistical mean and variance are invariant over time [25]. The autocorrelation of the random processes is a function of lag, which is the difference between two random values in time. Whereas, nonstationary processes have a variant statistical mean or variance. For simplicity, test statistics of spectrum sensing algorithms are normally constructed with the assumption that random variables are stationary. Therefore, a random variable in signal models is implicitly assumed to follow a stationary process.

Autocorrelation is the correlation between a sequence with a version of itself. Meanwhile, cross-correlation is calculated between two sequences. Auto/cross-correlation are normally used to construct a statistical criterion in spectrum sensing. In particular, the mean and variance of the test statistic, which follows a certain distribution in hypotheses, are main parameters for the probability of detection and error. For example, the autocorrelation of additive white Gaussian noise (AWGN) has zero mean. Differently, the autocorrelation of a desired signal has a nonzero mean when the signal conveys sequences such as cyclic prefixes, preambles, or pilots. Furthermore, a cross-correlation between the signal and a pattern can have high peaking amplitudes when the signal contains the same predefined sequence as the pattern. A

cross-correlation of AWGN with a pattern has no such peaking amplitudes. The mean of this cross-correlation is also zero. In this case, the PDFs of noise and the signal are not centered with each other. Therefore, it is helpful to determine the presence of the signal. Hence, cross-correlation can be a good method to develop spectrum sensing algorithms for the signal when the pattern is known. Alternatively, autocorrelation can be interchangeably presented with power spectral density via a Fourier transform. The Fourier theory is popularly applied to transform between autocorrelation and (power) spectral density [18]. Note that there are two theories to investigate on spectral coherence of random processes: the Fourier and Karhunen-Loeve theories [18]. Power spectrum analysis is also a tool for spectrum sensing. Noise and signals have different shapes of power spectral density. For AWGN, the average spectral density is flat in a whole channel bandwidth. Distinctly, manmade signals are not "white" since they have a centered spectral shape and spectral lines.

In addition to the two aforementioned random processes, cyclostationary is also a type of random process. Cyclostationary process is a special stationary since the statistical characteristics, mean and variance, vary periodically. This process is considered as a generalization of the stationary process. The cyclostationarity was extensively investigated by Gardner et. al [24, 26, 27]. Cyclic-autocorrelation and cyclic spectral correlation replace of autocorrelation and spectral density when examining cyclostationarity signatures.

From the above points, spectrum sensing needs to consider noise and signal with respect to statistical qualities such as autocorrelation and cross-correlation (for a stationary model) and cyclic autocorrelation or spectral correlation (for a cyclostationary model). The statistical qualities are important tools for spectrum sensing.

2.1.4 Statistical Criterions

Statistical criterion, noted by Λ, is a conventional quantity by which spectrum sensing can give a decision on hypotheses. For the detection task, this quantity is compared with a constant value to detect the presence of signal or noise. For classification/identification, the performance is calculated with different parameter values, and the maximum performance is selected to decide the highest possible hypothesis. To derive statistical criterions, main methods are mentioned as follows.

Likelihood Ratio (LLR)

This statistical criterion is defined by the ratio of the probability of correction to the probability of false alarm with respect to variable z, as in [28]

$$\Lambda_{LLR} = \frac{p\left(z|H_1\right)}{p\left(z|H_0\right)}.$$

The probability of correction and false alarm are changed with respect to the random variables. For binary hypotheses, the Neyman-Pearson theorem can be applied to derive an optimal statistical criterion. According to this theorem, the false alarm $p(z|H_0)$ is kept constant, while the probability of detection $p(z|H_1)$ is maximized.

Estimator-Correlator (EC)

The Estimator-Correlator (EC) was derived by Kay in [28] from the Neyman-Person theorem. This statistical criterion is applied for AWGN with a known variance σ^2 and a covariance matrix $\mathbb{R}_s$ of the received signal $\mathbf{x}$. The transmitted signal is estimated by minimum mean square error (MMSE) as $\mathbb{R}_s(\mathbb{R}_s + 2\sigma^2\mathbb{I})^{-1}\mathbf{x}$. The statistical criterion is a correlation between the estimated signal with the received signal as

$$\Lambda_{EC}\left(\mathbf{x}\right) = \mathbf{x}^H\mathbb{R}_s\big(\mathbb{R}_s + 2\sigma^2\mathbb{I}\big)^{-1}\mathbf{x}.$$

Generalized Likelihood Radio Test (GLRT)

Applying the Neyman-Person theorem in the case of no unknown parameter, a statistical criterion is formulated as the LLR. However, for hypotheses in which there are unknown parameters (e.g., a variance of noise and channel coefficients), an estimation method is taken to estimate the unknown parameters. This methodology is called the GLRT, as analyzed in [28]. The statistical criterion can be represented as

$$\Lambda_{GLRT} = \frac{\max\limits_{\theta} p(z|H_1, \theta)}{\max\limits_{\theta} p(z|H_0, \theta)}$$

where z and θ denote the random variable and unknown parameter, respectively.

2.1.5 Mathematic Tools

The GLRT is a framework to derive test statistics for spectrum sensing. The test statistics can be different forms due to the assumption placed on parameters. In principle, the statistics can provide a higher performance when the values of parameters are known to the detectors. Therefore, an estimation on unknown parameters needs to be handled before applying the GLRT framework. In statistics, there are some estimation methods: least squares, moments, Bayesian, and maximum likelihood estimation (MLE). MLE is a well-known method to estimate unknown parameters [29]. A likelihood function can be constructed from the given samples of the variables. The parameters are estimated by the values at which the likelihood function is at its maximum. To obtain the MLE of an unknown parameter, the likelihood function can be solved by some optimization tools, as applied in [30, 31]. In general, derivatives of the objective function (e.g., the numerator and denominator in the GLRT), with respect to the unknown parameters, are formulated to estimate the parameters. Convex optimization is also a powerful tool to find the MLEs of unknown parameters.

2.1.6 General Framework Formulation

A general framework formulation is presented here for the detection and classification of the desired signal. Based on this formulation, spectrum sensing approaches have clues to obtain test statistics. Fig. 2.1 visually presents the curves of PDFs under hypotheses H_1 and H_0. The right regions $z \geq \nu$ under hypotheses H_1 and H_0 present for the probability of presence for the desired signal and noise only, respectively. The two curves are overlap together. The region under hypothesis H_1 with $z \geq \nu$ presents the probability of detection (Pd) $P\left(z \geq \nu \,|H_1\right)$. The left region $z < \nu$ under hypothesis H_1 corresponds to the probability of miss-detection. The probability of error (false alarm, and denoted by Pfa) $P\left(z \geq \nu \,|H_0\right)$ is equivalent to the region under hypothesis H_0 with $z \geq \nu$.

For a good detector, Pd should be maximized, and Pfa should be minimized. However, Fig. 2.1 shows that it is difficult to solve the two objectives simultaneously. With the Neyman-Pearson theorem (denoted by *NP*), the ratio of Pd to Pfa is maximized with a constant false-alarm rate (CFAR). Therefore, the general framework is to construct a test statistic T for detection by

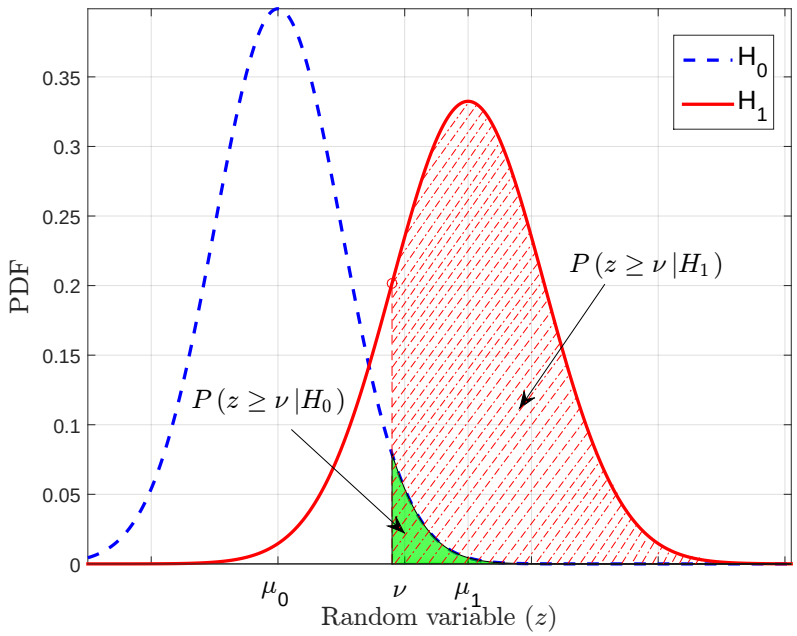

Fig. 2.1: The probability of detection and false alarm.

the GLRT [28], mentioned in 2.1.4, from the following inequation

$$\Lambda = \frac{\max\limits_{\theta_1} \{P(z\,|H_1\,,\theta_1)\}}{\max\limits_{\theta_0} \{P(z\,|H_0\,,\theta_0)\}} > \gamma. \tag{2.1}$$

After reducing Eq. 2.1, a *test statistic*, a reduced form from the statistical criterion, can be derived as follows

$$T_{dec} = f\left(z, \widehat{\theta}_1, \widehat{\theta}_0\right) \underset{H_0}{\overset{H_1}{\gtrless}} \eta \tag{2.2}$$

where $\widehat{\theta}_1 = \arg\max\limits_{\theta_1} \{P(z\,|H_1\,,\theta_1)\}$, $\widehat{\theta}_0 = \arg\max\limits_{\theta_0} \{P(z\,|H_1\,,\theta_0)\}$, and θ denotes a *threshold*.

Then the classification of signal, with respect to an identity parameter Θ under hypothesis

H_1 (when the target signal is detected), can be formulated as

$$\widehat{\Theta}_1 = \arg\max_{\Theta_1} \{T_{cls}(z|\Theta_1)\} \tag{2.3}$$

where T_{cls} is the test statistic of the classification. The identity of the detected signal is determined corresponding to the estimated value of $\widehat{\Theta}$.

2.2 Basic Approaches of Spectrum Sensing

A lot of work has been done on spectrum sensing algorithms. These algorithms are normally categorized into some approaches. From the perspective of the distribution function, spectrum sensing algorithms can be improved by tuning the variance and mean of PDFs under hypotheses H_1 and H_0. Therefore, two strategic methods should be focused on as follows:

- **Strategic method 1** – to increase the difference between the means of the test statistic under hypotheses H_1 and H_0. Visually, the two PDF curves, as in Fig. 2.1, need to be pushed far away from each other.
- **Strategic method 2** – to increase the variance of the test statistic under hypothesis H_1, compared to that under hypothesis H_0.

From literature reviews, as in [18, 20, 32, 33], spectrum sensing can be grouped as follows.

2.2.1 Matched-Filter Approach

The matched filter is a well-known linear time invariant filter to maximize SNR. For signal detection, the matched-filter approach was analyzed extensively by Steven M. Kay in his book [28]. With this approach, the received signal is processed through a matched filter, which has coefficients equal to those of the impulse response of the channels between the transmitter and detector [28, 34]. The test statistic is formulated from the correlation between the output signal of the matched filter $\widetilde{x}[n]$ and the known deterministic transmitted signal $s[n]$. Applying the

Neyman-Pearson theorem, the statistic is given in [28]

$$T_{mf}(x) = \sum_{n=0}^{N-1} \widetilde{x}[n] s[n] \underset{H_0}{\overset{H_1}{\gtrless}} \eta_{mf}.$$

The test statistic is a function of the transmitted signal vector. The transmitted signal is deterministic and considered as a pattern. The detector accomplishes a main function of primary receivers since it also takes a convolution between the received signal and the channel impulse response. The matched-filter approach can be applied when a detector knows the transmitted signal, channel impulse response, and variance of white Gaussian noise. With known noise power, the detector is an optimum method [20, 28] since SNRs are maximized throughout the matched filter. With unknown Gaussian noise (not only white), the *adaptive matched-filter* was proposed [35]. Originally, the adaptive matched-filter was derived for a radar target detection. The adaptive matched-filter uses an antenna array to estimate a unknown noise covariance by sample covariance matrix [35–38]. However, the adaptive matched-filter also works with assumption that the detector knows the steering signal vector. The enhanced algorithm in [38] is an adaptive matched-filter with a mismatch of the steering signal vector.

Similarly (but not identically), applying the mechanism of a matched filter, a sensing method exists when a detector knows a signature of transmitted signals. In DVB-T signals, for example, pilot symbols appear periodically. Based on this signature, [39] used a matched filter, which has coefficients equal to samples of the pilot symbols. The algorithm in [39] does not require knowing the noise power. However, the algorithm is not yet conveyed with the knowledge of environments.

2.2.2 Blind Approaches

This part presents approaches which require no or very limited knowledge about primary signals, noise, and environment. These such approaches are so-called *blind* or *semi-blind*, respectively.

Energy-Based Approach

The test statistic is based on the energy of the received signal. In the discrete time domain, the test statistic has the formula [40]

$$T_{ED} = \sum_{n=0}^{N-1} \|x(n)\|^2 \underset{H_0}{\overset{H_1}{>}} \eta_{ED}.$$

If it is assumed that noise is a Gaussian distrubuted random variable, then the test statistic will follow Chi-squared distributions, denoted by $\chi^2_{2N}(.)$, under hypotheses. The probabilities of detection and false alarm are in the closed forms, having Marcum Q-function and Gama functions [28]. With the large number of samples, the probabilities are asymptotically approximated by Gaussian distribution due to the central limit theory (CLT). Energy-based detectors consider the interference and thermal noise as a common noise floor. This detection is a popular method since it has a low complexity and requires no statistical characteristic of the signal. The detector is sub-optimal with a known noise power when compared to the matched-filter detection.

However, the knowledge of noise power is imperfect in practice. Noise power is estimated with an inaccuracy factor termed noise (level) uncertainty. It results in a significant performance degradation of the energy-based detector. The detector is disable at SNRs below a certain value, which is termed the SNR wall [41–43]. Normally, noise level uncertainty is about 1 dB to 2 dB [43–46]. The noise uncertainty (NU) factor is defined by $B \doteq 10\log_{10}\rho$. A low noise level uncertainty could increase the probability of false alarm more than the target of false alarm [47]. The detector is unreliable with inaccurate noise estimation. In practice, it is normally used as a coarse detector, which is combined with another detector (e.g., a feature-based detector) to improve the effectiveness of detection.

Note that ED is a certain kind of EC [28]. The statistical criterion EC formulates to the test statistic of ED when the desired signals and noise follow Gaussian distributions [28, 30, 47].

Eigenvalue-based Approach

To overcome the critical limitation of the energy-based approach, the eigenvalue-based approach is proposed in some work such as [31, 47–50]. This approach utilizes eigenvalue (spectral)

distributions of a random matrix to detect and classify signals and noise [49]. A basic idea of this approach is based on the fact that the power spectrum of primary signals has different statistical characteristics than those of the noise power spectrum. For primary signals, the shape of the power spectrum is non-flat, *"non-white"*. Normally, the spectral density concentrates at the center of the channel to obtain high energy efficiency. Whereas, the spectrum of noise is flat when noise is white Gaussian; it is not highly allocated at the center channel. The differences between the spectral density characteristics of signal and noise are exploited when the dimension of signal subspaces is smaller than that of the covariance matrix of received signals. Therefore, eigenvalue-based detectors need to be equipped with a higher number of antennas rather than the transmitter [31, 47–49].

Methodologically, the test statistics in this approach are derived from an eigenvalue decomposition (EVD) of the statistic covariance matrix of received signals $(\mathbb{R}_s + 2\sigma^2\mathbb{I})$. It is noted that this approach is equivalent to EC when the statistic covariance-matrix is known. An estimation of the statistic covariance-matrix can be revealed through a sample one. Here, assume that the eigenvalues are in a descending order $\lambda_1 \geq \lambda_2 \geq ... \geq \lambda_M$. Heuristically, Zeng et al. proposed *maximum-minimum eigenvalue* (MME) and *energy with minimum eigenvalue* (EME) ratios in [49]. Meanwhile, by the GLRT methodology, RuiZhang et al. derived the ratio *arithmetic-to-geometric* (AGM) in [31]. Wang et al. proposed another EV-based detection: $\lambda_{\max}/\sum \lambda_i$ by the GLRT in [47]. All of these methods are considered blind detection due to having no prior knowledge of channels, signals, and noise [47, 49]. The method *Signal-subspace eigenvalues* (SSE) was proposed in [31] with knowledge of noise variance as a requirement. It is not a good assumption as in the energy-based approach. This method is not categorized as a blind detection.

The PDF of the largest eigenvalue can be tractable by mathematical formulas through random matrix theories and is pre-computed into a table due to the high complexity of the formulas [49]. As the method proposed in [47], asymptotic forms were derived to reduce the computational complexity of the threshold and performance detection. In general, the EV-based approach has a high complexity since this approach is comprised of the covariance-matrix and EVD computation. The EVD computation contributes mainly to the complexity with $\mathcal{O}\big((MN)^3\big)$, where M and N denote the number of receiving antennas and observed samples, respectively. Therefore, this approach has an MN times higher complexity than that of the

energy-based approach.

From the aforementioned points, the EV-based approach can overcome the limitation of NU by which the energy-based detection is disable. However, these EV-based detectors are suitable in practice where the knowledge of primary signals, environments, and noise is limited or totally blind.

2.2.3 Feature-Based Approach

The transmitted signals in communication systems are manmade. These signals have distinctive features (e.g., modulation, CP, and a certain format) which are different with noise. The features could follow a known statistical distribution (e.g., a Chi-square distribution). Detectors can exploit these features to distinguish between the desired signals and noise. Hence, these detectors can overcome SNR walls and work well in low SNRs. Two basic methods in the feature-based approach are based on autocorrelation and cross-correlation. Autocorrelation is the correlation between a signal and a shifted version of itself. For autocorrelation, there are two main accumulation components that are contributed from the features and noise when the signals and noise are uncorrelated. Cross-correlation is computed from the signal and a predefined sequence for the features. In both methods, the component from noise reaches to zero with a large number of samples due to the characteristic of white additive Gaussian noise. The component accumulated from the features is non-zero and can be taken as a test statistic for a detection.

For the autocorrelation method, redundancy signatures in the received signals are utilized for detection. The signatures are used for multipath reduction, channel estimation, and synchronization. Algorithms based on an autocorrelation of the signals are proposed for detection. With *CP-based detection*, for example, the test statistic is constructed from the correlation between the samples in the CP areas and those in the original areas. A sliding window with the length of CP is used to gather samples in the CP and original areas. The correlation is computed between each sample and that at a sample distance equal to the useful part T_u of a OFDM symbol. In an AWGN channel, the signal samples in the CP areas are the same as those in the original areas. Hence, the correlation is maximum under hypothesis H_1. In multipath fading environments, the correlation is decreased but still strong, as proved in [51]. The main disadvantage of this method is real-time

processing for a correlation with a sliding window. This requires to compute the correlation of the samples in the original and CP areas at every shifted step. *Autocorrelation-based detection*, as in [52], accumulates the correlation between the sample not only in CP areas but also the others. This detection does not use a sliding window. The received signal is simply shifted by a lag τ equal to the useful part T_u. Therefore, the real-time processing is significantly reduced. The performance degradation is a trade off for this method in comparison to the CP-based detection. The TDSC-based detection was proposed by H.-S. Chen et al. in [53]. This detection utilizes the pilot pattern, which appears periodically in a number of OFDM symbols. The lag is equal to the length of the pilot pattern. The pilot cells can contribute to the accumulated correlation, which is non-zero. Meanwhile, the data cells and embedded noise introduce a mount of autocorrelation approaching to zero. Test statistics based on the autocorrelation method can be simplified to a summation formula of the noise variance and signal power when signal samples are uncorrelated with noise. The test statistics are asymptotically distributed to Gaussian distributions by applying the CLT when the number of samples is large.

For the cross-correlation method, the predefined sequences are normally signatures which are manipulated with useful data at transmitters. In cellular systems, for example, these signatures can be signals for symbol or slot synchronization at user-equipments (UEs). Yang Wen et al. [54] analyzed the correlation properties of primary and secondary synchronization signals (PSS/SSS). These authors proposed a detection algorithm based on the cross-correlation between the predefined PSS and received signals. The cross-correlation can be calculated by a convolution between the predefined sequences and received signals. Under hypothesis H_0, the test statistics are a summation of Gaussian random variables. These statistics would follow a Gaussian distribution. Similarly, the test statistics under hypothesis H_1 are distributed to Gaussian distribution with a statistical mean, which is shifted from that in H_0. The difference between the statistical means corresponds to the modulo of the predefined sequence.

2.2.4 Cyclostationarity-Based Approach

From the random processes' point of view, cyclostationarity-based approach is different from the feature-based approach. This approach is based on the probabilities of cyclostationary random variables. W.G. Gadner is the most outstanding pioneer in cyclostationarity research from his

works in [24, 26, 27, 55]. He proved that cyclostationarity random variables have cyclic statistical characteristics, which vary periodically, as means and variances. Cyclostationary models are *more complete* than stationary models, as mentioned in [56]. Cyclostationarity exhibits two dimensions: a lag time τ and cyclic frequency α in the time and frequency domains, respectively. The new dimension α leads to a new freedom for spectrum sensing. Exploiting cyclostationarity signatures from manmade signals will discover cyclostationarity-based detections, which can distinguish the presence of noise only and desired signals well in very low SNRs, as analyzed in [57]. Cyclostationarity signatures can be inherent in the desired signals when manipulating useful data or be intentionally embedded at transmitters, as proposed in [58, 59].

2.2.5 Waveform-Based Approach

Assume that the waveform of the desired signals is known. In the waveform-based approach [20, 60, 61], the test statistic is formulated by the correlation between the received samples and a waveform pattern of desired signals in the time domain. The pattern is a sequence of the transmitted samples, which are known at the detector. The test statistic can be given as

$$T_{wf} = \mathrm{Re}\left[\sum_{n=0}^{N-1} x\left(n\right) q^{*}\left(n\right)\right] \underset{H_0}{\overset{H_1}{\gtrless}} \eta_{wf}$$

where $x\left(n\right)$ and $q\left(n\right)$ are received samples and the pattern, respectively. The waveform-based detection outperforms an energy-based detection, especially at low SNRs [60]. This approach has a slightly higher complexity than an energy-based detection and is effective. However, it requires that detectors know the waveform of the desired signals. This assumption is realistic only when the sensing nodes must know perfectly: (1) the configuration parameters at the transmitter such as the multiplexing technique, modulation scheme, and pulse shaping filter, and (2) the environment to construct the waveform patterns. In particular, the waveform is affected by environments due to multipath fading and interference. Therefore, this assumption is not likely feasible in reality. Nevertheless, as the statistic formula, this approach could be concerned as a method of the feature-based approach when a main component comprising of the waveform is known instead of the waveform. The component is normally generated for synchronization purposes.

2.2.6 Concluding Remarks

The matched-filter approach, having the highest performance, is the optimal method. However, the detector requires a perfect knowledge for the primary-transmitting user and must demodulate the received signal as a coherent signal processing. A main disadvantage is that the approach is not suitable in the common practice in which the detectors have no such perfect knowledge of the primary user and environment. Besides, the complexity of the approach is high for implementation. For example, with a wideband spectrum, subband signals in each channel must be processed by a separate matched-filter detector. The waveform-based approach has a high accuracy of detection and a low computational complexity. However, the approach is difficult to apply since the pattern of transmitted signal must be known. The assumption for the approach is not feasible in common scenarios. The energy-based approach is popular, in general. The detector works well in high SNR regimes and has a low complexity. However, the detection performance is reduced significantly with an inaccuracy of noise power estimation. There exists an SNR wall at which the detection performance cannot exceed by increasing the observation duration.

Meanwhile, the feature-based approach exploits the statistical characteristics of the desired signals. The feature-based approach has a detection performance higher than the energy-based approach when noise is estimated with an uncertainty. Feature-based detectors can work in low SNR regimes. Besides, the computational complexity of these detectors is not as high as the matched-filter detector. The assumption of these detectors is also normally feasible. This approach can differentiate co-channel interference due to exploited statistical characteristics. The feature-based detector should be used to detect desired signals in certain spectrum parts which are not detected by a coarse detector (e.g., an energy-based detector) and applied at a fine-sensing stage of CCSs. Additionally, cyclostationarity-based approach is also effective for detection at very low SNRs due to the difference between cyclostationary signatures of noise and the desired signals. Nevertheless, the key assumption is that cyclostationary signatures must exist and be exploited.

2.3 Summary

The concept of CR has changed significantly since Mitola introduced it. Spectrum sensing plays a vital role in the context of CR. With the development of CR capabilities, spectrum sensing is changing as well. Currently, multi-dimensional spectrum sensing is a widely defined term. The tasks of spectrum sensing are the detection and classification of parameters or signal types. A general framework formulation of spectrum sensing is presented. From this framework, a test statistic in each spectrum sensing algorithm can be formulated. The enhancements or advantages of proposed solutions (algorithms and mechanisms) will show that they outperform or are more effective than previous work. From the statistical perspective, a key solution is to obtain the test statistic. Exploiting statistical characteristics of signals and noise is a primary issue. A background of statistical theory is presented with useful mathematic tools to construct test statistics that aim to improve the performance of spectrum sensing tasks. Basic approaches for spectrum sensing are categorized in this chapter. The feature-based and cyclostationarity-based approaches are mostly potential methods to enhance spectrum sensing algorithms. Studying approaches gives sign-pots and provides a good strategy for spectrum sensing, in general. Next, CCSs will be investigated. Spectrum sensing solutions will then be proposed for CCSs.

3 COGNITIVE CELLULAR SYSTEMS

This chapter presents the motivations on CR in current and future networks. Looking forward to the next generation of networks, CR could be located at a conceptual structure of the networks. As a core in CR, the roles of spectrum sensing in the networks will be mentioned.

3.1 Beyond 4G (B4G) Networks

Four generations (G) have been developed so far. The first generation (1G) was invented in the 1980s, and every decade since then, another generation has been developed. In about 2010, the LTE-Advanced technology was chosen by the ITU-T as the IMT-Advanced standard of 4G networks. It is standardized by the 3rd Generation Partnership Project (3GPP), as in Release 10. With the growing demands for mobile communications in modern society, higher data-rates and new scenarios are required for cellular networks. The market forecasts that there will be *a bottleneck* of mobile capacity in (approximately) 2020. By 2019, as predicted in [62], for example, there will be 1.5 billion wireless devices by which the mobile data traffic of 24.3 exabytes will be generated per month. Compared to 2014, data traffic is predicted to be tenfold in 2019. Per the prediction, 4G has not been a peak of deployment and will contribute 68% of total mobile traffic in 2019. Nevertheless, the pattern of one generation per decade strongly seems to continue. A vision of the ITU-R in 5G networks was launched as *"International Mobile Telecommunications (IMT) for 2020 and beyond"* (IMT-2020) in the World Radiocommunication Conference 2012 (WRC-12). In the even further long-term, 6G could be based on quantum technologies [63]. For the aspect of digital communications, quantum technologies could change the tradition bits to quantum bits, which are not in the two states (1s and 0s) but in superposition [64]. However, the author strongly believes that wireless communications spectrum bands are natural resources, which needs a high spectrum utilization, even in 6G, in order to

convey information over the air. Hereafter, the author specially mentions the networks later 4G (LTE-Advanced) and 5G to support the term B4G networks, in general.

Recently, research activities on 5G have been strongly encouraged. In Europe, a 5G vision with the term *the 5G Infrastructure Public Private Partnership* (5G-PPP) has been announced, as in [1]. In fact, the European commission is funding for big collaborative projects on 5G such as METIS [3] and 5GNOW [65]. Europe aims to reach a global agreement on 5G including a concept, killer services, a principal architecture, and key enabling technologies [1, 66]. Big players have been devoted to 5G research. For example, Samsung has pioneered breakthrough initiatives for 5G technologies [67–69].

The concept of 5G networks has not been finalized yet. This concept is still abstract, as mentioned in [70]. Nevertheless, a first concept of 5G has been agreed upon after collaborative discussions between between SDOs, vendors, and regulators.

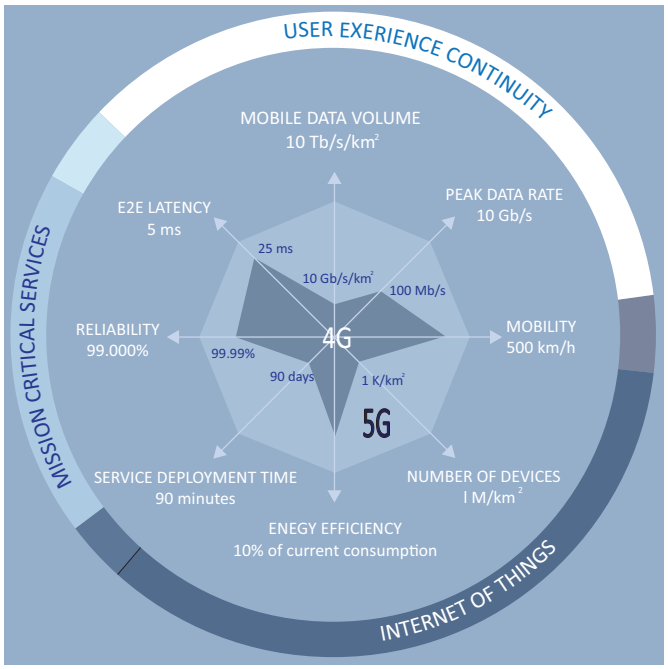

Fig. 3.1: 5G capacities. Reproduced from [1].

The disruptive capabilities of 5G are pointed out in [1, 3, 71–74]. These capabilities are depicted in comparison to 4G (in 2010) in Fig. 3.1 [1]. The mobile data capacity will be increased by 1000 times ($1000\times$) per area. In wireless communications, the limitations of channel capacity

is proven by Shannon theory (unit of pbs/Hz). The total system capacity is calculated as a formula: *Spectral efficiency x Bandwidth x Number of cells* and $pbs/Hz/cell \times Hz \times cell/km^2$. Therefore, to satisfy *1000*$\times$ for the system capacity, we must increase: spectral efficiency, bandwidth, and number of cells. As proposed by Nokia Siemen in [71], these quantities can be improved as $10 \times 10 \times 10$. For *spectral efficiency*, it can be handled by advanced technologies through diversity antennas. The technique with the most potential is massive MIMO, as mentioned in [68, 75, 76]. The cell coverage could be smaller with Pico/Femto-cells (and so on) to obtain higher cell densification (per km^2). The trend of small cells is described in [77]. Bandwidth can be improved by new spectrum bands and the utilization of unused spectrum spaces. New spectrum bands have been considered for cellular communications. Millimeter waves (mm-Wave) in the range of super high frequency (SHF), 3 GHz to 30 GHz, or extremely high frequencies (EHF), 30 GHz to 300 GHz, are potential candidates for 5G communications [68, 69, 78]. Nevertheless, a higher spectrum utilization of frequency ranges is coherently a good approach to provide a higher bandwidth for 5G. The spectrum usage is underutilized by about 14% in the spectrum range 30 MHz - 3 GHz [5, 7–10, 79]. Attaining a high spectrum utilization is the first priority before seeking new spectrum bands. This target can be achieved by boosting secondary transmissions and refarming the current assigned bands with a report on statistical spectrum usage from spectrum sensing. Therefore, CR will be an enabler in 5G by which 5G systems can address the capacity requirement and operate flexibly in different scenarios.

3.2 CR Framework in B4G Networks

3.2.1 Positioning CR in B4G Networks

The 5G concept has been just brought onto a track of finalization. Additionally, CRS has been at an initial stage of standardization. Nevertheless, CR in B4G can be shaped by looking forward to future generations. In this section, the position and principal roles of CR in B4G systems are described. SDOs have activities for the standardization of CRS. CR is under a specific task of working groups in SDOs. All SDOs focus on CR standardization but with particular kinds of communication systems. Standardizations of different SDOs are related and support each other

in concept. For example, the study group 5 of the ITU is working on CRS in terms of technical reports as M.2225 [80] and M.2242 [81]. The European Telecommunications Standards Institute (ETSI) has a technical committee on reconfigurable radio systems related to CRS. The IEEE DySPAN standards committee (IEEE and DySPAN are acronyms of The Institute of Electrical and Electronics Engineers and Dynamic Spectrum Access Networks, respectively) investigates on CRS in terms of TVWS for generic communications. For wireless regional area networks (WRANs), the IEEE 802.22 working group has launched a variety of standards for CRS—for example, the IEEE 802.22-2011 standard based on TVWS. For cellular communications, the 3GPP has considered to introducing CRS into technical specifications (TS), as expected in TS 36.211, Release 14. As in M.2242 [81], the CR in IMT systems yields capabilities that:

1. The CRS monitors traffic variation in time, geographic location, and frequency to improve spectral efficiency.

2. The CRS provides information to utilize resources flexibly such as bandwidths, transmit power, and carrier frequencies.

3. The CRS facilitates interference mitigation by choosing suitable spectrum portions and controlling power appropriately.

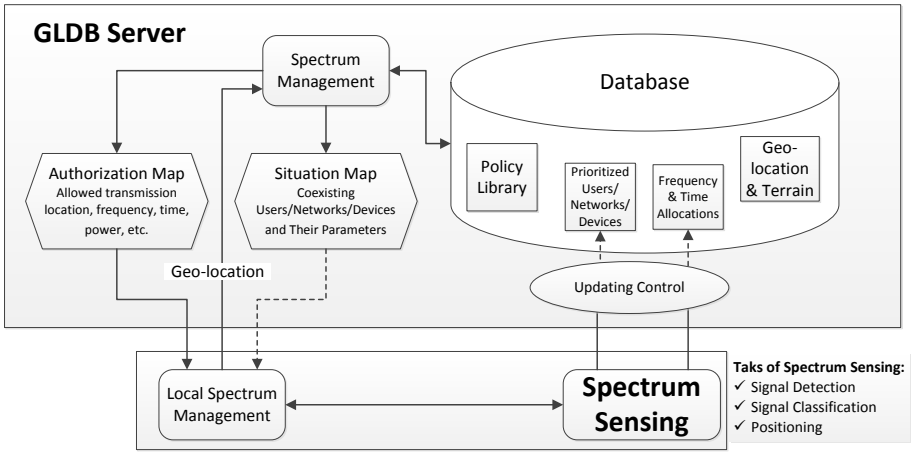

Fig. 3.2: A design of the spectrum awareness frame work in B4G systems. Adapted from [2].

For cellular communications, a CR framework (in general) is currently proposed to be deployed with LTA-Advanced technology. In B4G systems, the CR capabilities can be reused and developed since the next generations need to be backward standard-compliant. Moreover,

a CR framework can be conducted with different scenarios. CR-based B4G systems, as in the kogLTE [82] and ABSOLUTE [83] projects, for example, do not have the same design. In principle, a CR framework consists of main functional components: (a) spectrum sensing module(s) (to be aware of radio environments), a 'brain' (to make decisions), and databases (to store knowledge). Specifically, the CR framework for B4G systems was designed, as shown as in Fig. 3.2. The spectrum sensing in the CR framework, which is supported by the geo-location database (GLDB), can be more reliable.

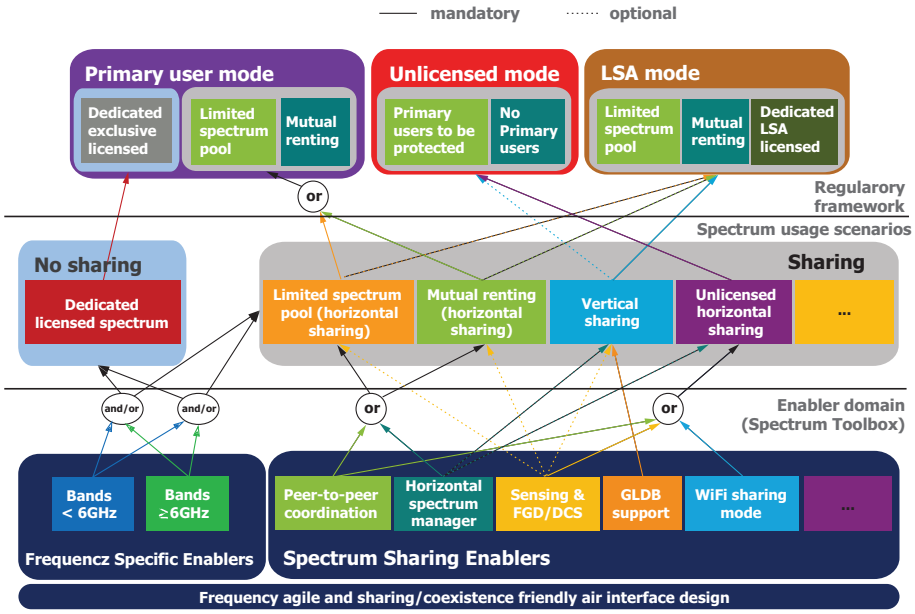

Fig. 3.3: The design of the Spectrum Toolbox for the METIS 5G system concept. Reproduced from [3].

A common vision of 5G was conducted from the collaboration in the METIS project between academic centers, vendors, and operators such as Ericsson, Alcatel-Lucent, Nokia, Huawei, and NTT DOCOMO. A 5G system concept was introduced by METIS in [3]. With the concept, METIS also proposed a 5G system architecture, which is comprised by the main enablers: Localized Contents and Traffic Flows, Dynamic RAN, Spectrum Toolbox, and Lean System Control Plane. *Spectrum Toolbox* is responsible for providing necessary radio resources. As shown in Fig. 3.3, Spectrum Sensing is an enabler of the Spectrum Toolbox for target services. It detects the presence of devices. For the spectrum sharing requirements of regulators, spectrum sensing can provide the information on spectrum usage to GLDB.

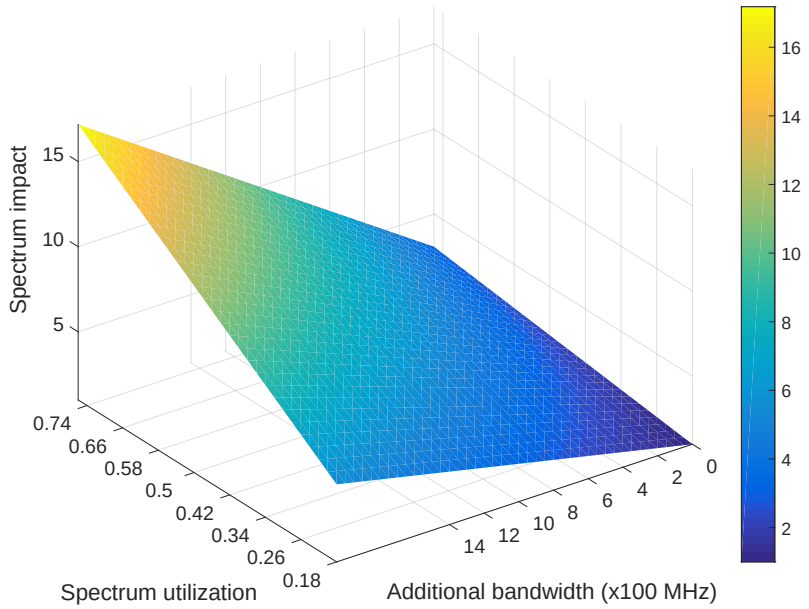

Fig. 3.4: Spectrum impact vs. additional bandwidth and spectrum utilization. Current bandwidth: 693 MHz.

3.2.2 Spectrum Utilization in B4G Networks

Spectrum impact is a factor measuring the improvement of spectral efficiency in B4G networks, as mentioned in Section 3.1. With spectrum utilization, CR can increase the spectral efficiency of CR-based systems [19]. Spectrum sensing in CR frameworks will detect white spaces in different bands, which are considered fragmented segments in spectrum bands. As a result, the CR-based systems obtain substantially higher spectral efficiency when utilizing the spectrum fragmentation. Spectrum impact, which affects the system capacity, can be estimated in the following form when considering only the contributions of CR frameworks in licensed bands as

$$q = (1 + \Delta_b/b_0\ ) \times u_1/u_0 \tag{3.1}$$

where b_0 and Δ_b are current spectrum bands, additional spectrum bands for the next generation, respectively; u_0 and u_1 denote for the spectrum utilization of the current and next generations. This form helps to estimate the additional bands and spectrum utilization to which the next generation needs to satisfy a targeted impact q.

Fig. 3.3 shows the impact of spectral efficiency with two dimensions: additional bandwidth and spectrum utilization. The higher spectrum utilization B4G can obtain, the less spectrum bands it requires. For the spectrum impact of 3.4, as in [3], the 5G systems need spectrum bands $\Delta_b = 1657MHz$ in addition to $b_0 = 693MHz$ of the current bands. Note that in the measurements of crowded cities such as Vienna [10], Chicago, and New York [79], the overall spectrum utilization, so-called spectrum occupancy, is about 13.6% for the frequency ranges 30 MHz–3 GHz. Here, assume the current spectrum occupancy for mobile communications is 25% on average. The spectrum impact will be $q = (1 + 1657/693\ ) \times 50/25\ \approx 6.8$ when spectrum utilization is improved to 50%. To gain the spectrum impact of 3.4, a CR-based B4G network requires additional bands of only $\Delta_b = (3.4 \times 0.25/0.5\ - 1) \times 693 \approx 485$ MHz with spectrum utilization: 50%.

3.3 Requirements for Spectrum Sensing in CCSs

Opportunistic transmissions must be harmless for primary devices. PUs are protected from secondary transmissions. Secondary transmissions must be stopped when primary signals are transmitted. To protect PU, regulators, such as the Federal Communications Commission (FCC) and the Electronic Communications Committee (ECC) must publish rigorous requirements. For example, the FCC requests a sensitivity of -114 dBm for DVB-T 6 MHz bandwidth [84]. At the sensitivity threshold of -114 dBm, detection probabilities for DVB-T 8 MHz bandwidth as in [85] should be higher 99% with the error probability of 1%. For licensed bands, spectrum sensing has to detect with the signal power lower than the sensitivity of PUs. For unlicensed bands, such as wifi bands, spectrum sensing recognizes the maximum power of transmitted signals to retain a sufferable interference level.

CR-based B4G systems must detect the desired-signals on each spectrum-band. These signals can be a primary, as in licensed bands, or secondary, as in unlicensed/shared bands. Specifically, 5G systems, as proposed by METIS, have spectrum sharing models [86] of which the different desired-signals have to be aware. In exclusive licensed-bands, for example, spectrum sensing detects LTE signals in the downlinks and uplinks with OFDM (or FBMC as a candidate for 5G multiplexing techniques [65]) and SC-FDMA, respectively; in unlicensed bands, as in TV, the desired signals is DVB-T (based on OFDM); in shared bands, as in wifi, the signals are

IEEE 802.11 (based on OFDM). Hence, spectrum sensing should be considered for multiplexing techniques (e.g., OFDM, and SC-FDMA).

For spectrum sensing, observations need to be short to release system resources for other operations and obtain a longer duration for secondary transmissions. For example, CRS can utilize quiet periods (QPs) [85], when all PUs do not transmit, to execute spectrum sensing tasks. Algorithms for sensing need to consider real environments in which transmitted signals suffer from a multi-path fading with some typical scenarios such as: urban/rural and fixed/portable UEs. Moreover, sensing algorithms have to be compatible with the imperfection of sensing nodes such as NU [42] and carrier frequency offset (CFO) [87].

In B4G systems, the operating bands will be much larger. This requires a kind of multiband sensing. Spectrum sensing for multiband signals has to take into account more channels in a large frequency-range [88]. The observation and detection need to be short (even for the multiband spectrum) with a simplified structure of multiband sensing compared to single-channel sensing. In the large spectrum, the sampling rate can be much higher, which result in the burdensome computation of multiband sensing. Simplifying this kind of sensing is a challenging issue.

3.4 Summary

A common 5G concept and its principle architecture will be standardized as the next step of SDOs. The standardization for CR has been under the study of WGs in SDOs. CR will have a part in B4G systems. CR-based B4G systems can contribute significantly to satisfy the requirements of system capacity and flexible operation. Spectrum sensing will be integrated into B4G systems as a core ingredient in CR frameworks. Spectrum sensing algorithms aim to improve the probability of correction with a constant probability of error. Additionally, the algorithms need to be allocated in realistic scenarios of system procedures, radio environments, and system constraints. The spectrum sensing should also be feasible in 4G systems since the development of 4G services has not been at a peak and future generations need to be backward standard-compliant.

4 SPECTRUM SENSING IN OFDM-BASED CCSS

4.1 Introduction

The feature-based approach is analyzed as a good approach for spectrum sensing. Signatures manipulated in the signals are utilized for spectrum sensing tasks. OFDM is a well-known multiplexing technique that is widely applied in wireless communications. CCSs need to work with OFDM signals when accessing current spectrum bands as TV. The signatures of OFDM signals can be cyclic prefixes (CPs), pilots, and preambles. Chapter 4 investigates the feature-based approach for OFDM signals. A general block diagram of the OFDM-based primary-transmitters and spectrum sensing algorithms is shown in Fig. 4.1. New algorithms for OFDM signals, one with pilots and the other with preambles, are introduced in Section 4.2 and 4.2, respectively.

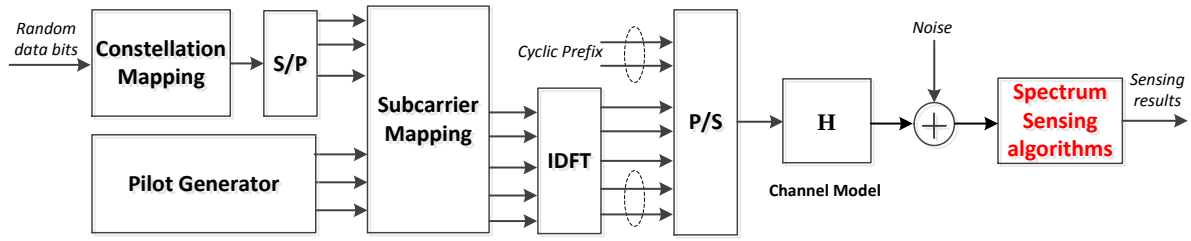

Fig. 4.1: OFDM model and spectrum sensing algorithms.

4.2 Enhanced Spectrum Sensing for Pilot-Added OFDM Signals

4.2.1 Overview

From literature reviews in [33], as analyzed in Section 2.2, the feature-based approach is considered as a good method for spectrum sensing. The detectors exploit unique characteristics of desired signals to distinguish the signals from noise. In wireless communications, pilots are normally generated for purposes such as channel estimation and synchronization. This section presents spectrum sensing algorithms for the signals which carry pilots. Specifically, the spectrum sensing algorithms for OFDM signals are investigated. Additionally, particular OFDM signals will be taken to derive test statistics. In principle, the spectrum sensing algorithms can be developed for other kinds of signal such as FBMC signals.

For pilot-added OFDM-based signals, the spectrum sensing algorithms extract statistical characteristics as the probability of distribution of the pilots to detect signals. For example, TDSC algorithms [53, 89, 90] were proposed and investigated intensively for DVB-T signals, which are based on OFDM and have pilot patterns. The basic idea of these algorithms is based on the fact that the cross-correlation between DVB-T symbols, which have the same pilot pattern, is nonzero and the cross-correlation of noise approaches to zero when increasing the number of observed symbols. In the DVB-T frame [91], pilot cells are repeated in a duration of four symbols, $4N_s$, while the amplitude of pilot cells is unchanged. TDSC algorithms are suitable for practical systems, as shown in [89], and are evaluated with captured real DVB-T signals. Moreover, TDSC detection has low performance reduction for carrier frequency offset.

The algorithms in [92] utilized the statistical difference between the subcarriers of pilots and these of useful data in the frequency domain. Due to using a fast Fourier transform (FFT), the performance of these algorithms could be degraded when increasing the carrier frequency offset.

In this dissertation, periodical peaks are exploited. The measurements and analytical forms show that the peaks can be contributed to the autocorrelation of pilot cells in OFDM signals. The positions of peaks are proved by formula derivations. For the DVB-T signal, two new spectrum sensing algorithms based on the periodical peaks are proposed. The periodical peaks are scaled up by constant precalculated coefficients to utilize a combination of the peaks. Simulations are

extensively investigated. The simulation results show that the new algorithms outperform TDCS algorithms, meanwhile inheriting the advantages of TDSC algorithms.

4.2.2 Periodical Peaks of Autocorrelation (PPA) Caused by Pilots

A. Exploiting PPA in Pilot-Added OFDM Signals

Let simplify the signal model with an AWGN channel, the transmitted signal under hypothesis H_1 is

$$y_m(n) = \frac{1}{\sqrt{N_C}} \sum_{k=0}^{N_C-1} x_{k,m} e^{jk\varphi_n} + w_m(n) \tag{4.1}$$

where n is the sample index, $\varphi_n = 2\pi\,(n - N_{CP})/N_C$; $y_m(n)$, $x_{k,m}$ and $w_m(n)$ denote the received signal, the data cell of the k^{th} subcarrier and noise in the m^{th} OFDM symbol, respectively; N_C is the FFT size; and N_{CP} is the CP length.

Several types of pilot pattern exist, as in [93]. Here, the pilot pattern of circular structure, which is commonly applied to OFDM systems, is investigated. The received signal can be written as

$$\begin{aligned} y_m(n) =& \frac{1}{\sqrt{N_C}} \sum_{p\in\Omega_{1,m}} x_{p,m} e^{jp\varphi_n} + \frac{1}{\sqrt{N_C}} \sum_{d\in\Omega_{2,m}} x_{d,m} e^{jd\varphi_n} \\ &+ w_m(n), \end{aligned} \tag{4.2}$$

where $\Omega_{1,m}$ and $\Omega_{2,m}$ are the set of pilot and data cells, respectively, $\Omega_{1,m} \uplus \Omega_{2,m} \equiv \{0, 1, .., N_c - 1\}$, $\Omega_{1,m} \triangleq \{p_0 + D_x m (\mathrm{mod} D_y) + D_x D_y i\}\,, i = \{0, .., N_{SP} - 1\}$ and N_{SP} is the number of scattered pilot cells in a symbol. For the circular structure, D_x and D_y denote the separation of pilot cells and number of symbols in one period, respectively, and $D = D_y \times D_x$.

The autocorrelation of the received signal is

$$R_{yy}\,(\tau) = E\,[y(n - \tau/2\,)y^*(n + \tau/2\,)] \tag{4.3}$$

where τ is lag. The autocorrelation is presented with symbol indices m_1 and m_2 at positions $(n - \tau/2\,)$ and $(n + \tau/2\,)$, respectively, and lag τ.

When $m_1 = m_2 = m$, substitute (4.2) into (4.3), with $\tau \neq 0$ the autocorrelation is derived as

$$R_{yy}(\tau) = \left(\sigma_d^2 / N_C\right) \left(\left(a^2 - 1\right)/D_y \; A + B\right) \tag{4.4}$$

where a is the boosted amplitude of pilot cells, σ_d^2 is the variance of data cells, and

$$\begin{cases} A = \sum\limits_{l=0}^{D_y-1} \sum\limits_{i=0}^{N_{SP}-1} e^{j(D_x l + Di)2\pi\tau/N_C} \; , \\ B = \sum\limits_{d=0}^{N_C-1} e^{jd2\pi\tau/N_C} \; . \end{cases} \tag{4.5}$$

Then, apply the geometric series, Eq. 4.5 is formulated as

$$\begin{cases} A = \frac{\sin(\pi\tau D/N_C)}{\sin(\pi\tau D_x/N_C)} \frac{\sin(\pi\tau N_{SP} D/N_C)}{\sin(\pi\tau D/N_C)} e^{j\pi\tau(N_{SP}D - D_x)/N_C} \; , \\ B = \frac{\sin(2\pi\tau)}{\sin(\pi\tau/N_C)} e^{-j\pi\tau/N_C} \; . \end{cases} \tag{4.6}$$

Hence, peaks of autocorrelation are found by scanning τ. $R_{yy}(n, \tau)$ has high amplitudes at the values of $\tau \in \{N_C/D_x \; , 2N_C/D_x \; , .., N_C\}$.

When $m_1 \neq m_2$, the autocorrelation is comprised of pilot cells with a step of N_C/D_x (not from data cells). Therefore, with all symbol indexes, the peaks appear periodically in D_y symbols.

The pilot pattern of DVB-T signals is shown in Figure 11 in ETSI EN 300744 [91]. In the pilot pattern, the scattered pilots are allocated periodically in a certain number of subcarriers and symbols. Continual pilots are assigned in fixed locations in the pilot pattern. In the 2k mode, the step of scattered pilot cells is of three subcarriers, $D_x = 3$. Thus, the three peaks of autocorrelation are expected for the DVB-T signal with this configuration in the duration of a symbol. The peaks are allocated at $\tau \in \{1/3 \; , 2/3 \; , 1\} \times N_c$. Moreover, after four symbols, $D_y = 4$, the pilot cells are repeated. Therefore, there will be in total 12 peaks expected in a duration of four symbols.

Fig. 4.2 presents the autocorrelation of the DVB-T signal, which is configured in the 2k mode with a CP ratio of 1/32 and a lag in a duration of four symbols. As observed in Fig. 4.2, four peaks are located at lag of $\{683, \; 1365, \; 2048, \; 2112\}$ in one symbol. The first three peaks

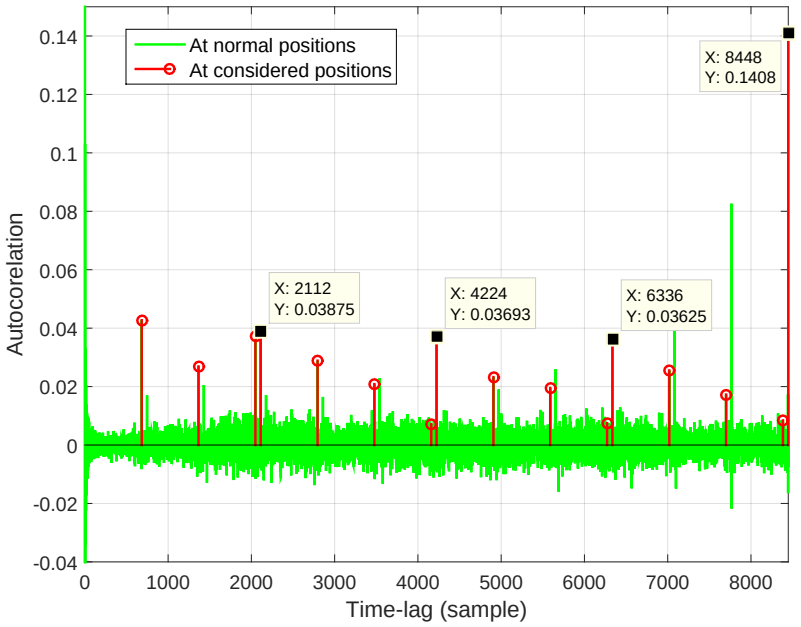

Fig. 4.2: Periodical peaks of autocorrelation for the DVB-T signal with $D_x = 3$ and $D_y = 4$.

are constructed by scattered pilot cells while the last peak is a sum of autocorrelation from the continual pilot cells and the edge ones in DVB-T frame [91]. Additionally, some floating-peaks are raised due to random values of autocorrelation. The floating-peaks are not allocated at fixed lags. Due to being at random positions, these floating-peaks can be ignored. Thus, four peaks appear at particular lags in a duration of one DVB-T symbol, N_s. In a period of four symbols, $T_0 = 4N_s$, 16 periodical peaks exist at considered positions, as in Fig. 4.2. Whereas, the peak at T_0 has the highest mean value due to the pilot pattern repeated in the periodicity T_0. Therefore, the characteristic periodical peaks could be utilized to enhance spectrum sensing algorithms for CR-based systems.

4.2.3 Proposed Algorithms for Detection

The exploited features of PPA can be used to detect the desired signals. TDSC algorithms [53] are proposed by utilizing the last peak, which is equivalent to the autocorrelation with T_0. As in [53], the NP theorem is applied to construct the statistic of the TDSC-NP algorithm. The MRC is used to accumulate symbol correlation for the test statistic of the TDSC-MRC algorithm [53].

This part introduces two enhanced sensing algorithms for the DVB-T signal, namely, PPA-

NP and PPA-MRC, respectively, by utilizing a sum of PPA peaks with weighting coefficients.

A. Formula of Test Statistic for PPA-NP

As mentioned in 2.1.6, the test statistics can be obtained when maximizing the joint distribution under hypothesis H_1 with unknown parameters: weighting coefficients. Under hypothesis H_0, the joint distribution does not vary with weighting coefficients. For simplification, assume that the peaks are independent of one another. As Eq. (30) in [90], the combination of independent random variables is maximized by scaling the real part of the variables with the coefficients. These coefficients are derived from the statistical mean of variables at a given SNR.

Nevertheless, the coefficients can be empirically computed by the average amplitude of the peaks. Due to the characteristics of zero-mean white-noise, the coefficients are calculated at one SNR value to determine the combination of periodical peaks. For example, the precalculated coefficients at an SNR of -13 dB are also used for an SNR range from -22 dB to -6 dB. In practice, at the location of the detector, the SNR could be estimated roughly from a radio environment map (REM) as shown in [39]. Therefore, the mean values of peaks are linearly scaled by constant coefficients for different SNRs. The accumulated autocorrelation from the peaks in the z^{th} period, $\tau \in \{zT_0 \div (z+1)\,T_0\}$, is formulated as

$$S(z) = \sum_{n=0}^{N-1} \left(\sum_{i \in \Omega_z} c_i R_{yy}(n, \tau_i + zT_0) + R_{yy}(n, T_0 + zT_0) \right) \tag{4.7}$$

where z, c_i, and τ_i are the period index from 0, the weighting coefficient, and the lag of the i^{th} peaks; Ω_z is the set of peaks; and N denotes the number of observed samples. The coefficients are calculated by averaging the amplitude of peaks in the considered lags at a given SNR level.

For the PPA-NP algorithm, the peaks in the first period T_0 are considered, and the sum of the peaks is factored as

$$S(0) = \sum_{n=0}^{N-1} \left(\sum_{i \in \Omega_z} c_i R(n, \tau_i) + R(n, T_0) \right). \tag{4.8}$$

Then, the module of $S(0)$ is taken and normalized by the coefficients, the test having the

formula of

$$T_{PPA-NP} = |S(0)| / \sqrt{\sigma_w^2 \left(\sum_{i \in \Omega_z} c_i + 1 \right)} \tag{4.9}$$

where σ_w^2 denotes noise power.

B. Formula of Test Statistic for PPA-MRC

To obtain further performance gain, the combination of the sum $S(z)$ with different indices z is taken. The weighting coefficients are the same as for PPA-NP.

A test statistic of PPA-MRC is accumulated by a sum of conjunction between $S(z)$. The test statistic is given by

$$T_{PPA-MRC} = \left| \sum_{z=0}^{N_{prd}-1} S(z) S^*(z+1) \right| \tag{4.10}$$

where N_{prd} is the number of periods.

C. Computation Procedure of Proposed Algorithms

- **Step 1 – Compute an averaged mean of the received signal under hypothesis H_1:**
  At a certain SNR (e.g., at SNR of -13 dB), calculate the weighting coefficients by averaging the autocorrelation of the signal at expected lags. These coefficients are divided by the mean amplitude of the peak at T_0. The coefficient for the peak at T_0 is equal to 1.

- **Step 2 – Compute the test statistic:**
  Calculate the amplitude of peaks for the received signal. Next, sum up the products of coefficients and amplitude of peaks, as in Eq. 4.8. The peaks are calculated in one period T_0 for the PPA-NP algorithm, in multiple periods, for the PPA-MRC algorithm. Then, the test statistic is computed by the absolute of the sum.

- **Step 3 – Make a decision:**
  Compare the test statistic with a predefined threshold. The presence of the desired signal

is assumed when the statistic is higher than the threshold. Otherwise, the absence of the desired signal is confirmed.

D. Complexity of Proposed Algorithms

Table 4.1: Comparison of complexity of proposed algorithms with TDSC algorithms.

Algorithm	Complexity
TDSC-NP [89]	$4N_s\left(N_{prd}-1\right)$
TDSC-MRC [89]	$2N_sN_{prd}\left(N_{prd}-1\right)$
PPA-NP	$4N_s\left(N_{prd}-1\right)N_P$
PPA-MRC	$2N_sN_{prd}\left(N_{prd}-1\right)N_P$

As shown in Table 4.1, the complexity of PPA-NP/MRC algorithms is equal to that of TDSC-NP/MRC algorithms, multiplying along with the period number N_{prd}. Besides, N_P is the number of periodical peaks in one period. For the DVB-T signal, with $N_P = 16$, the complexity of PPA algorithms is 16 times greater than that of TDSC algorithms. PPA algorithms outperform TDSC algorithms by approximately 1 dB but with the cost of complexity.

4.2.4 Simulation Results

In simulations, the DVB-T signal is generated with a bandwidth of 8MHz, an FFT-size of 2k, and the pilot pattern extracted as in [91]. To obtain good statistic values, the simulations are carried out with 10,000 and 8,000 Monte-Carlo trials for thresholds with a CFAR of 1% and the probability of detection, respectively.

Table 4.2: The mean value of PPA for the DVB-T signal with 42 symbols, CP ratio: 1/16, SNR: -13 dB, and noise variance σ_w^2: 1.

$Symbol/Peak$	P1	P2	P3	P4
Symbol 1	0.644844	0.311306	0.786491	0.643230
Symbol 2	0.370261	0.182691	0.043152	0.612116
Symbol 3	0.379901	0.190188	0.046907	0.597460
Symbol 4	0.372756	0.177803	0.042282	2.206068

Table 4.2 shows the mean amplitude of peaks computed by simulations for the DVB-T signal at an SNR of -13 dB. In this table, the last peak of Symbol 4 is the highest. The weighting coefficients are derived by dividing the amplitudes by the highest one. Therefore, the last peak has the weighting coefficient of 1.

Fig. 4.3 plots the probability of detection for the PPA-NP/MRC algorithms compared to the TDSC-NP/MRC algorithms with a sensing time of 10 ms for different CP ratios, as defined by the DVB-T standard and with noise uncertainties of 0 dB and 1 dB. To verify the performance gain of PPA algorithms, the SNRs at which the performance is over 90% are considered. Besides, as shown in Fig. 4.3, the performance degradation of PPA and TDSC algorithms in the two cases of NU are approximately equal together. The performance gain of PPA algorithms compared to TDSC algorithms is maintained with NU. As shown in Fig. 4.3a, the performance gain is 2.5 dB with CP ratios of 1/4. In Fig. 4.3b, the performance gain is about 1 dB with a CP ratio of 1/32. The reason is that the peak at $\tau = N_c$ is accumulated more from the correlation of the samples in CP areas with ones in the original areas than the three peaks at $\tau = N_c + iN_s$ with $i = 1, 2, 3$. This leads to a higher performance gain when CP ratio is higher. The amplitude of the peak at $\tau = N_c$ will be approximately equal to that of the three peaks comprised from the autocorrelation of pilots when the CP length is shortened to zero. With a CP ratio of 1/32, the gain is mainly constructed by pilot cells. The performance gain is kept at 1 dB with short CP ratios. The performance gain of the PPA-MRC algorithm compared to the TDSC-MRC algorithm is 1 dB for all CP ratios. Therefore, PPA detection could be applied as well for FBMC signals [94], whose CP ratio is zero. Assuming that FBMC signals have the same pilot pattern as the DVB-T standard, the performance gain of PPA-NP/MRC algorithms will be 1 dB.

Fig. 4.4 shows the probability of detection for PPA-NP/MRC compared to TDSC-NP/MRC with a sensing time of 20 ms and CP ratio of 1/8. Comparing PPA-NP to TDSC-NP and PPA-MRC to TDSC-MRC, the performance gains are 1.5 dB and 1 dB, respectively. Hence, when increasing the sensing time from 10 ms to 20 ms, while keeping the CP ratio of 1/8, the gains remain. In contrast, the performance gain given in [92] is reduced when the sensing time is increased. Therefore, this is an advantage of PPA algorithms in comparison with TDSC algorithms.

Fig. 4.5 plots the performance of PPA-NP detection in different environments and with NU of 0 and 1 dB. The above results are extracted from the simulations in AWGN and multipath fading

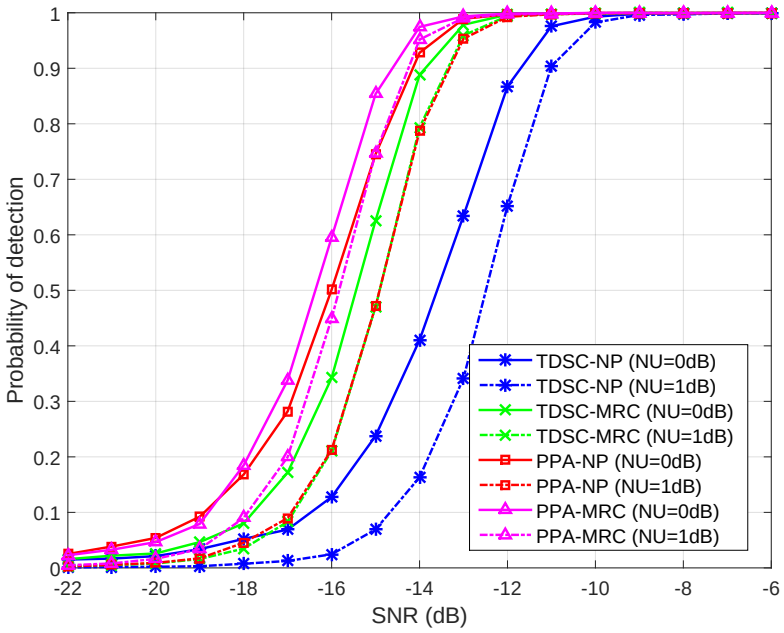

(a) CP ratio of 1/4

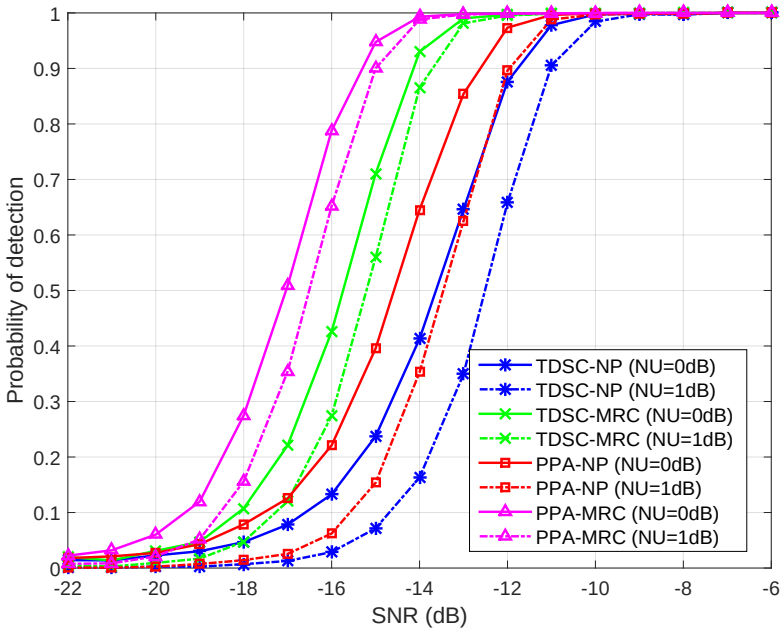

(b) CP ratio of 1/32

Fig. 4.3: PPA versus TDSC in the COST207 environment with a sensing time of 10 ms, a CFAR of 0.01, and different CP ratios.

environments, including the profiles of WRAN [95] and COST207 [96]. In the environments, with NU of 1 dB the performance degradation of the PPA-NP algorithm is about 0.85 dB.

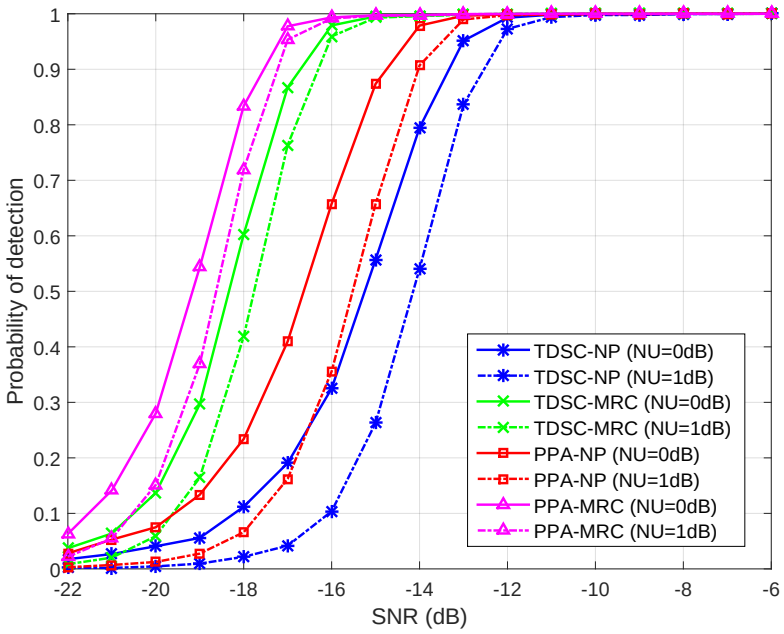

Fig. 4.4: PPA versus TDSC in the COST207 environment with a sensing time of 20 ms, a CP ratio of 1/8, and a CFAR of 0.01.

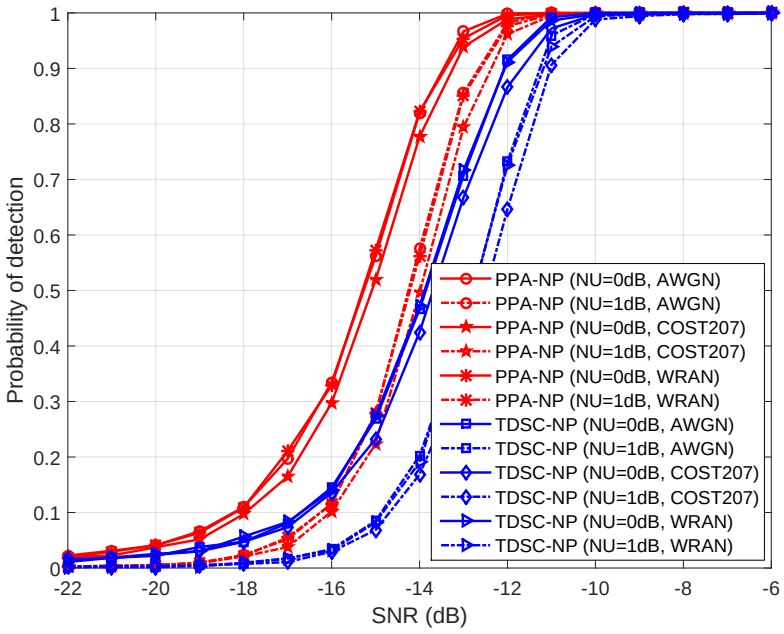

Fig. 4.5: PPA-NP versus TDSC-NP in different environments with NU of 0 and 1 dB, and a CFAR of 0.01.

The degradation is comparatively equal to that of TDSC algorithms. In all environments, the performance gain of PPA algorithms compared to TDSC algorithms is about 1.5 dB in both cases NU of 0 dB and 1 dB. In an AWGN environment, the performance is the highest. The performance in WRAN environments is close to one in an AWGN environment and is reduced slightly in COST207 environments.

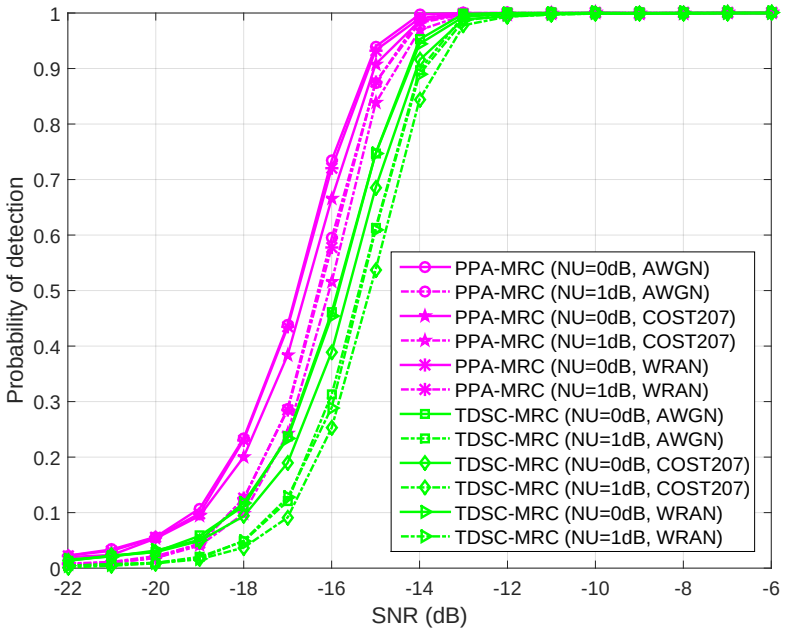

Fig. 4.6: PPA-MRC versus TDSC-MRC in different environments with NU values of 0 dB and 1 dB, a CFAR of 0.01, and a CP ratio of 1/8.

Similarly, Fig. 4.6 depicts the performance of PPA-MRC detection in different environments with NU of 0 dB and 1 dB. In the environments with NU of 1 dB, the performance degradation of the PPA-MRC and TDSC-MRC algorithms are about 0.55 dB. PPA-MRC outperforms TDSC-MRC by 1 dB in all environments. The results, as shown in both Fig. 4.5 and Fig. 4.6, indicate that PPA detectors work well in different environments and are low sensitive to NU.

In Fig. 4.7 and Fig. 4.8, the curves of receiver operating characteristic (ROC) are plotted for the algorithms. To compare with TDSC algorithms, a probability of detection of about 90% is considered. At given SNRs, the false alarms of PPA-NP/MRC algorithms compared to that of TDSC-NP/MRC algorithms are roughly reduced by 20% and 30%, respectively. The curves in Fig. 4.7 and Fig. 4.8 are plotted with the same weighting coefficients, which are calculated at

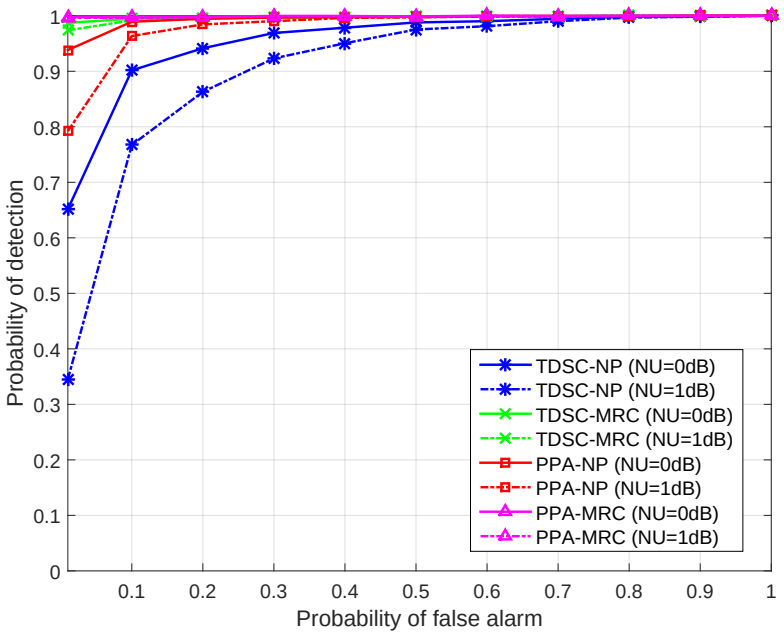

Fig. 4.7: ROC of PPA versus TDSC in the COST207 environment at an SNR of -13 dB with a sensing time of 10 ms and a CP ratio of 1/8.

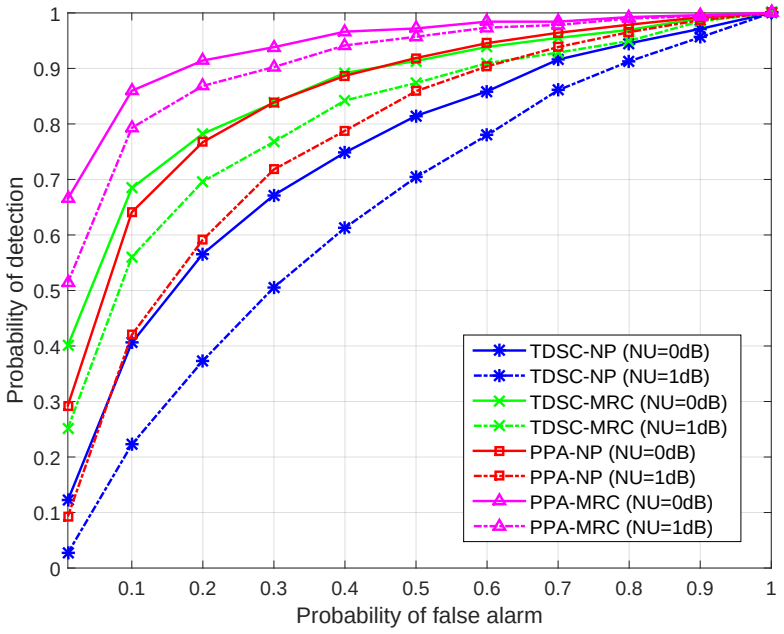

Fig. 4.8: ROC of PPA versus TDSC in the COST207 environment at an SNR of -16 dB with a sensing time of 10 ms and a CP ratio of 1/8.

SNR of -13 dB. Empirically, it is unnecessary to calculate the weighting coefficients for each SNR value. The coefficients could be used for a range of SNRs surrounding the reference SNR. This usage supports practical implementation because PPA algorithms could take a roughly estimated SNR to look up the predefined coefficients.

4.2.5 Concluding Remarks

Periodical peaks caused by pilots in OFDM-based signals are exploited. DVB-T signals were presented as an example which can generate periodical peaks. The peaks are statistically independent from one another. The peak amplitudes were computed by simulations. Based on the periodicity of peaks, two spectrum sensing algorithms, called PPA-NP and PPA-MRC algorithms, were proposed to detect DVB-T signals. The weighting coefficients can be calculated by averaging the amplitude of the peaks measured at an SNR value. The SNR value can be in a range. The PPA-NP/MRC algorithms were compared with TDSC-NP/MRC algorithms in different environments and noise uncertainties, respectively. The simulation results show that PPA-NP and PPA-MRC algorithms outperform TDSC-NP and TDSC-MRC algorithms by 1 dB to 2.5 dB and 1 dB, respectively. Additionally, the new proposed algorithms work well in multipath fading environments.

4.3 Enhanced Spectrum Sensing for DVB-T2 Signals

4.3.1 Overview

In CR-based systems, DVB-T [91] is one of the most important kinds of signal used by the primary users in TV bands. The effective sensing approach is based on the characteristics of the DVB-T signal. The signal has the CP fractions of 1/4, 1/8, 1/16, and 1/32 and a fixed pilot pattern. With the above characteristics, the CP-based algorithms [51, 90] and the pilot-based algorithms in the time domain [53, 90] were proposed. For example, the pilot-based algorithm in [53] works well with a 0.9 detection probability at the SNR of -20.5 dB with a sensing time of 50 ms and a false alarm of 0.1.

However, the DVB-T2 standard [97] was introduced as the next generation of DVB systems. The new standard gives various configurations depending on signal characteristics. With the pilot

characteristic, there are eight patterns for each mode of single-input single-output (SISO) and multiple-input single-output (MISO). Also, the pilots are modulated by a pseudo-noise sequence. As a consequence, the existing algorithms based on the pilots in the time domain do not work for the DVB-T2 signal. With the CP feature, the DVB-T2 standard offers a low fraction for some fading environments. When the CP fraction is shorter, the algorithm based on CP needs a longer sensing time. Additionally, the DVB-T2 standard has many CP choices. Therefore, the implementation of CP-based detection for the DVB-T2 signal is more complex than for the DVB-T signal.

Motivated by a demand of spectrum sensing for the DVB-T2 signal, this dissertation proposes a new sensing algorithm based on the first preamble symbol (denoted by P1). The new algorithm works well at the SNR of -10 dB in an AWGN channel as well as in multipath fading environments. Additionally, it does not depend on the configuration of the pilot pattern or CP length. Another advantage of the new algorithm is that the sensing time is significantly shorter than that of other algorithms.

4.3.2 Signal Model

The signal model of a CCS can be given as

$$\begin{cases} H_0 : y(n) = w(n), & n = 0, ..., N-1 \\ H_1 : y(n) = \tilde{s}(n) + w(n), & n = 0, ..., N-1 \end{cases} \tag{4.11}$$

where

$$\tilde{s}(n) = \sum_{l=0}^{L-1} h\left(l\right) s\left(n-l\right)$$

where $h\left(l\right)$ denotes the channel coefficient according to the path index of l. The signal follows the complex Gaussian $s(n) \sim \mathbb{C}N\left(0, \sigma_s^2/2\right)$. Assume that noise is independent and identically distributed (i.i.d.), circular symmetric complex Gaussian (CSCG) $w(n) \sim \mathbb{C}N\left(0, \sigma_w^2/2\right)$. Simplify the signal model by assuming that there is a single transmitting antenna and that SNR is defined by $SNR = \left(\sum_{l=0}^{L-1} \left\|h\left(l\right)\right\|^2 \sigma_s^2\right) / \sigma_w^2$.

4.3.3 Other Detection for Comparison

Energy-based Detection

The test statistic of the detector is constructed from the energy of the received signal as follows

$$T_{ED} = \sum_{n=0}^{N-1} \|\tilde{s}\,(n)\|^2. \tag{4.12}$$

Due to the above assumptions that the complex signal and the noise follow Gaussian distribution, the test statistic has Chi-squared distributions [28]. With a large number of samples, the statistic is asymptotically Gaussian-distributed due to CLT. The asymptotic forms are derived in [47]. ED is a popular method due to the low complexity of the test statistic, as in Eq. 4.12. It works well when the noise power is known perfectly. The detection performance of ED is significantly degraded by noise uncertainty [42]. Here, the ED is used as a benchmark for new algorithms.

CP-based Detection

OFDM-based signals, such as DVB-T/T2, have a CP part, which is copied from samples at the end of symbol, as a guard-interval. CP-based detection was investigated in many works [51–53, 90, 98, 99]. The test statistic in [53] is the maximum correlation between the CP and original parts as follows

$$T_{CP} = \max_{d} |R_{CP}(n)| \tag{4.13}$$

where the correlation is defined by

$$R_{CP}(n) = \frac{1}{SL} \sum_{u=0}^{S-1} \sum_{n=0}^{L-1} y\,(d+n+uM)\,y^*\,(d+n+N+uM).$$

The CP length of DVB-T2 is designed flexibly. With 8 MHz channels, DVB-T2 has 31 configurations, as Table 67 in [97], compared with eight configurations in DVB-T, as shown in Table 14 in [91]. Without the prior knowledge of CP length, the detector must execute the algorithm for each configuration. Furthermore, the new CP fraction of 1/128 will increase the

sensing time substantially. Therefore, CP-based detection for the DVB-T2 signal has a higher complexity in implementation. The performance of CP-based detection is used as a comparison for P1-based detection. Moreover, CP-based detection cooperates with P1-based detection in the CR system in Subsection 4.3.6.

4.3.4 Spectrum Sensing Based on the Preamble P1

In the DVB-T2 standard, the P1 format is described by Figure 51 in [97]. The P1 symbol lasts 0.224 ms with two guards. The guard intervals B and C are copied from the useful part A. Therefore, the parts B and C are correlated with the original parts from part A. A detection of DVB-T2 signals can be detected by utilizing this feature. In the following, the test statistic based on P1 is constructed.

The total correlation is formed as

$$\begin{aligned} &R(d) = R_{N_C}(d) + R_{N_B}(d + 2N_C), \\ &d \in \{1, 2, 3..., 2\left(N_C + N_B\right) - 1\} \end{aligned} \tag{4.14}$$

where d denotes the index of the starting sample; N_B and N_C are the length of the guard intervals B and C, as in [97], respectively; and R_{N_B} and R_{N_C} are correlations from the parts B and C with the formula as follows

$$R_{N_s}(d) = \sum_{n=d}^{d+N_s-1} y\left(n\right) y^*\left(n + N_s\right). \tag{4.15}$$

To obtain the total correlation, a sliding window with a length is 2048 samples is used and shifted one by one sample. Then, the test statistic has the following formula

$$T_{P1} = \mathrm{Re}\left\{R(d)\right\}. \tag{4.16}$$

A. Analysis of the Test Statistic

The CLT is applied to construct the test statistics of the parts C and B. For convenience, the test statistic is derived first with the part C. The autocorrelation of the part B has a similar formula. Under hypothesis H_0, the formula of test statistic P_1 is derived by replacing N_C with

$N_A = N_C + N_B$. Under hypothesis H_1, using the sum of two Gaussian random variables of the two parts, the asymptotic formula is derived for the test statistic of P_1.

1. Under Hypothesis H_0 The autocorrelation of part C is

$$R_{N_C}(d)\,|H_0 = \sum_{n=d}^{d+N_C-1} [w(n)w^*\,(n+N_c)]. \tag{4.17}$$

The mean is

$$m_{N_C,H_0} = E\left[\mathrm{Re}\left\{R_{N_C}(d)\,|H_0\right\}\right] = 0,$$

and the variance is

$$\sigma^2_{N_C,H_0} = E\left[\left(\mathrm{Re}\left\{R_{N_C}(d)\,|H_0\right\} - m_{N_C,H_0}\right)^2\right] = N_C\sigma_w^4/2.$$

Replacing N_C with N_A, the test statistic of P1 in H_0 is

$$\begin{cases} m_{H_0} = 0 \\ \sigma^2_{H_0} = (N_C + N_B)\,\sigma_w^4/2. \end{cases} \tag{4.18}$$

2. Under Hypothesis H_1

$$\begin{aligned} R_{N_C}(d)\,|H_1 = \sum_{n=d}^{d+N_C-1} & \{\tilde{s}(n)\tilde{s}^*\,(n+N_C) \\ & + w(n)w^*\,(n+N_C) + \tilde{s}(n)w^*(n+N_C) \\ & + \tilde{s}(n+N_C)^* w(n)\}\,. \end{aligned}$$

The mean is

$$m_{N_C,H_1} = N_C\|h\|^2\sigma_s^2 \tag{4.19}$$

where $\|h\|^2 = \sum_{l=0}^{L-1} \|h_l\|^2$.

The variance is

$$\sigma_{H_1}^2 = E\left[\left(\mathrm{Re}\left\{R_{N_C}(d)\,|H_1\right\} - m_{H1}\right)^2\right].$$

After removing some zero terms, the variance reduces to

$$\begin{aligned}
\sigma_{N_C,H_1}^2 = & E\left[\mathrm{Re}\left\{\sum_{n=d}^{d+N_C-1} \tilde{s}(n)\tilde{s}^*\left(n+N_C\right)\right\}^2\right] \\
& + E\left[\mathrm{Re}\left\{\sum_{n=d}^{d+N_C-1} w(n)w^*\left(n+N_C\right)\right\}^2\right] \\
& + E\left[\mathrm{Re}\left\{\sum_{n=d}^{d+N_C-1} \tilde{s}(n)w^*(n+N_C)\right\}^2\right] \\
& + E\left[\mathrm{Re}\left\{\sum_{n=d}^{d+N_C-1} \tilde{s}(n+N_C)^*w(n)\right\}^2\right] \\
& - \left(N_C\|h\|^2\sigma_s^2\right)^2 \\
& = N_C\sigma_w^4/2 \; + 2N_C\sigma_w^2\left(\|h\|^2\sigma_s^2\right)/2.
\end{aligned}$$

The variance is derived as

$$\sigma_{N_C,H_1}^2 = N_C\sigma_w^4/2 \; + N_C\sigma_w^2\left(\|h\|^2\sigma_s^2\right). \tag{4.20}$$

It is a reasonable assumption that the parts B and C are independent variables. Applying the sum of two Gaussian uncorrelated variables, the mean and the variance are given by

$$\begin{cases} m_{H_1} = N_A\|h\|^2\sigma_s^2 \\ \sigma_{H_1}^2 = N_A\sigma_w^4/2 \; + N_A\sigma_w^2\left(\|h\|^2\sigma_s^2\right). \end{cases} \tag{4.21}$$

The test statistic follows the Gaussian distribution as

$$\begin{cases} H_0 : T_{P1} \sim N\left(m_{H_0}, \sigma_{H_0}^2\right) \\ H_1 : T_{P1} \sim N\left(m_{H_1}, \sigma_{H_1}^2\right). \end{cases} \tag{4.22}$$

The detection performance can be given by

$$P_d = p\left(\frac{T_{P_1}(y)}{\sqrt{\sigma_{H_1}^2}} > \frac{\eta_{P_1}}{\sqrt{\sigma_{H_1}^2}} | H_1, \sigma_w^2, \sigma_s^2, \|h\|^2\right) \tag{4.23}$$

$$= Q\left(\frac{\eta_{P_1} - N_A\|h\|^2\sigma_s^2}{\sqrt{N_A\sigma_w^4/2 \ + N_A\sigma_w^2\left(\|h\|^2\sigma_s^2\right)}}\right) \tag{4.24}$$

where η_{P_1} denotes a threshold; Q is the complementary cumulative distribution.

As in [28], the probability of detection can be approximated by

$$Q(t) \approx \frac{1}{\sqrt{2\pi}t} \exp\left(-\frac{t^2}{2}\right). \tag{4.25}$$

3. In Multipath Fading Environments: Recalling the definition of SNR, the formula does not depend on the type of fading. Therefore, the P1 detector could apply to multipath fading. In the simulations, the detection performance is verified in an AWGN channel, the multipath fading channels of the wireless regional area networks (WRAN) with the profile B, and the COST207 channels.

4. With Timing and Frequency Offsets: Since P1-based detection uses the sliding window to compute the test statistic, the timing offset can be eliminated. Hence, the timing offset is considered ideal. The frequency offset can be estimated, as in the Table 1 of [90]. In this dissertation, the ideal frequency offset, which is equal to zero, is used.

B. False Alarm and Threshold Computation

Similar to the performance of detection, the formula of false alarm is

$$P_{fa} = p\left(\frac{T_{P_1}(Y)}{N_A\sigma_w^4/2} > \frac{\eta_{P_1}}{N_A\sigma_w^4/2}|H_0, \sigma_w^2\right) \tag{4.26}$$

$$= Q\left(\frac{\eta_{P_1}}{\sqrt{N_A\sigma_w^4/2}}\right). \tag{4.27}$$

The threshold is derived as

$$\eta_{P_1} = \sqrt{N_A\sigma_w^4/2}\, Q^{-1}(P_{fa}). \tag{4.28}$$

4.3.5 Simulation Results

In the simulations, the complete DVB-T2 signal is generated with the FFT size of 2k, the pilot pattern 1, one closing frame, and the antenna mode of SISO.

The simulations are carried out by the Monte Carlo method with 8000 trials. When computing the performance of detection, the P_{fa} is kept at the constant of 0.01. In the ROC, the P_{fa} is in the range of 0.01 to 0.1 with a step of 0.01. To further compare with the CP-based detection (4.13), the detection performance with the norm of (4.15), denoted by P1Norm, is also investigated in simulations. The proposed detection in (4.16) is called a P1-based detection (or, explicit, P1Real). The simulation results and analytical results are denoted by $(sim.)$ and $(ana.)$, respectively.

In Fig. 4.9, the P1 sensing significantly outperforms ED with the noise uncertainty (NU) of 1 dB. In the simulations, ED is investigated with the observation time of 5 ms, corresponding to 18 symbols and a CP fraction of 1/4. The results also reveal that, with the NU of 1 dB, the detector is disable when the SNR is below -6 dB. The performance of ED is not improved at the SNR values when increasing the sensing time. The P1 detector has a low sensitivity to noise uncertainty.

In Fig. 4.10, the performance of the P1-based detection is the same in different types of channels. The detection works well in multipath environments, and the performance of P1Real in simulation method fully agrees with the performance in the analytic method. The performance

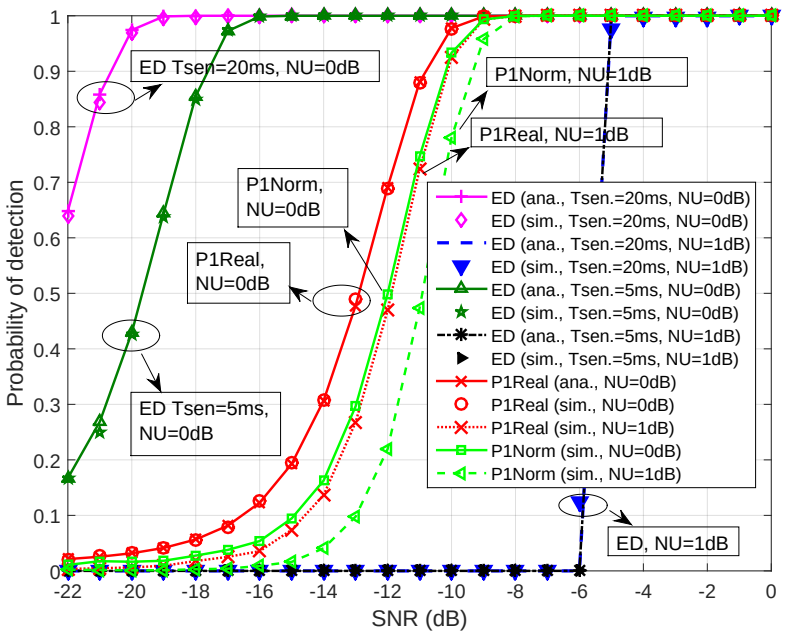

Fig. 4.9: P1-based detection and energy-based detection with a CFAR of 0.01 and in AWGN.

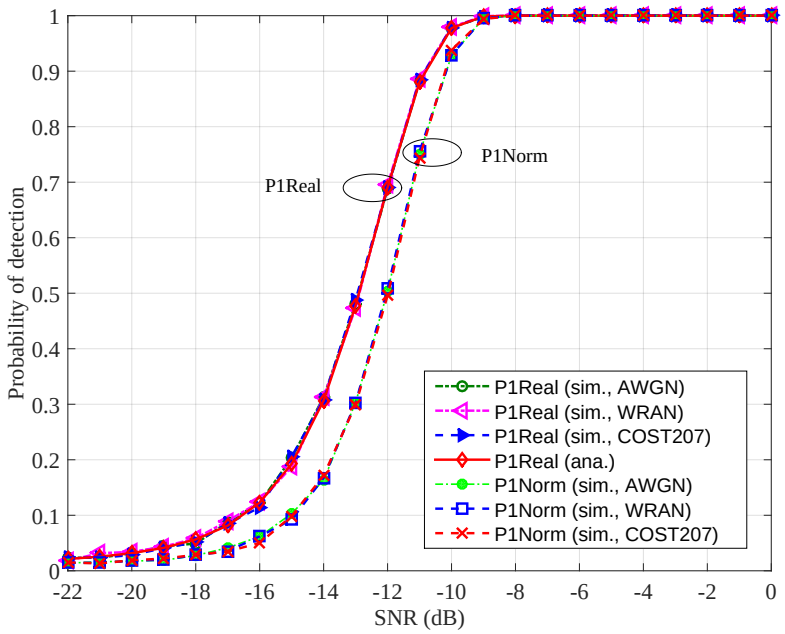

Fig. 4.10: P1Real detection and P1Norm detection with a CFAR of 0.01 and an NU of 0 dB.

of P1Real is about 0.5 dB higher than that of P1Norm.

In Fig. 4.11, the P1-based detection is compared with the CP-based detection. The length of

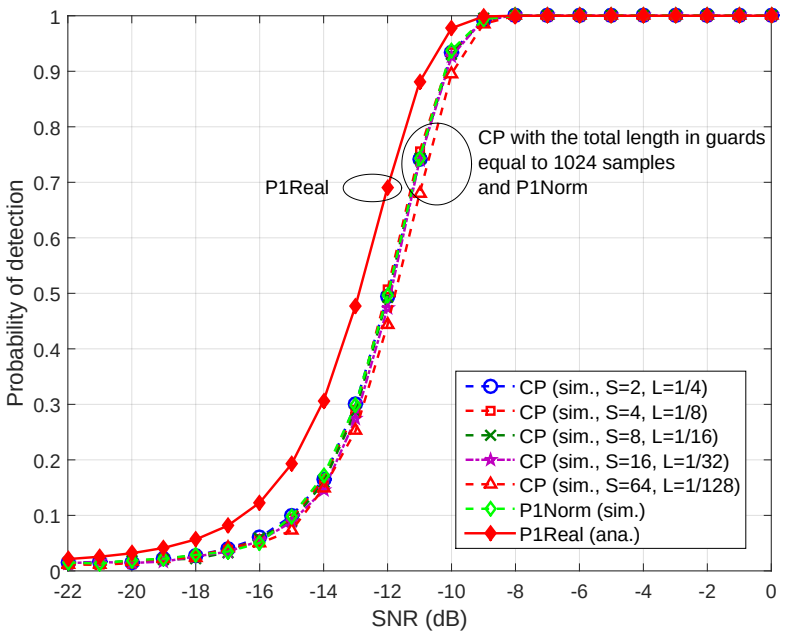

Fig. 4.11: P1-based detection and CP-based detection with the accumulation of samples in guard intervals equal to the length of 1k symbol in a COS207 environment with a CFAR of 0.01 and an NU of 0 dB.

the two guards in P1, a 1k symbol, is 1024 samples. In addition, the CP-based detection has the formula of magnitude as in (4.13). Therefore, for a good comparison, the P1Norm detection is compared with the CP-based detection, having the accumulation of samples in guard intervals equal to 1024 samples. As in Fig. 4.11, the performance of the P1Norm detection is roughly as high as that of the CP-based detection with the sensing time of $\{14.448, 3.696, 1.904, 1.008, 0.56\}$ ms and the CP choices of $\{1/128, 1/32, 1/16, 1/8, 1/4\}$, respectively. When taking the real part of the autocorrelation as the test statistic (4.16), the performance of detection is improved by 0.5 dB. In the DVB-T2 standard, the CP length is designed flexibly and is reduced intentionally for more useful data. Since the P1-based detection does not depend on the choices of CP, the detection is obviously more beneficial than the CP-based detection with a short CP length.

In Fig. 4.12, the ROC of the P1-based detection is shown with an SNR of -10 dB. Considering the recommendation of miss-detection from regulators and the false alarm for the efficiency of practical CR systems, the simulations focus on the ROC with the false alarm in the range of 0.01 to 0.1. At an SNR of -10 dB, the performance of the P1Real detection is $92, 84\%$ and $99, 67\%$ false alarms of 1% and 10%, respectively.

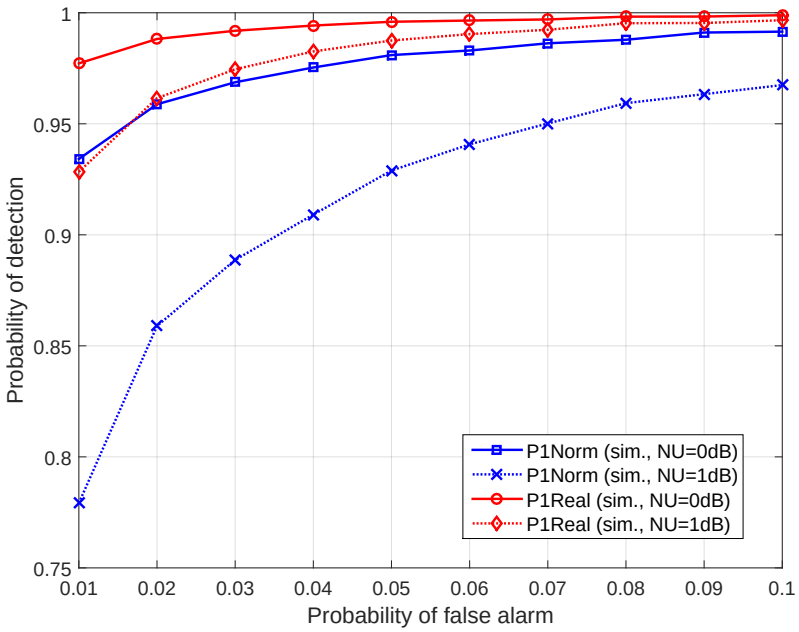

Fig. 4.12: ROC of the P1-based detection with an SNR of -10 dB and NUs of 0 and 1 dB.

4.3.6 Proposed Scheme for a CCS

This section proposes the sensing scheme of the P1-based detection, as shown in Fig. 4.13, for an in-band sensing mode in practical CR systems operating with a DVB-T2 signal. In the mode, CR systems must instantly stop the secondary transmission currently occupying the frequency range of the primary signal when the primary signal returns. Therefore, sensing time is a critical task. With a fast sensing of 0.224 ms, the P1-based detection satisfies the issue excellently. A CCS can deploy the scheme for an in-band sensing on the uplink. In the CCS, the scheme is one function of the spectrum sensing module. This function is invoked in a in-band sensing mode to detect the DVB-T2 signal in real-time. Therefore, the CCS stops secondary transmissions just after the primary signal is transmitted. In out-band sensing, when there is no secondary transmission, the sensing module can invoke another detection (e.g., a CP-based detection) with a long enough sensing time before switching to in-band sensing.

The FCC [100] recommends that the performance of detection at the SNR of -21 dB should be higher than 90% and that the false alarm should be less than 10%. From the simulation results, we can set the SNR regime of the P1 detector from -10 dB. Therefore, the effective SNR regime is higher than -21 dB (as recommended). However, in practical CR systems, this issue is satisfied

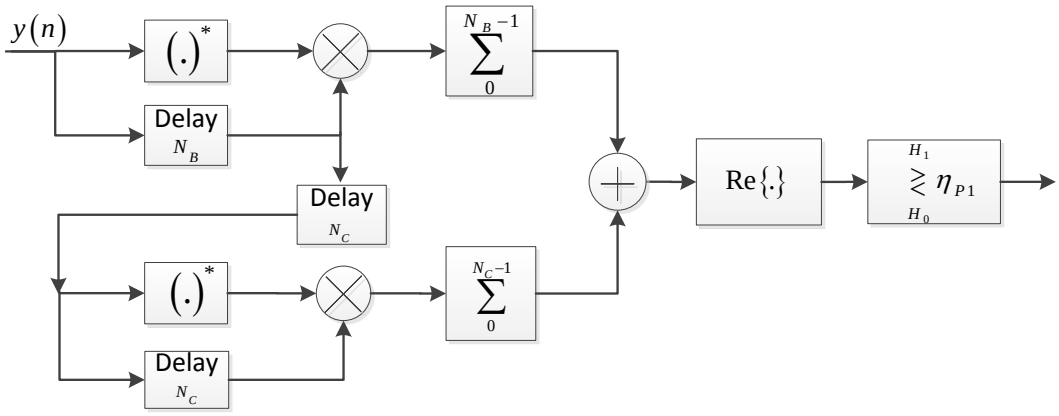

Fig. 4.13: The proposed sensing scheme based on P1.

by the support of a REM [39], which has the prior knowledge of average power transmitted in DVB-T2 channels. Based on the prior information, the P1 sensing is applied to channels with an SNR of -10 dB. The SNR in DVB channels is commonly higher than the above value.

The P1 detector loses the detection in the whole remaining part of the DVB-T2 frame if it is turned on after P1 is transmitted. However, in the in-band sensing mode, the P1 detector is activated and caries out the sensing in real-time. Therefore, the issue of the missing P1 in the sensed part is solved and the detector does work properly. The detector uses a sliding window to calculate the test statistic, which requires real-time computation. However, it could be simply implemented by a hardware, as in [101].

4.3.7 Concluding Remarks

In this section, the sensing algorithm for the DVB-T2 signal based on the P1 symbol is proposed. The P1-based detection is effective for all configurations of the DVB-T2 signal. The sensing time of the P1-based detection is very short at 0.224 ms. The P1 detector works well at an SNR of -10 dB. The detector has a low sensitivity to noise uncertainty and the effect of timing offset, and can be applied in multipath environments. Furthermore, the asymptotic formula of the performance, the false alarm, and the threshold for the P1-based detection are derived. The simulation results match with the analytical results. P1-based detection is feasible with CR-based systems. The sensing scheme based on P1 is proposed, and can be applied to the in-band sensing mode of CR-based LTE-Advanced systems.

4.4 Summary

The periodical peaks of autocorrelation for pilot-added OFDM signals are exploited. DVB-T signals are taken as an example for the exploitation. The results from this exploitation lead to an approach to enhance spectrum sensing tasks including detection and classification. Two enhanced sensing algorithms for DVB-T signals are proposed: PPA-NP and PPA-MRC. The new algorithms outperform the existing algorithms. The algorithms can work with short CP lengths at which CP-based detection is disable. This point gives clues to sensing algorithms for FBMC, a potential multiplexing technique without CP in the future. For OFDM signals with preambles as DVB-T2, a new sensing algorithm based on the first preamble symbol is proposed. Analytical forms of the detection are derived. The new algorithm works well with a very short sensing time and with all configurations of DVB-T2. Moreover, a sensing scheme based on this algorithm is introduced for practical CR-based systems. All of the new algorithms can be applied for spectrum sensing tasks in unlicensed spectrums, such as TV bands, which are a most promising spectrum to find white-spaces.

5 SPECTRUM SENSING IN SC-FDMA-BASED CCSS

5.1 Introduction

Spectrum sensing needs to be reliable at low SNRs. Regulators such as the FCC and ECC encourage the research on spectrum sensing. Nevertheless, they recommend requirements for spectrum sensing such as a high detection performance Pd with a CFAR at given SNRs. For example, the FCC requires that Pd is higher than 90% with a CFAR lower than 10% at a low signal-level (e.g., -116 dBm for digital TV, normally corresponding to the SNR at -21 dB) [100].

Spectral correlation is considered as a good approach [18] for spectrum sensing to realize the aforementioned goal. Gardner is a pioneer in the research on spectral correlation, and the theory of spectral correlation was well investigated in his work [24, 26, 27]. As pointed out by Gardner, many manmade signals contain components which vary periodically due to the underlying mechanism of signal manipulations. Some *hidden periodicity* [26] can be exploited by techniques of spectral analysis—for example, *a quadratic time-invariant* (QTI) transformation for signals. They are second-order periodicity. This periodicity with (cyclic) frequency is equivalent to the spectral lines of output from the QTI transformation that appear in a specific period. Therefore, it is called spectral correlation. This spectral correlation of noise is significantly different from that of desired manmade signals. For noise, the spectral correlation approaches zeros. Meanwhile, the spectral correlation is non-zero for desired signals, even at low SNRs. Therefore, the spectral correlation is applicable in modulation classification and signal detection. In CR, this approach helps to detect the desired signal in a low SNR regime as the one specified by relevant regulators.

For desired signals, their spectral correlation is related to the parameters of the signals: the baud rate and the carrier frequency. Sutton extensively analyzed (in [57]) the effect of the parameters on spectral correlation in a plane of cyclic frequency α and spectral frequency f. A

sum of correlation could be computed with the whole αf plane for a test statistic of detection. This method is called the conventional algorithm. However, the high burden of computation for sensing nodes is due to the high number of correlation peaks in the plane. To reduce the complexity, Fehske proposed an algorithm in [102] which selects the maximum correlation peaks along the α axis and puts them into a α profile. Basically, this algorithm computes the correlation for half of the peaks in a plane. Therefore, its complexity is significantly decreased compared to the conventional algorithm. For a further enhancement, Wu and Eric et al. [103, 104] proposed an algorithm based on the αf profile, which consists of the maximum peaks in both axes of the αf plane. They proved that the αf-profile-based algorithm has significantly low-complexity and outperforms those of the α-profile-based and conventional algorithms.

This chapter considers not only the confident regions of spectral correlation peaks in the αf plane but also the amplitude of the peaks. This chapter introduces a new algorithm which uses the peaking amplitudes of the αf profile as weighting coefficients. The new algorithm outperforms the αf profile algorithm. An additional complexity in the new algorithm compared to the αf profile algorithm is the multiplication between the amplitude of peaks and weighting coefficients.

5.2 Background of Cyclic Spectral Correlation

The second-order periodicity of a signal is examined by the cyclic autocorrelation function (CAF), which is a kind of QTI transformation. For an envelop signal $y\left(t\right)$, the CAF is defined, as in [26]

$$R_{y}\left(\tau,\alpha\right)=\lim_{\Delta t\rightarrow\infty}\int_{-\Delta t/2}^{\Delta t/2}y\left(t+\tau/2\ \right)y^{*}\left(t-\tau/2\ \right)e^{-j2\pi\alpha t}dt \tag{5.1}$$

where τ and α denote time lag and cyclic frequency, respectively. The CAF exhibits the second-order periodicity in the time domain with the cyclic frequency α. In the above form, the CAF is considered to be a generalization of conventional autocorrelation and reduces at conventional autocorrelation at $\alpha=0$. Meanwhile, the CAF presents the correlation between two components $y\left(t+\tau/2\ \right)e^{-j\pi\alpha t}$ and $y\left(t-\tau/2\ \right)e^{j\pi\alpha t}$. This is also called spectral correlation.

In the frequency domain, the CAF is transformed by the Fourier operation into the spectral correlation function (SCF) as

$$S_y^{\alpha}(f) = \int_{-\infty}^{\infty} R_y(\tau, \alpha) e^{-j2\pi ft} dt. \tag{5.2}$$

To estimate the spectral correlation, a spectrally smoothed cyclic periodogram is defined in [26] as

$$S_{y_{\Delta t}}^{\alpha}(t, f) = \frac{1}{\Delta t} Y_{\Delta t}\left(t, f + \frac{\alpha}{2}\right) Y_{\Delta t}^{*}\left(t, f - \frac{\alpha}{2}\right) \tag{5.3}$$

where

$$Y_{\Delta t}(t, f) = \int_{t-\Delta t/2}^{t+\Delta t/2} y(v)\, e^{-j2\pi fv} dv.$$

This equation shows that the SCF is equivalent to the correlation between a spectral line and its shifted version of a frequency α. Thus, a SCF is approximated by the periodogram as

$$\widehat{S}_y^{\alpha}(f) = \lim_{\Delta f \to 0} \lim_{\Delta t \to \infty} \frac{1}{\Delta f} \int_{f-\Delta f/2}^{f+\Delta f/2} S_{y_{\Delta t}}^{\alpha}(t, u)\, du. \tag{5.4}$$

Parameters Δt and Δf are temporal resolution and spectral resolution [57], respectively. These two parameters are so chosen that their product is much greater than unity: $\Delta f \Delta t \gg 1$. Temporal resolution Δt is normally determined by the baud rate of signal. However, it can be a multiple integer of the symbol duration. Meanwhile, spectral resolution Δf is calculated for a reliable $\widehat{S}_y^{\alpha}(f)$ as analyzed in [105], by which the spectral correlation peaks of confident regions can be observed in the αf plane.

5.3 Proposed Algorithm

5.3.1 Profile of Spectral Correlation

For cellular networks—for example, the uplinks—data modulation can be binary phase-shift keying (BPSK) or higher quadrature amplitude modulation (QAM) due to the density of users. The αf profile varies with modulation types. The profile of SCF for BPSK and 16QAM are shown in Fig. 5.1 and Fig. 5.2, respectively. For BPSK, SCF is symmetric with respect to α and f axes because the BPSK symbol is symmetric data: $\{+1, -1\}$. When $\alpha = \{0, 0.5\}$, SCF is high due to the carrier frequency. Other peaks appear due to the pulse-shape filter of transmitter: $\alpha = \{0.125, 0.375, 0.75\}$. The SCF is nonsymmetric for high-order modulation such as 16QAM. There are only high peaks at $\alpha = 0$, equivalent to conventional power spectral density, and low peaks at $\alpha = 0.125$.

In realistic scenarios, the α and f profiles are computed when the parameters of the underlying signals at the transmitter are known. The baud rate and carrier frequency can be looked up from a REM, as described in [2, 82].

5.3.2 Test Statistic

The αf profile is selected, as in [103]. The profile contains the position cyclic frequency, spectral frequency, and amplitudes of the peaks. To utilize the advantages of MRC, the amplitudes of some selected peaks are taken as weighting coefficients. This combination can give further performance gain compared to existing algorithms in which all coefficients are equal to 1. The test statistic of the new algorithm is as follows

$$T_{proposed} = \left\| \sum_{a,k} c_{a,k} \widehat{S}_y^{\alpha} (f) \right\| / \left(\sum_t \| y(t) \| \times \sum_{a,k} c_{a,k} \right) \tag{5.5}$$

where $c_{a,k}$ are coefficients of the spectral peaks of selected confident regions at cyclic and spectral frequencies with the indices a and k, respectively.

In the denominator, the component $\sum \| y(t) \|$ normalizes the signal power. Hence, the computation for predefined thresholds does not depend on noise estimation. It results that the proposed algorithm is completely intensive to the noise-uncertainty phenomenon [42]. The

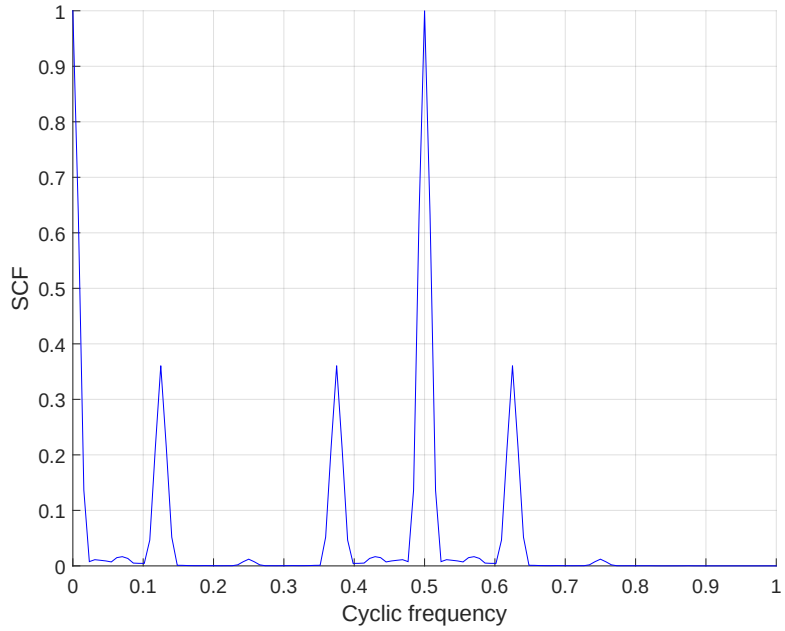

(a) α profile

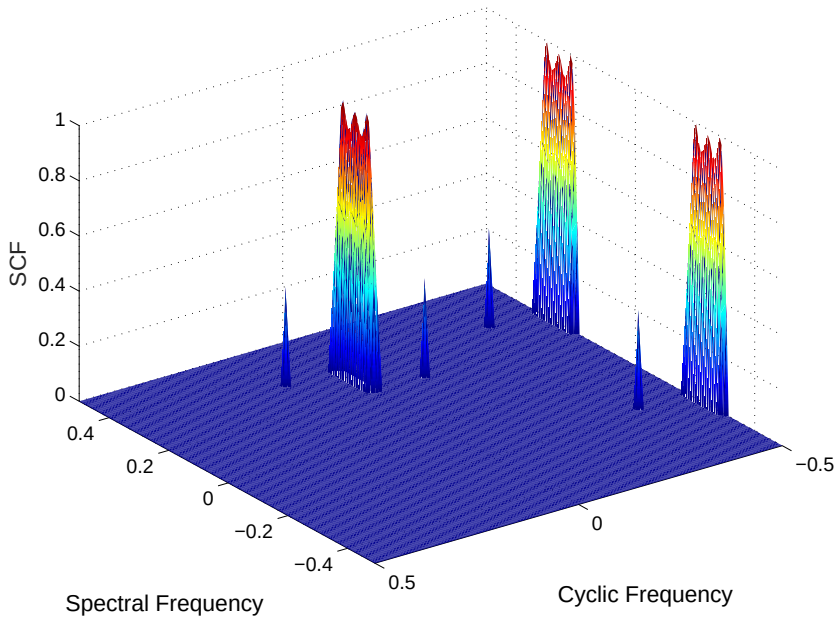

(b) αf profile with coefficients

Fig. 5.1: SCF of BPSK.

numerator is a sum of the complex-amplitudes of selected peaks. For convenient comparison, subscripts αf and $\alpha f co$ denote the algorithms based on the αf profile without/with the weighted

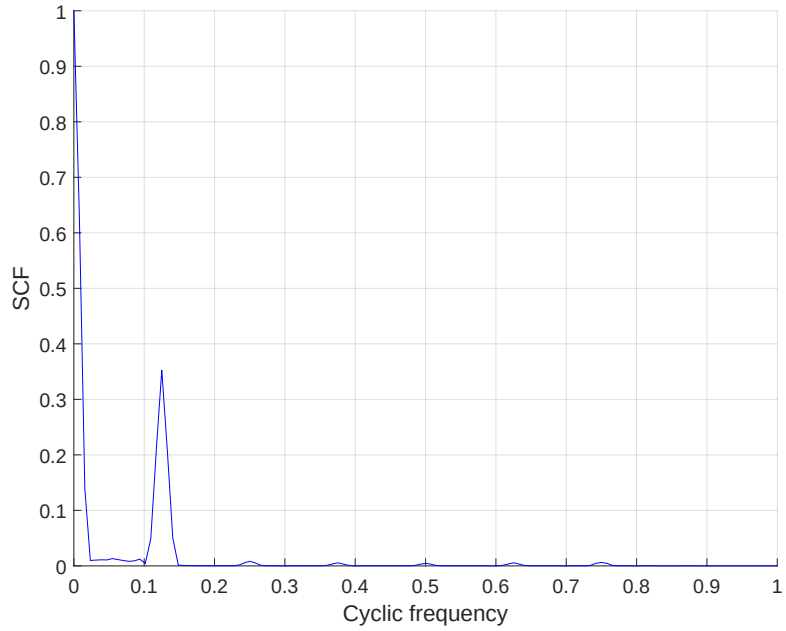

(a) α profile

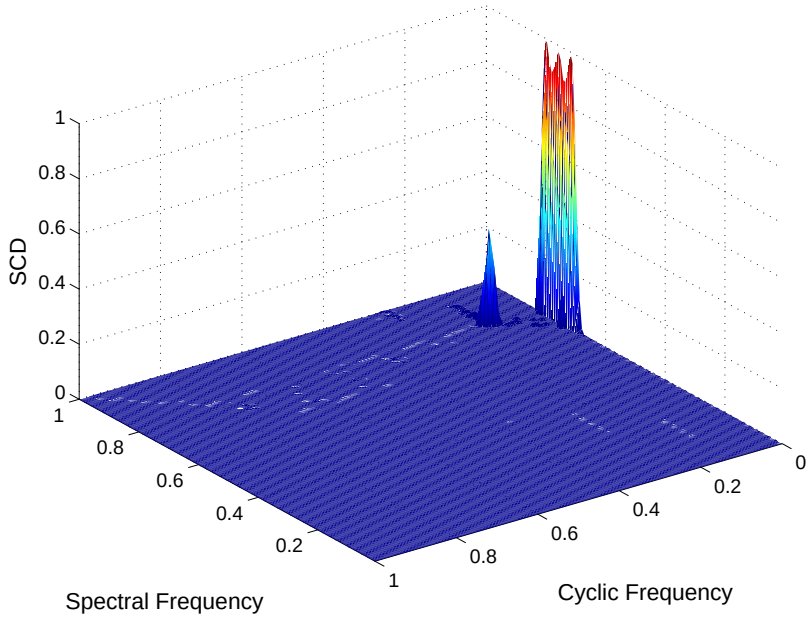

(b) αf profile with coefficients

Fig. 5.2: SCF of high order modulation: 16QAM.

coefficients, respectively. In previous work as in [102–104], there is no explicit formula of test statistic. Hence, algorithms are evaluated here with explicit formulas. The subscripts abs and

$complex$ are used to indicate the two different statistic forms with the numerators as $\sum \|(.)\|$ and $\|\sum (.)\|$, respectively. The proposed algorithm is equivalent to $\alpha f co_{complex}$.

As shown in Eq. 5.5, the additional complexity of the proposed algorithm is the multiplication operation for the coefficients and SCF peaks compared to the αf algorithms. Therefore, the additional complexity can be neglected.

5.3.3 Flowchart of the Proposed Algorithm

The flowchart of the new algorithm is described as follows.

- **Step 1 – Measure the average of SCF:**
  The average of SCF can be statistically measured by collaborative sensing nodes or computed by a neutral network with the knowledge of baud-rate and carrier frequency stored in a REM. The sensing node acquires the αf profile from the SCF before it computes a test statistic. In this step, thresholds are also computed as the expected values of the CFAR.

- **Step 2 – Compute the SCF of the received signal:**
  The received signal is transformed into the frequency domain by FFT. Spectral lines are selected to compute spectral correlation peaks as a part of the SCF corresponding to the spectral and cyclic frequency in the predefined αf profile.

- **Step 3 – Combine for the test statistic:**
  The selected peaks are scaled to the weighting coefficients as defined by the averaged SCF. Next, the test statistic is combined, as given in Eq. 5.5, and is compared with a predefined threshold to decide whether or not the desired signal appears.

5.4 Simulation Results

The proposed algorithm is simulated with the two modulation types: BPSK and 16QAM. The main simulation parameters are listed in Table 5.1. CFAR is sensitive to the predefined thresholds. Therefore, the number of simulation trials for threshold computation is highly sufficient to compute the thresholds. The accuracy of threshold computation leads to the exact comparison

for the algorithms. In simulations, the performance of algorithms are verified, including our proposed algorithm in Eq. 5.5, $\alpha f co_{abs}$, αf_{abs}, and $\alpha f_{complex}$.

Table 5.1: Simulation parameters of cyclostationarity-based spectrum sensing algorithms

Parameter	Values
Modulation	BPSK, 16QAM
FFT size	128
Sampling frequency	1.92 MHz
Over-sampling ratio	8
Channel model	AWGN
Threshold	1%
Simulation trials	CFAR: 6000, Pd: 1200

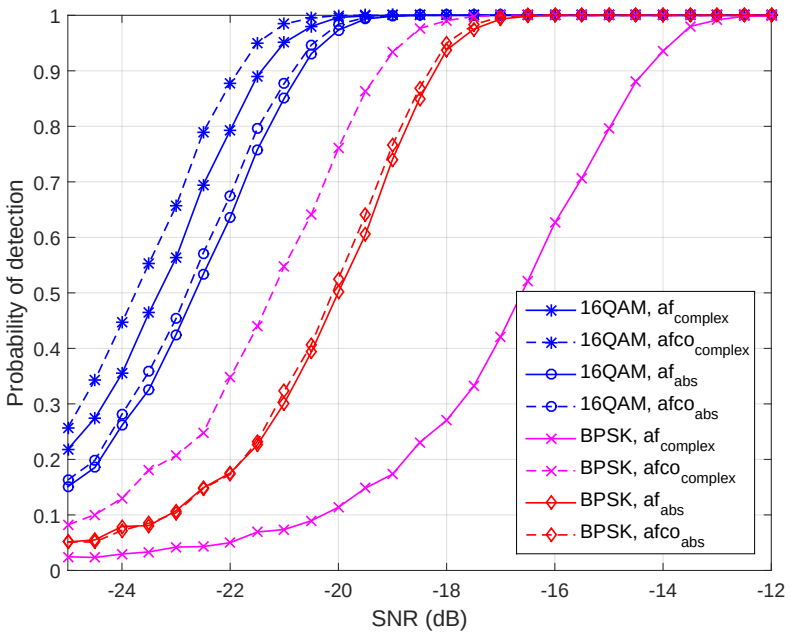

Fig. 5.3: The probability of detection with a CFAR of 1% and an observation time of 5 ms.

The proposed algorithm outperforms αf algorithms for different modulations, as shown in Fig. 5.3. Nevertheless, there is a low performance gain between $\alpha f co_{abs}$ and αf_{abs}. The reason is that the summation of scaled peaks with the complex SCF (in the case of the proposed algorithm) eliminates noise components more effective than that of the absolute SCF (in the case of $\alpha f co_{abs}$ algorithm). For BPSK modulation, the performance gain of the proposed algorithm is 1 dB and 5 dB when compared to αf_{abs} and $\alpha f_{complex}$, respectively. With a summation of the real-part, af

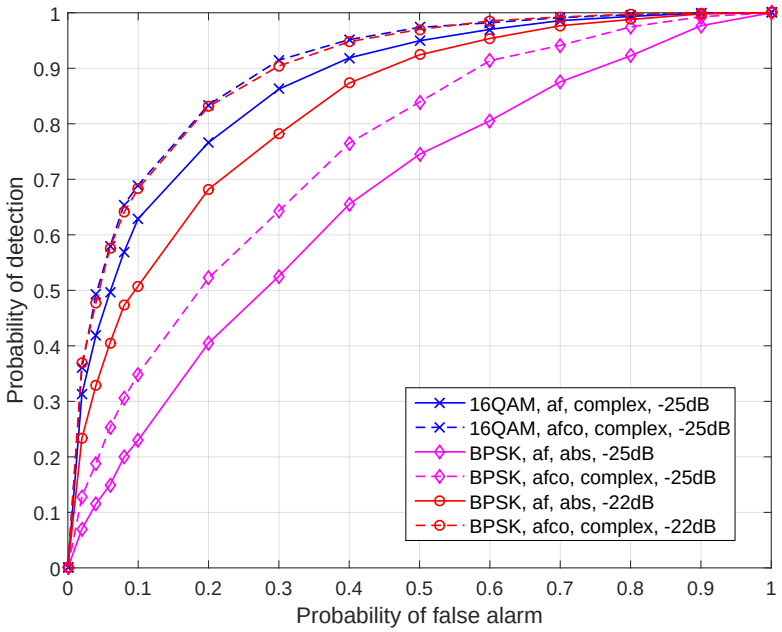

Fig. 5.4: The curves of ROC with an observation duration of 5 ms.

algorithms have a higher performance of 4 dB than that of a summation of the complex-part. The performance gain of αf_{abs} compared to $\alpha f_{complex}$ can be explained by the reflective symmetry of the SCF as shown in Fig. 5.1b. This symmetry appears only if the SCF is computed with the real-part of the envelop signal. For 16QAM, meanwhile, the SCF with the real-part is no difference to the complex form. The performance of the proposed algorithm is about 1 dB and 0.5 dB higher than that of αf_{abs} and $\alpha f_{complex}$, respectively.

The curves in Fig. 5.4 present comparisons among the algorithms at very low SNRs. The new algorithm has better performance than existing algorithms, αf. For example, with the false alarm of 10% and BPSK, the performance gain is 12% and 19% at the SNR of -25 dB and -22 dB, respectively. With 16QAM, the performance gain is 6% at the SNR of -25 dB.

From the simulation results, some remarks can be concluded: (1) the αfco algorithm outperforms the αf algorithm. The performance gain depends on the αf profile. (2) For BPSK, spectrum sensing should use the absolute SCF for αf algorithms; for higher-order data modulation (e.g., QAM), spectrum sensing should use complex SCF for both the αf and αfco algorithms.

5.5 Promising Application for SC-FDMA Signals

Spectrum sensing based on cyclostationary signatures can be applied for a detector in spectrum sensing schemes, as in [106–109], to detect SC-FDMA signals. The SC-FDMA is adopted for multiple access in the uplink of LTE-Advanced systems [110]. By schemes which utilize cyclostationarity-based spectrum sensing, the SC-FDMA signals are detected in each resource block in two resource-mapping modes: localized and interleaved. For example, the schemes in [106] and [107, 108] are to detect the SC-FDMA signals in localized and interleaved uplink mode, respectively. There are six resource blocks with respect to the frequency domain. Each resource block contains 12 subcarriers. Resource blocks are assigned for UEs. The schemes use the cyclostationarity signatures from the subcarriers to detect the presence of SC-FDMA signals. Particularly, the detector of the sensing scheme in [106] (given by E.q (5)) is equivalent to the αf-profile-based algorithm since the coefficients of a block window, which is used to compute the cyclostationarity signagures, are equal to 1. Hence, the new cyclostation-based spectrum sensing can be deployed for the detector to obtain performance gain such as the simulation results in Section 5.4. Therefore, the scheme can apply the new cyclostationarity-based spectrum sensing for a detection of SC-FDMA signals in resource blocks, which are assigned for the uplink of cellular systems.

Moreover, D2D communications, in which devices communicate with each other directly without a base station, will be a prominent capability of mobile devices, as mentioned in [111–114]. These D2D communications use resource blocks of the cellular systems, which are used for the uplink and downlink [112–114]. The devices are normally handy equipment which are limited by hardware capabilities and a power supply. The SC-FDMA is considered a suitable multiplexing technique for the communications since this technique has low peak-to-average power ratios which need lower computational complexity hardware, and consumes less power than the OFDM technique. Therefore, the mobile devices should use the SC-FDMA technique for D2D communications. This shows that schemes which deploy the cyclostationarity-based spectrum sensing signatures can be also applied to a detection of the signals in D2D communications.

From the above points, the new spectrum sensing algorithm can be potentially applied to the detection of the signals in the uplink and in D2D communications.

5.6 Summary

This chapter presented a new enhanced spectrum sensing, which is based on the MRC of spectral correlation. The new and existing algorithms were evaluated using modulation schemes. The simulation results shows that the new algorithm outperforms the existing algorithms with a marginal increase in the computational complexity. The forms of test statistics were investigated with the modulation scheme. Based on the performance detection of each form, implementation guidelines for cyclostationarity-based detection were given. The algorithm can be deployed in a spectrum sensing scheme for the detection of SC-FDMA signals in the uplink of cellular systems and D2D communications.

6 SPECTRUM SENSING IN MULTIBAND CCSS

6.1 Introduction

The demand of high data rates in mobile communication is growing fast. SDOs and some industry preventatives attempt to propose new technologies for the improvement of data rates. To meet the defined requirements of the 4G networks from the ITU, in 2011, the 3GPP published the Release 10 for LTE-Advanced, which is the most prominent candidate for the network. LTE-Advanced networks can provide a data rate of up to 1 Gpbs for the downlink and 500 Mbps for the uplink. Currently, 4G LTE frequency bands 1 to 25 and 33 to 43 are already defined and planned by regulators. These bands are allocated at the frequency of 800 MHz to 3.4 GHz. Thus, the frequency bands are more crowded. Additionally, while LTE-Advanced networks are developed and launched as trials in some countries, the concepts of 5G networks are raised with further requirements. It results that the spectrum scarcity for mobile communications is demanded intensively. Nevertheless, the spectral efficiency in some other frequency bands is under-utilized. For example, from 30 MHz to 30 GHz, spectrum occupancy is only about 13.6% in cities such as Dublin, Chicago, and New York [79]. Therefore, mobile networks (e.g., LTE-Advanced newtworks) could utilize unoccupied spectrum spaces for opportunistic transmissions. The total spectral efficiency would be improved.

Motivated by the secondary transmission, a testbed has been developed as the description in [2, 82] for LTE-Advanced networks with the cognitive function by which TV white-spaces are detected and used for LTE-Advanced transmissions. Some challenging tasks need to be handled in realistic scenarios, including the procedure of initial-cell-search for the secondary user-equipment (UE) and the co-ordination among the secondary networks. In literature reviews, the detection of the LTE signals, which is based on the primary synchronization signal (PSS), was proposed by Yang Wen in [54] and investigated in [21]. These works consider the detection

in a single channel with the implicit assumption that the LTE signals are perfectly extracted from a certain frequency band. The spectrum sensing approach for multiple channels with filter bank spectral estimators (FBSEs) was proposed by Farhang-Boroujeny in [115]. However, in the work, the detection algorithm for subband signals is an energy-based method. For the detection of the digital video broadcasting-terrestrial signal, a low-complexity filter bank realization was introduced, as in [116].

In this chapter, a spectrum sensing scheme will be proposed with some enhancements compared to previous works. Firstly, the proposed scheme can handle a sensing task simultaneously for subband LTE signals transmitted in multiple primary channels. The subband signals are extracted by a polyphase implementation of the filter-bank with a flexible design of the prototype filter. Additionally, the sensing task is not only to detect the LTE signals but also classify them. To verify the scheme, secondary LTE transmissions in TV channels are modeled. Spectrum sensing for single channels, where subband signals are extracted perfectly, is considered as a benchmark for a comparison against that of the proposed scheme. The simulation results show that the LTE subband signals in multiple channels are detected and classified well from the multiband signals. The detection and classification performance of multiple channels by the proposed scheme are close to those of single channels with the same observation time. Based to the scheme, secondary UEs can quickly perform the procedure of initial-cell-search normally as in the primary transmission; secondary LTE networks can negotiate with each other to utilize TVWSs.

6.2 Identified Information

In CR, detectors work under different conditions to normal transmission. For example, the detectors have to detect the desired signal in a low SNR regime with a short observation. Due to these conditions, the information which could be identified by spectrum sensing is also limited. Nevertheless, using the cell-identities, it could to look up other additional information about the signal. For example, with help from a REM, as shown in [39], other necessary information about the signal is tracked with the cell-identity.

To attach with LTE networks, UEs acquire the physical-layer cell identity (or called cell identity, denoted by Cell-ID) by the initial-cell-search procedure [110], as well as other system

information such as bandwidth, antenna configuration and CP length. A Cell-ID comprises of two parameters: the physical-layer cell-identify group (or Sector-Group, denoted by NID1) and the physical-layer identity (or Sector-ID, denoted by NID2) which are extracted from the PSS and secondary synchronization signal (SSS), respectively. The Sector-ID has three choices, $NID2 = \{0, 1, 2\}$, to generate the sequence of PSS from two Zadoff-Chu sequences [110] in the frequency domain. The Sector-Group determines the sequence of SSS and two scrambling sequences. This parameter has a value range $NID1 = \{0, 1, ..167\}$. Thus, the Cell-ID has 504 different identifies with the equation given as: $Cell\_ID = 3 * NID1 + NID2$.

In LTE signals, the PSS occurs in every five subframes equivalent to the duration of 5 ms. For frame structure type 1, which is applicable to the frequency division duplex (FDD) mode, the PSS is mapped to the last OFDM symbol in slots $0th$ and $10th$. For frame structure type 2, the PSS is allocated in the third OFDM symbol of the subframes $1st$ and $6th$. Both the PSS and SSS occupy six resource blocks, 1.08 MHz, at the center of the frequency range. Due to more simplification than time division duplex (TDD) mode, the FDD mode would be more interesting for secondary LTE networks in the context of CR. In licensed bands of LTE networks, the information is known based on the bands. However, in unlicensed bands for secondary transmission, the information of the frame structure type is not mentioned or known in advance. However, it is reasonable to assume that the FDD mode is applied in secondary transmission. For the detection function, a convolution between the received signal and the pre-generated sequences of the PSS is computed. This is to determine the presence of LTE signals. Besides, this function predicts the sector identity. When performing the classification function, the symbol of SSS in the received signal will be located to classify the sector group. Mapping $NID1$ to m_0 and m_1, as shown in Table 6.11.2.1-1 in [110], determines the three sequences to construct SSS. This signal is allocated in the slots $0th$ and $10th$ for the FDD mode. Then, the location of the maximum peaks of the convolution are used to determine the position of the frame boundary, in which the PSS is first allocated in the slot $0th$ or $10th$.

6.3 Multiband Spectrum Sensing Scheme

The multiband spectrum sensing scheme is proposed here to detect and classify LTE signals in two main stages. The first stage adequately extracts subband signals in multiple channels by

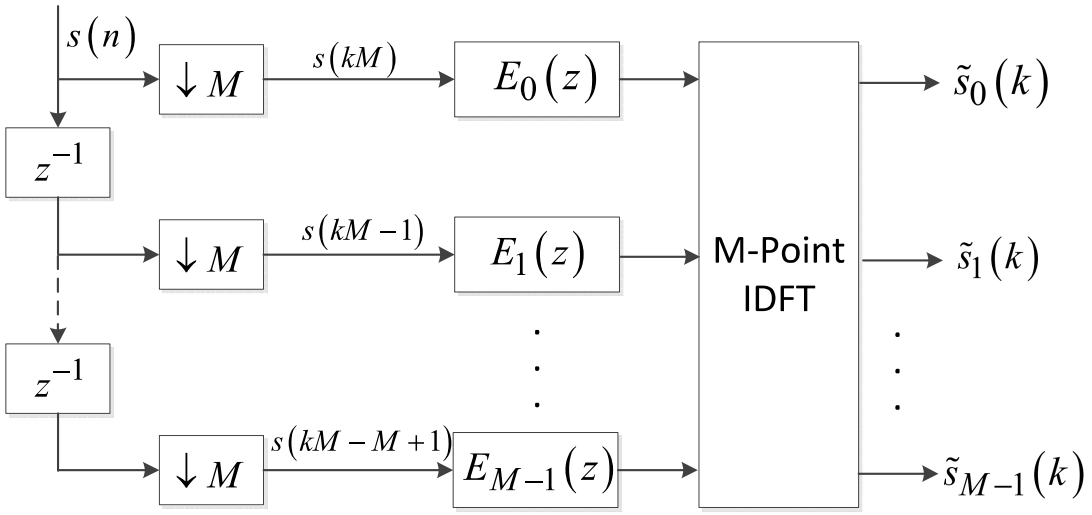

Fig. 6.1: Polyphase implementation of a filter bank.

employing a filter-bank realization. Then, the next stage performs a detection of the LTE signal and a classification of the detected subband signals by the Cell-ID of the LTE networks.

6.3.1 1st Stage: An Implementation of Filter Bank

Fig. 6.1 presents the filter-bank realization with a low-complexity polyphase, as in [116], for the first stage of the proposed scheme. At this stage, the multiband signals are analyzed into subband signals. In each channel of the multiband spectrum, the subband signals are extracted as

$$\tilde{s}_m(k) = \sum_{l=0}^{M-1} [s(kM-l) * h(kM+l)] W_M^{ml} \tag{6.1}$$

where k and m denote the indices of received samples of subband signal and the channel, respectively, M is the number of channels, h is the impulse response of the prototype filter in the filter-bank, and the W_M^{ml} are blocks of the inverse discrete Fourier transform. The decimation by a factor of M is applied to reduce the computational complexity of the polyphase implementation of the filter-bank. This implementation does not raise any spectrum aliasing for the signal allocated in each subband channel [116].

The prototype filter is a kind of low-pass filter (LPF), which can be designed as a finite impulse response (FIR) type 1. To reduce the number of multiplications at the first stage, this LPF is designed with the pass-band of 1.08 MHz instead of the whole effective bandwidth of

LTE signals. With 5 MHz LTE signals, this pass-band replaces that of 4.5 MHz. Therefore, the transition-band can be expanded from 0.5 MHz to 3.92 MHz. The filter length will be shortened by about eight times. For windowing methods, a Blackman window can be selected to obtain a small ripple in the pass-band. An example design for the prototype filter with 5 MHz LTE signals is: $\omega_p = 0.216\pi$, $\omega_s = 0.9\pi$, and $\omega_c = 0.558\pi$, where ω_p, ω_s, and ω_c are the pass bandwidth, the transition bandwidth, and the normalized cutoff frequency, respectively, and Blackman window with the filter length of 18. The transition bandwidth can also be increased when the total bandwidth carrying LTE signals is larger. The 5 MHz LTE signals are transmitted by secondary LTE networks in 8 MHz TV channels.

At the second stage, the tasks of detection and classification are executed for all channels in the multiband spectrum in parallel. These tasks are presented as follows.

6.3.2 2nd Stage: PSS-Based Detection

Recall that the general framework formulation in Eq. 2.2, the physical-layer identity $NID2$ is an unknown parameter. This unknown parameter is estimated by maximizing the probability of the case in which a PSS can exist. Basically, cross-correlation between a predefined PSS with the received signal is utilized to measure the probability. The test statistic of the detection is equivalent to the case of the estimated value of $NID2$.

The cross-correlation between the received signal and the predefined feature sequences of PSS is given by

$$c_i(t) = \frac{\left| \int_0^{T_p} \tilde{s}_m(t-\tau)\, p_i^*(\tau)\, d\tau \right|^2}{\int_0^{T_p} |\tilde{s}_m(\tau)|^2 d\tau \int_0^{T_p} |p_i^*(\tau)|^2 d\tau} \tag{6.2}$$

where $i = 0, 1, 2$ denotes the root indices of the PSS and $p_i(\tau)$ are the feature sequences of the PSS in the time domain.

With each physical-layer identity $NID2$, the maximum of the sum peaks is selected by

$$\Lambda_{PSS_i} = \max_{0 \le t < T_{frm}} \{d_i(t)\} \tag{6.3}$$

where

$$d_i(t) = \frac{1}{N_P} \sum_{l=0}^{N_P-1} c_i(t + lT_{frm})$$

where T_{frm} is the length of a frame and N_P is the number of half-frames.

The maximum value in Λ_{PSS_i} is selected. Thus, the test statistic is derived as

$$T_{PSS} = \max_i \{\Lambda_{PSS_i}\}. \tag{6.4}$$

Then, the test statistic is compared to a predefined threshold as

$$T_{PSS} \underset{H_0}{\overset{H_1}{\gtrless}} \eta_{PSS}. \tag{6.5}$$

Recall Eq. 6.2. This formula applies the dimension cancelation method [117]. The test statistic, therefore, requires no knowledge of noise power. This PSS-based detection is completely tolerant of noise uncertainty [42]. Under hypothesis H_1, the root index of the PSS is determined by

$$NID2 = arg\max_i \{\Lambda_{PSS_i}\}. \tag{6.6}$$

6.3.3 2nd Stage: Signal Classification

The detected LTE signals can be classified with respect to the parameter Cell-ID which is comprised of the parameters cell-identity group $NID1$ and physical-layer identity $NID2$. The parameter $NID2$ is estimated when detecting the LTE signals. Here, the parameter $NID1$ will be estimated to compute the parameter Cell-ID. A test statistic of classification with respect to the parameter $NID1$ will be constructed. The estimated value of the parameter $NID1$ is equivalent to the case when the test statistic is maximized. Similarly, with the PSS-based detection, the test statistic of the $NID1$ classification is based on the cross-correlation of the detected signals with the predefined SSS sequences.

In LTE frames, the SSS is located at the symbol, which is one symbol preceding the detected PSS. For the awareness of the SSS order (between $0th$ and $10th$ slot) in the LTE frames in FDD

mode, each candidate of $NID1$ with the two slots is selected as

$$\Lambda_{SSS_i} = \max\{z_{i1}, z_{i2}\} \tag{6.7}$$

where z_{i1} and z_{i2} denote the correlation between the received signal and the SSS sequences at the $0th$ and $10th$ slot, respectively, and $i = \{0, 1, .., 167\}$ denotes the value of $NID1$.

The correlation is given as

$$z_{i1} = \left| \int_{\theta}^{\theta+T_u} \tilde{s}_m(t-\tau)\, q_{i1}^*(\tau)\, d\tau \right|^2 \tag{6.8}$$

where θ is equivalent to the position preceding one symbol at which the PSS is detected and T_u is the length of the symbol conveying the SSS.

Then, the physical-layer cell-identity group $NID1$ is determined by

$$NID1 = arg\max_i \{\Lambda_{SSS_i}\}. \tag{6.9}$$

From Eq. 6.6 and 6.9, the detected signals are classified with respect to the Cell-ID, which is equal to $3 \times NID1 + NID2$. Thus, the subband signal is identified by the Cell-ID.

6.4 Simulation Results

In simulations, secondary LTE signals are assumed to transmit in multiple channels of TV bands in the ultra-high frequency range (from 470 MHz to 790 MHz). The secondary UEs require to detect the secondary transmission and obtain the Cell-IDs for the network attachment later. Therefore, the UEs will apply the proposed spectrum sensing scheme to complete the two tasks. For simplification of the hardware, some configuration parameters, such as the sampling rate of the receiver and the FFT-size, are fixed. In the kogLTE project [82], the testbed of CR-based LTE-Advanced networks, which is also described in [2], is under the same conditions. Due to the conditions, LTE signals in our simulations have configuration parameters: the bandwidth of 5 MHz with 300 effective subcarriers, the FFT-size of 2048, the sampling rate of 30.72 MHz, and the access mode of FDD.

Based on the simulator of TU-Wien [118], LTE signals are generated from the defined configuration. Then, the signals are processed by resampling to allocate the effective bandwidth into an 8 MHz TV channel. Finally, the LTE signals are shifted by frequency steps and are mapped arbitrarily into TV channels. Note that SNRs are computed by the ratio of pure-signal power to noise power in the time domain and are then scaled to the ratio of the number of effective subcarriers with the FFT-size $300/2048$. At the first stage, the prototype filter is designed with the cutoff frequency of 4.5 MHz, which is equal to the effective bandwidth of subband LTE signals. To be convenient for simulations, the subband signals are resampled back to the original sampling rate. Then, the PSS-based detection and classification are computed. Besides, the simulations for single channels with the perfect filter (by which there is no bias of spectrum estimation) are carried out. Therefore, the performance of spectrum sensing for single channels is considered as a benchmark to evaluate that of the proposed scheme. The probability of detection and classification by the proposed scheme is compared with that of the case for single channels.

For PSS-based detection, the thresholds are pre-computed with a CFAR of 1%, and the feature sequences for the PSS with the three values of $NID2$ are pre-generated. For Cell-ID classification, all 504 feature sequences for the SSS, which include three choices for $NID2$ and 168 choices for $NID1$ are also generated in advance. When the signal is detected with a value of $NID2$, 168 sequences (which correspond to 168 values of $NID1$) are selected to compute the cross-correlation with the SSS, as given by Eq. 6.8.

Fig. 6.2 pictorially demonstrates the power spectrum density (PSD) as the output of FBSEs for the signals in eight TV channels with the bandwidth of 8 MHz. With an assumption of sensing the primary signal in advance, a secondary LTE network utilizes the empty TV channels for its opportunity transmission. As observed from the figure, the eight TV channels are used by the secondary signals, and each secondary signal occupies 4.5 MHz, in the total bandwidth 5 of MHz, of LTE signals. In simulations, the secondary LTE signals are randomly transmitted into the TV channels. Consider the probability of detection and classification at low SNRs; the SNR range is from -22 dB to 0 dB in our simulations. The filter-bank analyzes the wideband signal in the 64 MHz bandwidth into subband signals corresponding to eight separated channels. At the next stage, the subband signal in each channel is processed to identify the expected information.

The cross-correlation between the predefined PSS sequences and the received signal is demonstrated in Fig. 6.3. As observed in this figure, periodical peaks of the cross-correlation

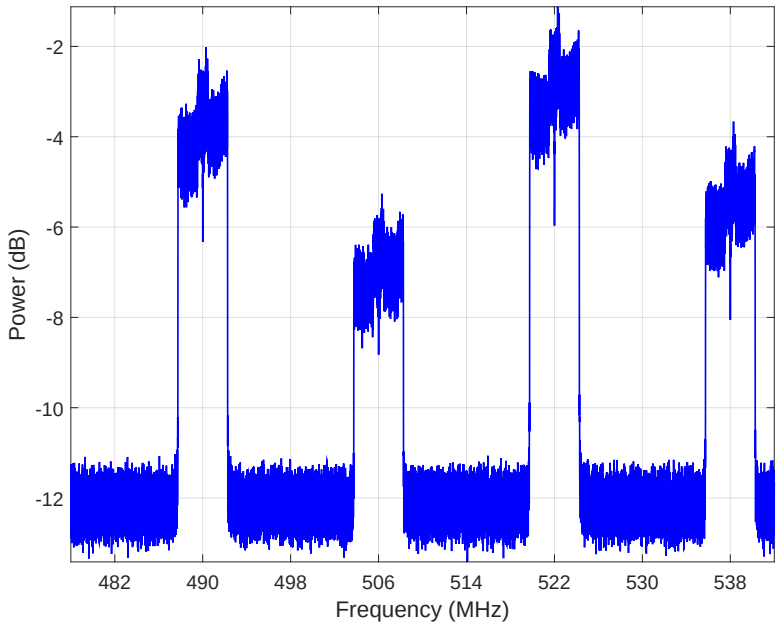

Fig. 6.2: A snapshot of the power spectrum density, which is estimated by FBSEs, of secondary LTE signals transmitted in eight TV channels.

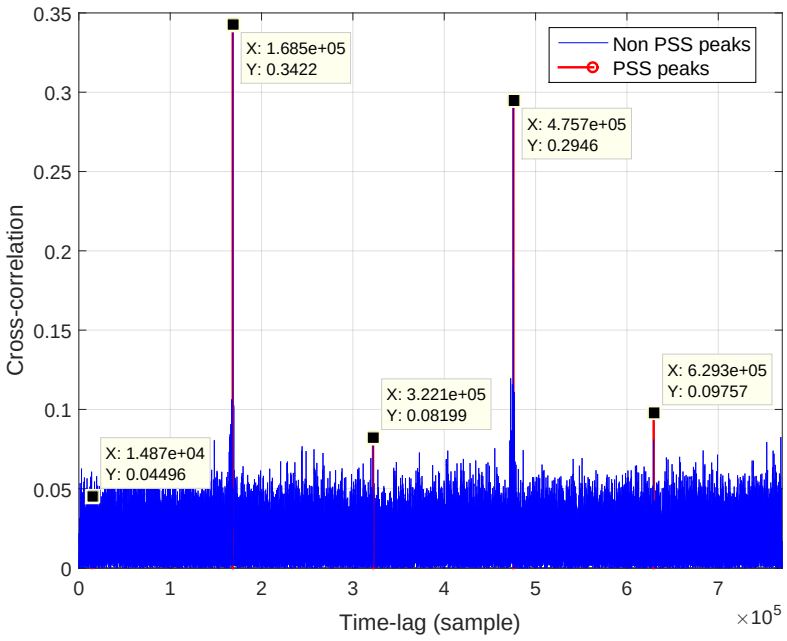

Fig. 6.3: Peaks of cross-correlation between the received signal and the pre-generated feature of the PSS with a bandwidth of 5 MHz at the SNR of -6 dB.

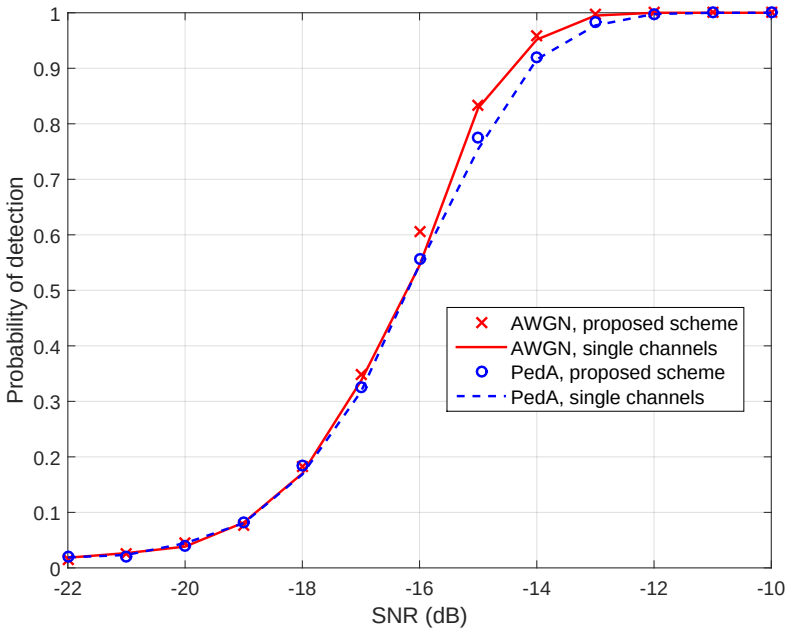

Fig. 6.4: The probability of the detection based on PSS in different environments with the observation time of 10 ms and CFO of 0 ppm.

exist when a predefined sequence and the signal have the same parameter sector identity, $NID2$. The periodicity of these peaks is half of the LTE frame. The probability of the detection based on the PSS for subband signals, through the filter-bank as the first stage in an AWGN channel and ITU Pedestrian (PedA) channels with an observation time of 10 ms and a CFO of 0 ppm, is observed in Fig. 6.4. These results show that the detection performance in both environments is comparatively close together. Hence, the PSS-based detection works well in multipath fading environments. The comparison between the detection performances for different CFOs is shown in Fig. 6.5. In simulations, CFOs are configured with two cases of 0 ppm (perfect local oscillators) and 6 ppm for imperfect local oscillators. Considering the detection performance of over 90%, the performance of the CFO of 0 ppm is higher 1 dB than that of the CFO of 6 ppm. Thus, the PSS-based detection by the proposed scheme is tolerant well of CFOs. For the carrier frequency of 514 MHz, the CFO of 6 ppm is equivalent to 3084 Hz. Additionally, in Fig. 6.4 and 6.5, the detection performance of the proposed scheme is fit well to that in the case of a single channel. It proves the anti-aliasing of the polyphase implementation of the proposed scheme and the idea to design the prototype filter, whose pass-band is smaller than the whole effective bandwidth of subband LTE signals.

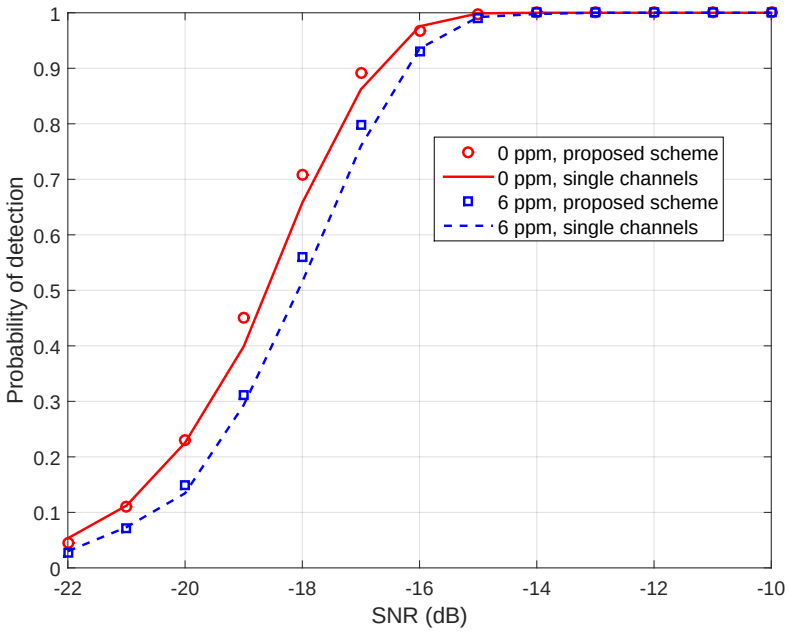

Fig. 6.5: The probability of detection based on PSS in 20 ms with a CFO of 6 ppm in PedA channels.

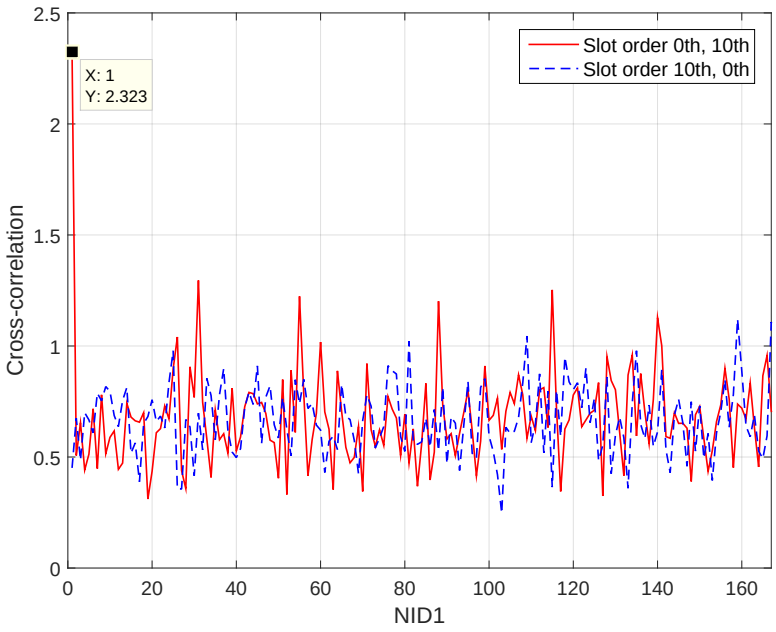

Fig. 6.6: A snapshot of classification with the physical-layer cell-identity group in SSS at -6 dB in 40 ms.

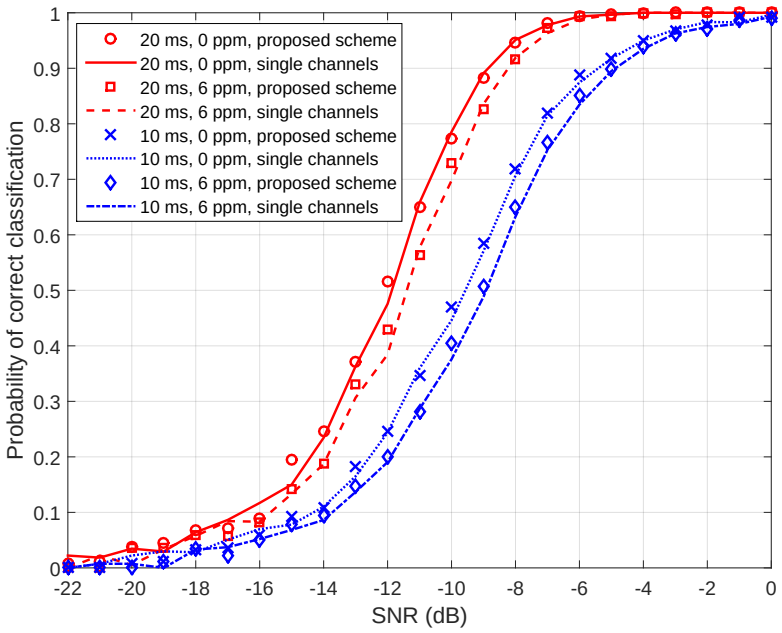

Fig. 6.7: The probability of correct classification (PCC) when detected with CFOs of 0 ppm and 6 ppm in PedA channels.

The methodology of Cell-ID classification is pictorially presented, as in Fig. 6.6. It shows a snapshot of the cross-correlation as Eq. 6.7, between the predefined features, which convey the Cell-IDs induced by Sector-ID, $NID2$, of the detected LTE signal and the extracted SSS. The highest peak of the cross-correlation is corresponding to the parameter Sector-Group, $NID1$. As observation for this snapshot, the detected $NID1$ is equal to 1, and the order of the slot in which the first PSS peak appears is the $0th$ in the frame. Finally, Fig. 6.7 depicts the PCCs, which are considered when LTE signals are detected, with different CFOs. Compared with the performance of the CFO of 0 ppm, the PCC of the CFO of 6 ppm is less than 1 dB. When increasing the observation time from 10 ms to 20 ms, the PCCs obtain 3 dB performance gain with the same CFOs. Moreover, Fig. 6.7 shows that the PCCs of the proposed scheme comparatively fit with those for single channels. These observed clues show that the wideband spectrum sensing is highly effective due to (1) the anti-aliasing by the polyphase implementation and (2) the proper design of the prototype filter.

6.5 Summary

This chapter investigated multiband spectrum sensing for LTE signals in the downlink of cellular systems. A multiband spectrum sensing scheme was proposed for the detection and classification of LTE signals in multiple channels. The mathematic formulas were introduced for the multiband spectrum scheme, including a filter-bank realization and detection and classification algorithms for LTE signals. The detection and classification performances of LTE signals were evaluated by simulations in which LTE signals are transmitted into multiple channels of TV bands. The simulation results show that the proposed scheme works well in multipath fading environments with an imperfect CFO and is tolerant of NU. The performances of the scheme are approximated to those in the case of single channel spectrum sensing. Moreover, this chapter has presented a realistic scenario for CCSs, which need to detect and utilize vacant TV channels for secondary transmissions. In the scenario, a design of the scheme was introduced with main parameters. This design gives useful guidelines to implement the scheme in CCSs.

7 CCS EXPERIMENTS

7.1 Introduction

The experiments are carried on with the testbeds, which are developed and integrated as the kogLTE [82] and ABSOLUTE [83] projects. The two testbeds are compatible to LTE-Advanced systems and have cognitive capabilities of CR frameworks, which are comprised of a spectrum sensing module. CR frameworks in the testbeds are different to each other due to the target scenarios.

In the kogLTE project, a main target of the cognitive capability is to utilize the unoccupied-spectrum in the unlicensed spectrum such as TV bands. Differently, the testbed in the ABSOLUTE project aims to recover cellular communications when the existing infrastructure of cellular systems is unexpectedly destroyed. Therefore, the LTE-Advanced transmission is described in the experiments with the testbed of the kogLTE project. The CR frameworks and other related entities will be mentioned with specific scenarios. Due to the cognitive capabilities of the two projects, the experiments can be carried on as follows:

- **The PPA algorithms:** The proposed algorithms, as in Section 4.2, will be evaluated with the testbed of the kogLTE project [82]. DVB-T signals are primary signals to be processed by a CR framework deployed with the PPA algorithms.
- **The multiband spectrum sensing scheme:** The proposed scheme, as in Chapter 6, will be assessed with the testbed of the ABSOLUTE project [83]. LTE signals in multiple channels are primary signals in a licensed spectrum. The LTE signals in each channel will be detected and classified by the multiband spectrum sensing scheme.

This chapter presents the experiments of the PPA algorithms and multiband spectrum sensing scheme in Sections 7.2 and 7.3, respectively. Each section will mention the main targeted

scenarios and methodologies of the experiments. The experimental results will be analyzed in the context of cellular communications to verify simulation results in previous chapters.

7.2 Spectrum Sensing in OFDM-Based CCSs

7.2.1 Overview

In spectrum sensing, the feature-based detection is considered as a good approach [18]. With this approach, many algorithms have been proposed for OFDM signals, whose modulation is popular in wireless communications. Specifically, the algorithms are proposed to pilot-added OFDM such as the TDSC-based detection [53] and the PPA-based detection introduced in Section 4.2. These detections can be applied to exploit TVWSs, which are promising frequency ranges for secondary transmissions of cognitive systems [119]. The TDSC-based detection is evaluated in simulations, as in [53, 120], and in a testbed, as in [89]. However, these works were implemented with a long observation duration, 50 ms, compared to a demand for short durations, which are in order of milliseconds, to improve the effectiveness of the whole network. For example, the networks only need to be idle [85] in a short interval to perform sensing tasks. The performance of the PPA-based detection is evaluated by simulations in Section 4.2 with DVB-T 2K mode signals, which have a higher number of symbols than 8K mode signals, which are popularly deployed in Germany [121].

Recently, testbeds have been developed for CR-based systems. Spectrum sensing algorithms need to be assessed in testbeds with realistic conditions. Standardization organizations publish recommendations and requirements for CR-based systems. For example, CR-based IEEE P802 and CR-based cellular systems are recommended, as in [122] and [85], respectively. CR-based IEEE P802 systems are designed specially for the IEEE P802.22 standard with the VHF/UHF TV bands. CR-based systems [85] are supposed to operate with cellular communications. As a good trend, CR-based cellular systems operate for cellular communications with radio cognitive capabilities. For the development of the capabilities, it is essential and challenging to evaluate the reliability of spectrum sensing algorithms in a testbed.

Here, this dissertation presents experiments to assess the reliability of the spectrum sensing algorithms for pilot-added OFDM signals: the TDSC algorithms and PPA algorithms in Section

4.2 with a testbed. This testbed has been developed from the kogLTE project for CCSs, which are CR-based LTE-Advanced systems. The radio front-end of this CCS can operate with frequencies of TV bands. Experiments are carried out with real signals captured by the testbed. Moreover, a transmission between a vector generator and a spectrum analyzer is used to cross-check with results by the testbed. The experimental results will assess the algorithms in real environments and with NUs and observation times. The PPA algorithms and TDSC algorithms will be compared with one another when taking into account the observation time as the system constraint.

Particularly, the contributions of these experiments are: (1) the algorithms are evaluated in practice by a CR-based LTE-Advanced system with end-to-end operations; (2) the experiments give comparisons by which CR-based systems can utilize the advantages of the two algorithms in different sensing modes.

7.2.2 Spectrum Sensing Algorithms for Pilot-Added OFDM Signals

Pilots are used to estimate the channels between transmitters and receivers. Normally, pilots are designed with certain patterns in a frequency-time grid. Based on this characteristic, the TDSC and PPA algorithms are proposed for the spectrum sensing of OFDM signals. The TDSC algorithms compute the cross-correlation between symbols shifted the symbol interval of pilot patterns to detect the desired signals. Differently, the PPA algorithms exploit autocorrelation peaks, which are based on both subcarrier and symbol intervals of pilot patterns. Each algorithm has two sub-methods named by suffixes NP (Neyman-Pearson) and MRC (maximum rate combination). The TDSC-NP and PPA-NP are briefly presented in the following part. The NP test statistic of the two algorithms can be further improved by a MRC for symbol cross-correlation terms in multiple pilot periodicities. The test statistics of the TDSC-MRC and PPA-NP algorithms are introduced in [53] and [13], respectively.

Time domain symbol cross-correlation (TDSC)-based detection

For DVB-T signals [91], the TDSC algorithms calculate the cross-correlation between the symbols, $R(k, m)$, whose indices are different from each other by four. With the NP approach, a

test statistic is computed from an accumulation of the cross-correlation. It is given as [53]

$$T_{TDSC-NP} = \frac{1}{N_{4sbl}} \left| \sum_{m-k=4} R(k,m) \right| \tag{7.1}$$

where N_{4sbl} is a multiple integer of the symbol pairs.

Periodical peaks of autocorrelation (PPA)-based detection

The PPA algorithms [13] calculate a summation of the autocorrelation peaks from the signals at the lag with respect to subcarrier and symbol indices. The summation is given by

$$S(0) = \sum_{n=0}^{N-1} \left(\sum_{i \in \Omega_z} c_i R(n, \tau_i) + R(n, T_0) \right). \tag{7.2}$$

For DVB-T signals, the test statistic of PPA-NP has the formula of

$$T_{PPA-NP} = |S(0)| / \sqrt{\sigma_w^2 \left(\sum_{i \in \Omega_z} c_i + 1 \right)} \tag{7.3}$$

where σ_w^2 is the noise variance.

7.2.3 Design of a CR-based LTE-Advanced System

A. Overall Architecture

In LTE-Advanced systems, two main entities are UE and evolved-node-B (eNodeB or eNB). With CR-based LTE-Advanced systems, CR capabilities can be deployed in UE or eNodeB. Here, a design for CR-based eNodeB is introduced. The overall architecture of CR-based eNodeB is described as in Fig. 7.3. This architecture has been developed from the testbed initially presented in [14, 123]. In this architecture, the spectrum sensing module (SSM) plays a crucial role in the physical layer (PHY) and is associated with other modules for normal LTE-Advanced transmissions. This module handles spectrum sensing algorithms with requirements from cognitive engine (CE) whose configuration parameters for sensing can be configured by a host personal computer (PC), which is used for configuration and applications (e.g., REM).

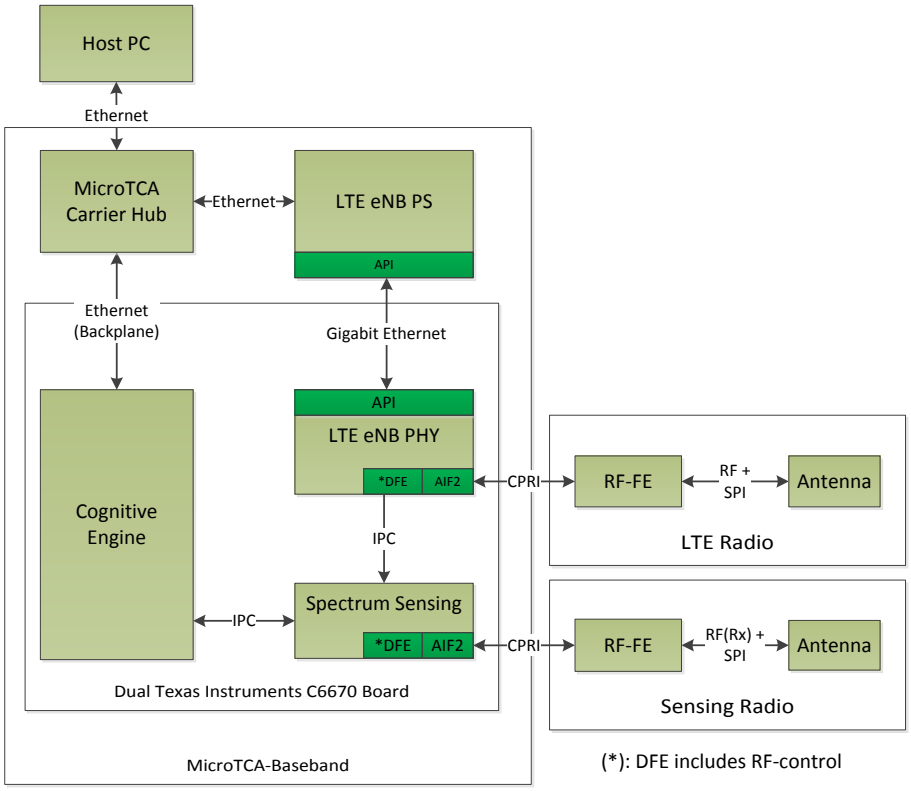

Fig. 7.1: Functional blocks of a CR-based eNodeB.

The SSM obtains the necessary signals needed to be detected/classified from a radio-frequency front-end (RF-FE) separated with or integrated to that of LTE transmissions.

The RF-FE for spectrum sensing (termed Sensing Radio) is separated from that of LTE transmissions (termed LTE Radio). These two RF-FEs facilitate sensing tasks with two modes: out-band and in-band sensing. In out-band sensing mode, bass-band signals are transferred to the RF-FE in Sensing Radio via a serial peripheral interface (SPI). The RF-FE down convert the pass-band signals to base-band signals. They have an antenna containing matching circuits. The base-band signals are supplied to the SSM thought an antenna interface 2 (AIF2) via a common public radio interface (CPRI). The SSM uses a digital front end (DFE) to convert the base-band signals to digital signals for a sensing process. In the in-band sensing mode, the pass-band signals are processed and transferred to the SSM via an inter process communication (IPC). The CR-based eNodeB can flexibly handle sensing tasks in the two modes by using the two RF-FEs. The SSM provides sensing results to the CE for decision making on secondary transmissions. For example, the CE uses the sensing results to determine the vacant channels and power for

transmissions.

The SSM, CE, and LTE eNB PHY are implemented in a Texas Instruments digital signal processor (DSP) board. These elements are physically connected with each other and other modules via a micro telecommunications computing architecture (MicroTCA) chassis. These modules communicate with others operating at layer 3 as the Host PC and LTE eNB PS (PS denotes protocol stack) via ethernet connections.

B. Implementation of Software-Defined Radio in a DSP Platform

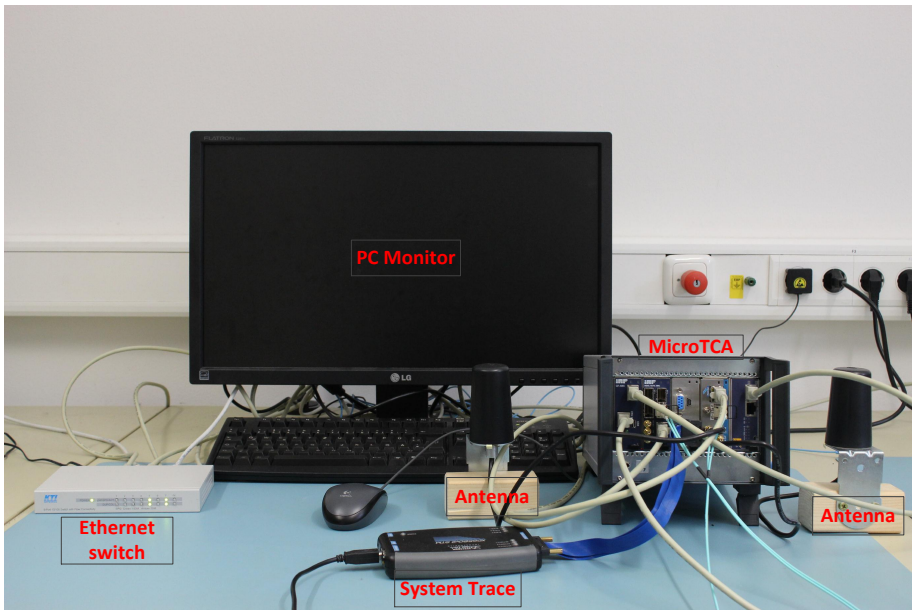

Fig. 7.2: Main productive components of CR-based eNodeB.

The CR-based eNodeB has main productive components, as shown in Fig. 7.2. The DSP board is plugged into the MicroTCA chassis. Modules on the DSP board are monitored via a system trace. They connect with layer 2 and layer 3 softwares and RF-FEs via ethernet connections and the CPRI, respectively.

Fig. 7.3 shows module-interfaces of the SDR platform, on which physical layer functions are software-defined [23] in a CR-based eNodeB. With this design, the SDR is comprised of three main modules: SSM, CE, and LTE eNB PHY. The SSM and CE were designed and have been developed on a DSP platform. A platform of Texas Instruments (TI) is selected: a dual 6670 AMC board. The other modules are based on computers such as the external data-base.

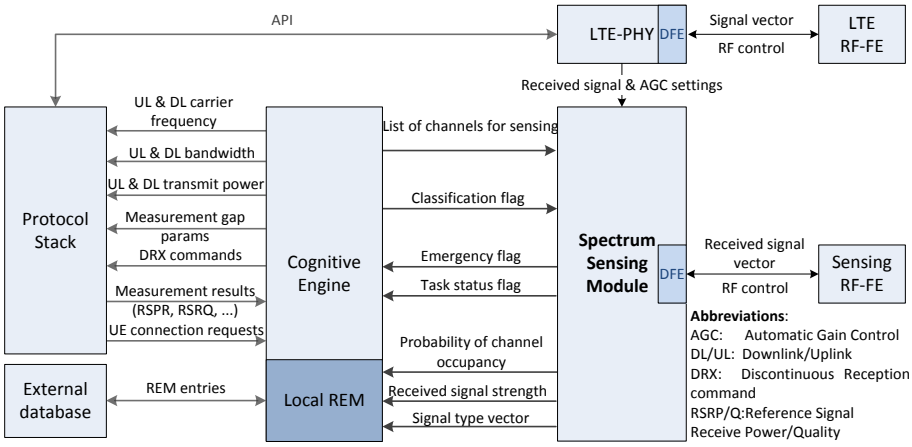

Fig. 7.3: Module interfaces of SDR in CR-based eNodeB.

The DSP platform is selected to implement LTE eNB PHY effectively. Logically, the DSP-based modules independently implement (a) DSP core(s) and transfer parameters (params) to each other via an Inter-Process-Communication (IPC).

The SSM has main logical in/outputs as shown in Fig. 7.3. The inputs are stored in a dynamic random-access memory (DRAM). This design aims at accelerating the processing time for sensing tasks. However, a main constraint factor here is the storage capacity of DRAM, which is normally small. In the system, it can contain DVB-T signals in orders of milliseconds. It results that the observation time should be short from the memory-storage aspect. Therefore, short observations are taken into account when spectrum sensing algorithms are deployed in such systems.

7.2.4 Methodology of Experiments

Experiments are carried out to verify the performance of algorithms: PPA and TDSC, in practice, with the above CR-based LTE-Advanced system. For a reliable comparison, the methodology of the experiments is as follows.

Reference (Ref.): Signals are generated by a vector generator, MXG N5182B, with a high SNR of 35 dB. To avoid unknown noise and interference, the signals are transmitted directly to an analyzer, MXA 9020B, via a cable. In this case, the channel between the transmitter and receiver is AWGN.

Experiments (Exp.): Signals transmitted over the air (OTA) are captured. OTA signals are fed

into the SDR platform (via DFE, as in Fig. 7.3). Due to the memory capacity of DRAM, the MXA is used instead of the RF-FE to capture OTA signals for long observation durations higher than 5 ms.

The signals captured by the two approaches are processed with the same steps to compute the performance of the mentioned algorithms. The performance with the pair of the MXG and the MXA is considered as a reference value for that of the testbed. Main steps are taken to compute the performance of algorithms.

- **Step 1 – Threshold computation:**

  The SSM is fed with noise to calculate a probability of error (false alarm), Pfa. Thresholds are adjusted to a value when the Pfa meets the constant rate of 1%. 3000 iterations are set up for each adjustment.

- **Step 2 – SNR control:**

  This step manufactures signals with precise SNRs. Embedded noise in captured signals is ignored because the signals are captured with a high SNR. Therefore, the signals are scaled up/down and combined with noise at certain SNRs in Matlab.

- **Step 3 – Probability of correction:**

  The scaled signals are fed into the inputs of SSM to calculate the probability of detection. At each SNR value, 1000 iterations are carried out to obtain good statistic values of a detection with an observation duration.

DVB-T signals at the UHF band 470 MHz–790 MHz are targeted for experiments. In Nordrhein-Westfalen, Germany, DVB-T base stations transmit signals with main parameters [121]: 8K mode, 8 MHz bandwidth, and CP ratio of 1/4. For the in-band sensing mode, cognitive LTE-Advanced systems normally utilize temporal gaps between downlink and uplink transmissions to detect primary signals [85]. The gaps are called quiet periods (QPs), in which elements in a network are idle and stop transmitting. Observation durations can be a combination of multiple QPs to meet requirements of spectrum sensing such as probability of detection. However, observation durations should be as short as possible to improve the effeciency of the whole network. Similarly, for the out-band sensing mode, observations should not be long to obtain good opportunistic access in unoccupied spectrum spaces. In experiments, the observation durations are equal to 5 ms, 10 ms, and 20 ms with a false alarm of 1%.

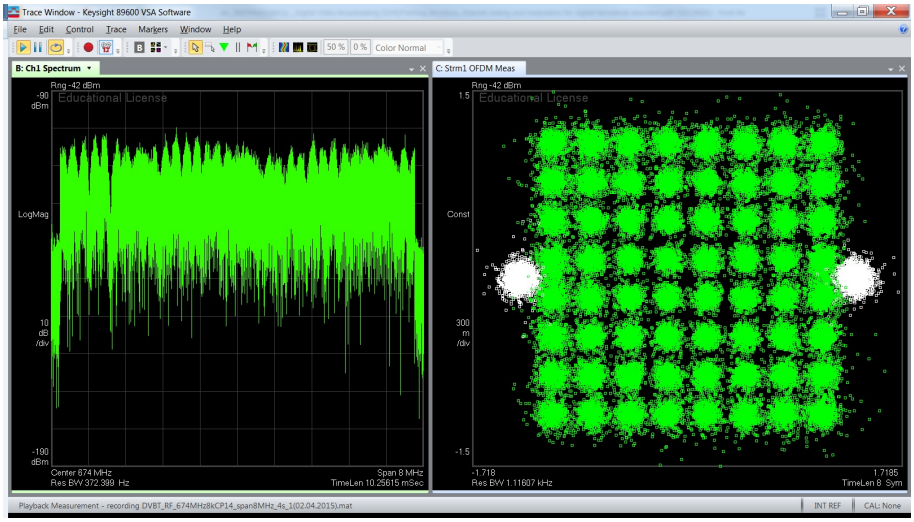

(a) PSD and constellation

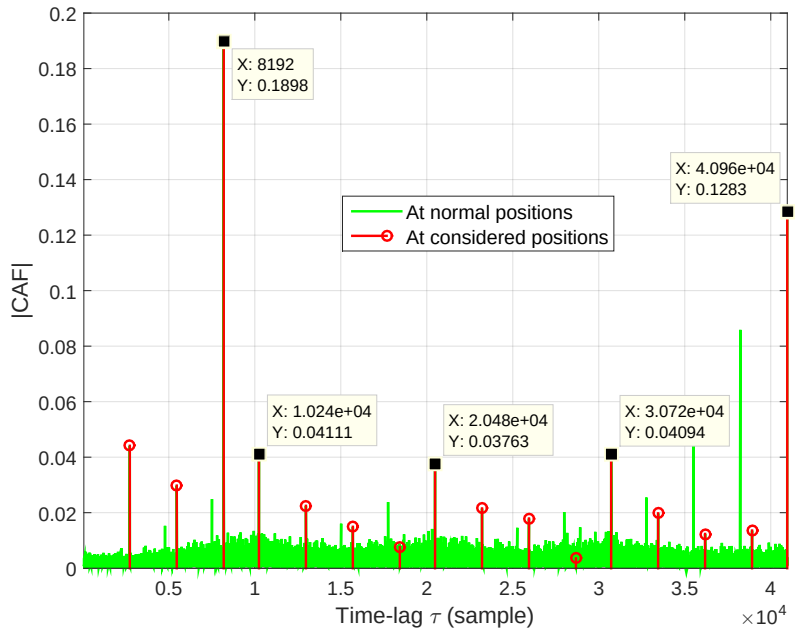

(b) A snapshot of CAF in 10 ms

Fig. 7.4: DVB-T signals with 8K mode captured at $f_c = 674MHz$.

7.2.5 Experimental Results and Analysis

Fig. 7.4a shows the PSD of captured 8K DVB-T signals at the channel 46: $f_c = 674MHz$, 8 MHz bandwidth, and 64QAM. For pilots, the BPSK modulation with a boosted amplitude can be observed from the constellation in the figure. For DVB-T 8K mode signals, scattered pilots are assigned in subcarriers with the subcarrier and symbol steps: $D_x = 3$ and $D_y = 4$,

respectively. As proven in [13], the autocorrelation peaks are high at the subcarrier gap as $1/D_x$ of the symbol length and at the end of symbols. These peaks appear periodically in D_y symbols. Fig. 7.4b presents a snapshot of CAF for the captured signals in 10 ms. There are three peaks $2731, 5461, 8192$ due to scattered pilots. The peak at sample index 10240 is mainly accumulated by continual pilots. The peak at index 8192 (FFT-size) is the highest in this measurement because it is contributed from pilots and CP samples. Meanwhile, the peak at index 40960 (4-symbols length) is the second highest. This peak is equivalent to the autocorrelation for TDSC algorithms. Key points can be drawn by observing the peaks in the experiments and those in simulations 4.2. These points give insight into the analysis of the performance of TDSC and PPA algorithms in different observation durations.

- The peak at 4-symbols length (as the TDSC algorithms) is decreased when decreasing the number of symbols.
- The other peaks can contribute considerably to a total accumulated autocorrelation.
- The peak at FFT-size is high, corresponding to CP ratios, and approaches to other peaks when the CP ratio is small.

Fig. 7.5a shows that the performance by the experiment method with the RE-FEs is insubstantially degraded to that of the MXA, which can be explained by the fact that the MXA is a piece of commercial equipment dedicated to measurements. From testbed's perspective, therefore, it is reasonable for the experiment method to use the MXA as an alternative of the RE-FEs when the algorithms are evaluated with long observation durations. Compared to the reference method, the performances by the experiment method (with the RF-FE and MXA) are slightly less than those by the reference method, as shown in Figs. 7.5 and 7.6. The reason is that the channels are multipaths fading in real environments; meanwhile, they are AWGN in the reference method. This agrees with a comparison between AWGN and a multipath fading environments, as in [13]. Therefore, the experimental results are reliable. As shown in Figs. 7.5 and 7.6, both TDSC and PPA algorithms degrade the performances by about 1 dB with a noise uncertainty (NU) of 1 dB. This performance degradation is much slightly compared to the limitation of SNR walls for energy-based detection [43].

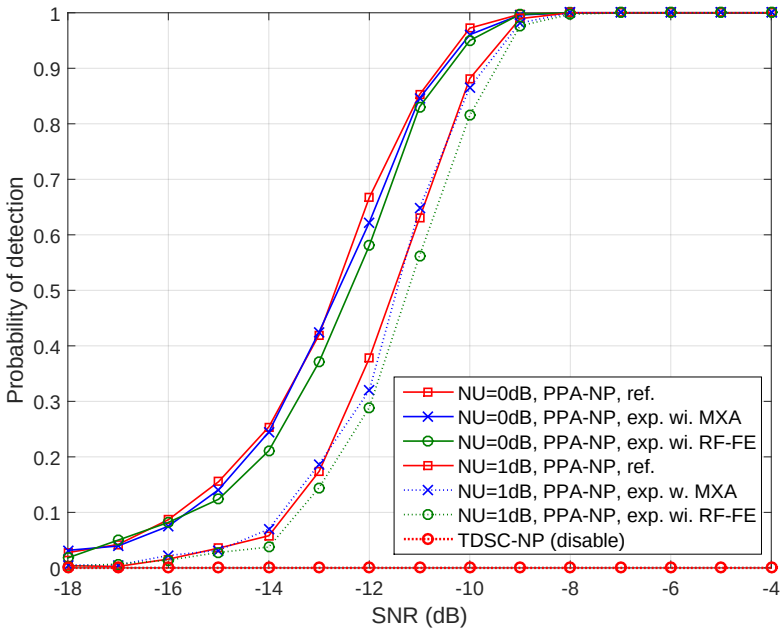

(a) Observation duration: 5 ms

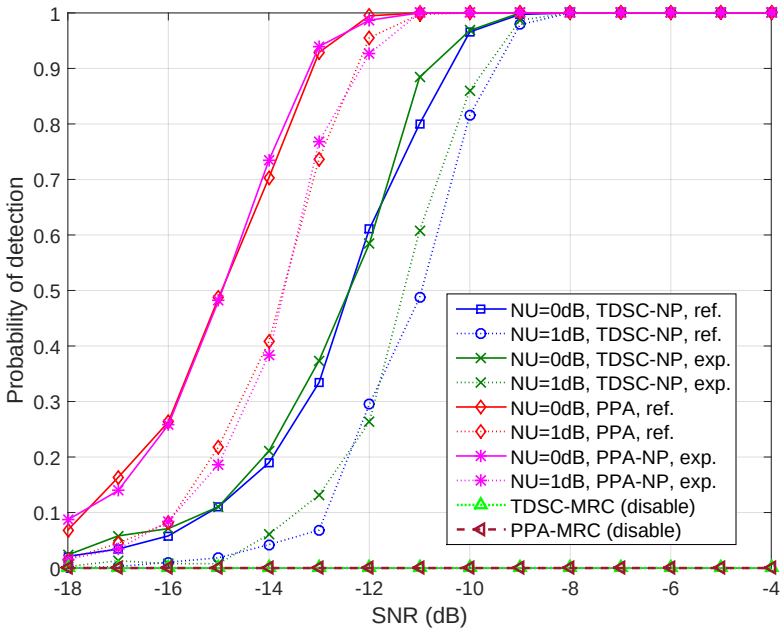

(b) Observation duration: 10 ms

Fig. 7.5: Comparison of performances between PPA and TDSC detectors with the DVB-T 8K mode captured at $f_c = 674MHz$.

With DVB-T 8K mode signals, the TDSC-NP algorithm does not work if the observation duration is less than or equal to 5 ms. In a 5 ms duration, there are 4.5 symbols of DVB-T 8K

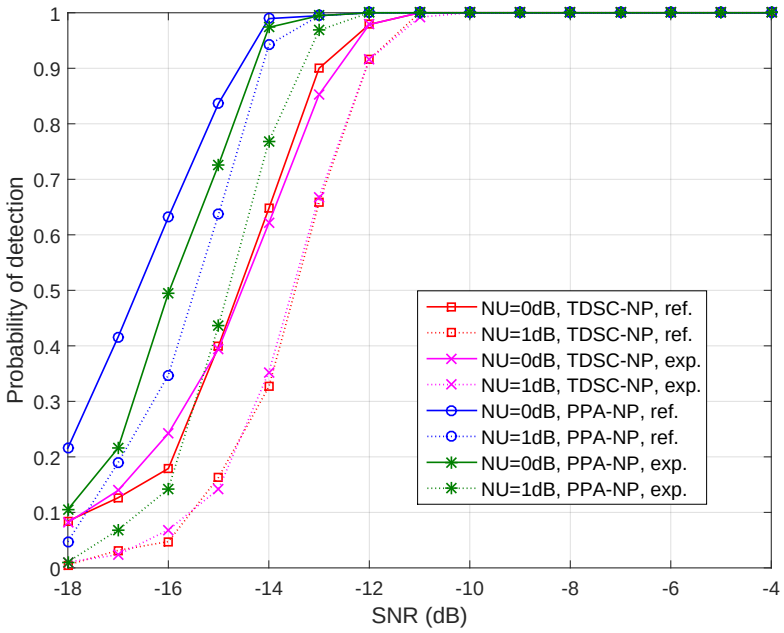

(a) NP

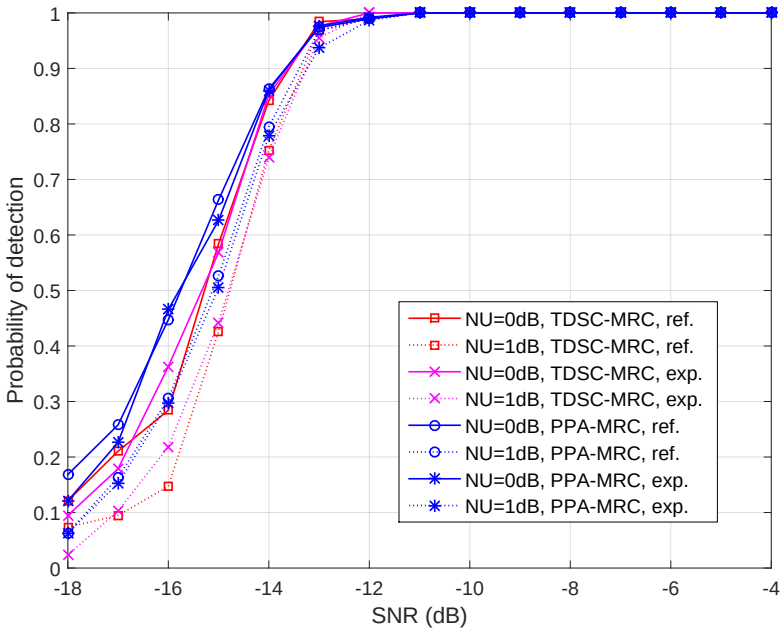

(b) MRC

Fig. 7.6: Observation duration: 20 ms.

mode signals. There is almost no sample left for a cross-correlation between symbols when the signals are shifted in four symbols. Similarly, there are two periods for the 8K mode signals

with a 10 ms observation. There are not enough periods for a MRC of correlation in periods. Therefore, only the PPA-NP algorithm and the TDSC-NP algorithm work in 5 ms and 10 ms observations, respectively; the other algorithms are disable.

The PPA-NP algorithm has a performance higher than the TDSC-NP/MRC algorithms with all the observation durations. With a 5 ms observation, only the PPA-NP algorithm works and has a performance approximated to that of the TDSC-NP algorithm with a 10 ms observation. With a 10 ms observation, the PPA-NP algorithm outperforms the TDSC-NP algorithm by 2.5 dB. With a 20 ms observation, the PPA-NP algorithm has a 1 dB performance higher than that of the TDSC-MRC algorithm.

8K mode signals have a performance about 1 dB less than that of 2K mode signals, simulated in [13] with a same observation duration of 10 ms. The reason is that the symbol length of 8K mode signals is four times longer than that of 2K mode signals. It results that 8K mode signals require three more symbols (compared with 2K mode signals) to utilize the pilot periodicity.

With DVB-T 8K mode signals, there is no performance gain for the PP-MRC algorithm compared to the TDSC-MRC algorithm with the observation times. With the DVB-T 2K mode signals, meanwhile, the PP-MRC algorithm gives performance gain of about 1 dB more than the TDSC-MRC algorithm, as simulated in [13]. Nevertheless, the PPA-NP algorithm outperforms the PPA-MRC and TDSC-MRC algorithms by 1 dB in a 20 ms observation.

7.2.6 Concluding Remarks

The PPA and TDSC algorithms were evaluated in a real testbed of CCSs. The algorithms work well in real environments with noise uncertainties and at low SNRs. These algorithms work well in real environments and are insensitive to NU. Besides, the experimental results show that the PPA algorithms outperform the TDSC algorithms by 1 dB–2.5 dB. The performance gains of the PPA algorithms compared to the TDSC algorithms in the experiments agree with those in the simulation results. The PPA algorithms can work with short observation durations (e.g., with 5 ms of DVB-T 8K mode signals); meanwhile, the TDSC algorithms cannot. Depending on the observation duration in sensing modes, CCSs can select a suitable algorithm to detect the desired signal.

7.3 Spectrum Sensing in Multiband CCSs

7.3.1 Overview

To obtain high effectiveness of the operation, CR-based networks require that sensing tasks be performed in a short duration. This requirement will be more challenging when the operating frequency range of the CR-based networks is wider. For example, CR-based networks extend the frequency range to search the vacant spectrum; or the spectrum bands of PU are broadened. It results that CR-based networks need to execute sensing tasks in the wide frequency range. For example, the frequency range can be 320 MHz (470 MHz–790 MHz) in the UHF band or 70 MHz (2620 MHz–2690 MHz) in LTE band 7 when CR-based networks operate in these bands. Therefore, the CR-based networks must detect white-spaces in multiple channels, which is called multiband spectrum sensing. Besides, spectrum sensing has been developed with the concepts of CR. It does not only detect white spaces but also needs to be aware of other information on radio environment surrounding. Specifically, for CR-based LTE networks, spectrum awareness should have abilities to detect and identify LTE signals. With these abilities, user equipments (UEs) can choose and quickly attach to a target LTE base station (eNodeB). CR-based eNodeBs can collaborate effectively with each other due to the identified information in the channels.

An approach based on filter-banks is proposed, as pioneered by Farhang-Boroujeny [115] for spectrum sensing in multi-channels. Filter-bank spectral estimator (FBSE) is compared with Thomson's multi-taper spectral estimator (MTSE). From the spectral estimator's perspective, both of these methods have advantages and disadvantages. In the work, the spectrum sensing task is to detect signals by the energy-detection algorithm. In the work [116], authors proposed a scheme with a filter-bank using a polyphase network to detect DVB-T signals by a matched-filter algorithm. For LTE signals, a spectrum sensing scheme with a filter-bank is proposed in Chapter 6 for the detection and classification of the signals by feature-based detection algorithms. In Chapter 6, simulation results prove that the spectrum sensing scheme works well with mostly no degradation compared to the spectrum sensing performance for single channels. For about two decades, many efforts have been tried to develop testbeds for CCSs. Also, pilot applications have been deployed. For cellular communications, CR-based LTE networks bring benefits to many scenarios such as in emergency situations mentioned in [21]. They have to detect

the unoccupied spectrum and identify themselves for a good collaboration when operating in wideband spectrums. Besides, the networks can collaborate effectively with each other due to the knowledge of identified information in channels. From the testbeds' perspective, the evaluation of spectrum sensing algorithms is an essential step, specially when it is considered in realistic scenarios with a context of end-to-end procedures.

This section presents emergency situations in which eNodeBs are rapidly deployed to serve UEs, instead of destroyed eNodeBs, due to catastrophes. In such situations, the CR-based eNodeBs need spectrum awareness on the current channels in LTE bands. Therefore, a spectrum sensing scheme, as proposed in Chapter 6, can satisfy this demand, by which the multi-channels are processed to detect unoccupied channels and identify the serving eNodeBs. These base stations are called CR-based eNodeBs. A SDR platform of a CR-based eNodeB is used to evaluate the spectrum sensing scheme with OTA signals in emergency scenarios. This evaluation essentially contributes to the successful development of CR-based eNodeBs, which can perform multiband spectrum sensing in practice.

In the remaining parts, Section 7.2 is organized as follows. First, this section mentions the discipline and design of the scheme with the main parameters of target channels and signals. Then, the experiments of a testbed are introduced, including the scenarios, overall architecture of the testbed, and implementation of the main modules. Next, the experiment results are presented and analyzed. Concluding remarks are finally drawn.

7.3.2 Multiband Spectrum Sensing with Filter-Bank Realization

As presented in Fig. 7.7, there are two stages of the scheme for multiband spectrum sensing as in Chapter 6. At the first stage, subband signals are extracted from multiband signals by a filter-bank realization. The subband signals are detected and classified with cell identities in parallel. Aiming to assess the scheme for the scenarios, the above scheme is designed with main configurations for each stage. In the first stage, the core issue is to design the filter-banks, which are a polyphase realization of a prototype filter. The prototype filter processes 10 MHz bandwidth LTE signals. The prototype filter is a low-pass filter, which can be carried out by a FIR type I. In the experiments, the signals are processed with the effective bandwidth of the LTE channels. The main parameters of this filter are: $\omega_p = 0.9\pi$, $\omega_s = 0.1\pi$, which denote the normalized

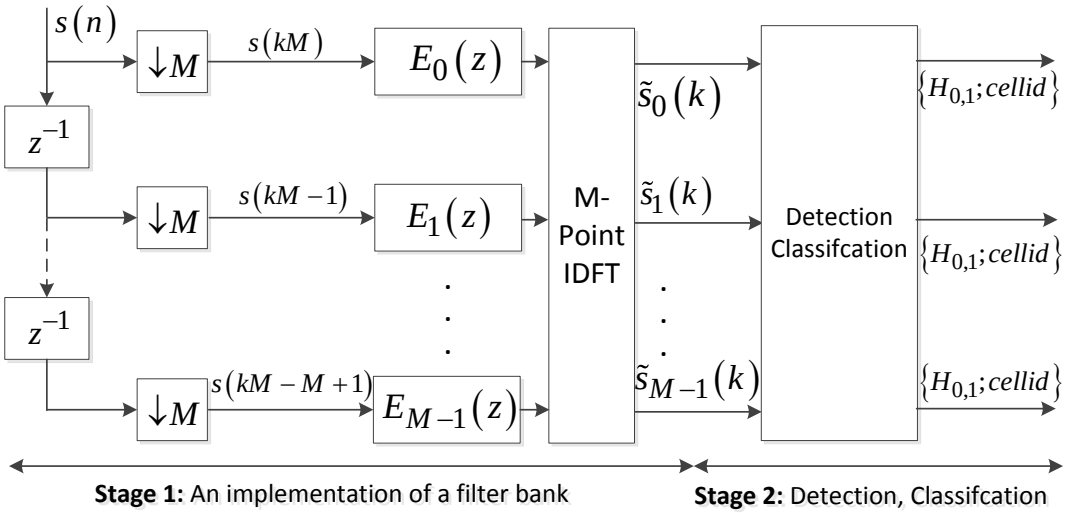

Fig. 7.7: The multiband spectrum sensing with filter-bank realization, as proposed in [4].

passband frequency and transition bandwidth, respectively. The ideal cutoff frequency will be at $\omega_c = 0.475\pi$, where the amplitude decreases by 3 dB. Choosing a windowing function is the first step of FIR designs. The Blackman window is chosen due to its low spectral leakage of about -58.1 dB, as shown in [124]. The mainlope depends on the filter length L_{flt} and is given as $12\pi/L_{flt}$. For the passband ripple of -74 dB, the filter length must be larger than 121. The response function of the designed prototype-filter is presented, as in Fig. 7.8. In the second stage, the detection and classification of LTE signals are carried out by the cross-correlation between the subband signals and the predefined PSS and SSS. The PSS and SSS sequences are used to calculate the correlation, as Eq. 6.2 and 6.8 in Chapter 6, for the detection and classification of the test-statistic, respectively. The sequence of PSS is generated from Zadoff-Chu, as in [110]. PSS is the output of an inverse fast Fourier transform with 1024 bins. Thresholds of test statistics are computed by the Monte-Carlo method in advance. The synchronization signals and threshold are stored in a database of CR-based eNodeBs.

7.3.3 Experiments with CR-Based LTE-Advanced Systems

A. Emergency Scenarios

In cases of natural disasters, such as an earthquake or a flood, a formerly existing telecommunication infrastructure is destroyed in a region. Emergency aids must be carried out as quickly as

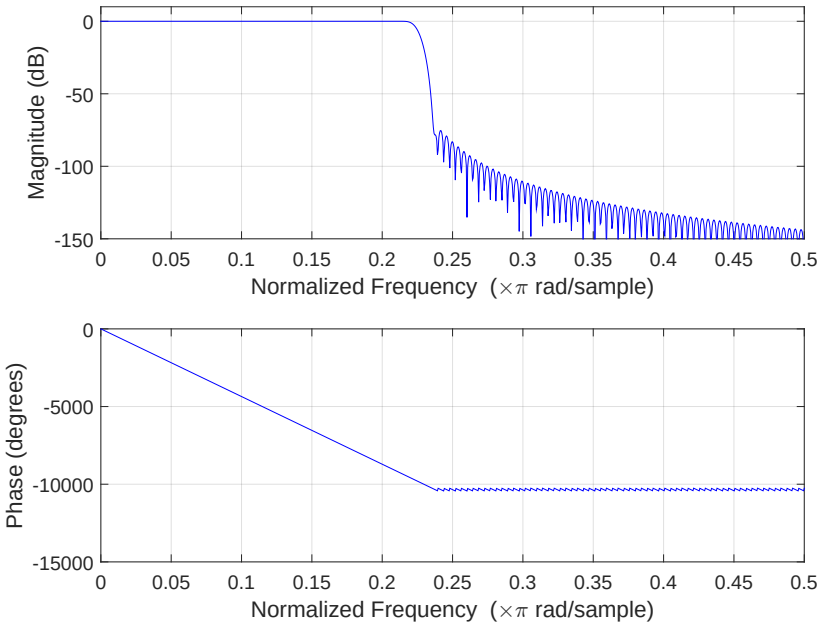

Fig. 7.8: The design of the prototype filter.

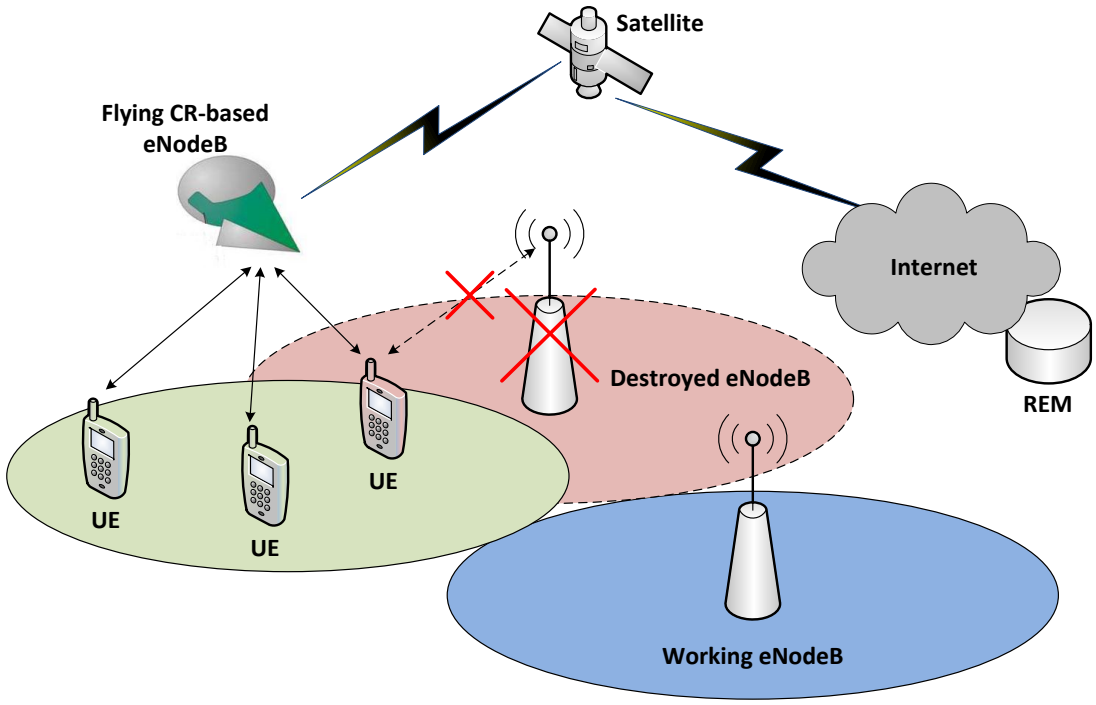

Fig. 7.9: Flying CR-based eNodeBs in emergency scenarios.

possible for citizens in the region. Cellular communications would be incredibly useful to help the people in terms of sharing messages, images, and videos, not only among each other but also

with their respective headquarters. Thus, a temporally infrastructure must be set up to replace or complement destroyed base stations. New coming eNodeBs need to be carried on either a balloon, a helikite, or a pole, as described in the ABSOLUTE project [83]. These eNodeBs are enhanced by the CR function to do spectrum sensing in the multi-channels. They must search for unoccupied LTE channels in the wide spectrum to provide cellular communications. Next, they register a set of parameters to an REM, which is shared for other necessary entities. The registered parameters, for example, indicate the maximum/minimum transmit power in selected LTE channels (or the geography positions). It results that cellular communications are restored as normal in a short duration and in a good manner. In CR-based eNodeBs, detection/classification tasks are handled by an SSM. The SSM executes the sensing tasks for the multiple channels periodically to keep the REM updated.

B. Combination between Spectrum Sensing and Geo-Location Database

In the emergency scenarios, a combination between the SSM and REM is configured. The combination improves the reliability of spectrum sensing and the effectiveness of the collaboration between the CR-based eNodeBs. It could be considered as an extended suggestion from the 3GPP for CR systems as in [85]. A general framework with this combination was introduced in [39]. Here, it introduce a framework with further details for such emergency scenarios and parameters in environments. In these scenarios, an SSM interacts with an REM via a layer 2/3 connection, as shown in Fig. 7.10. For example, the SSM queries the REM by a Python script. The REM is instructed by the GRASS GIS software [125], which stores a geography map, radio environments, and the parameters of the eNodeBs such as carrier frequency, channel bandwidth, transmitted power, and channel models. The access to the database is depicted in Fig. 7.10. The eNodeBs send requests with their current positions (latitudes, longitudes, and heights above a ground level), a kind of desired systems, and frequencies (bands, bandwidths, and sub-channel numbers). In a response, the REM replies to configuration parameters and assigns a calculated maximum transmit-power for the eNodeBs.

7.3.4 Methodology of Experiments

The methodology of the experiments has some main point, as follows:

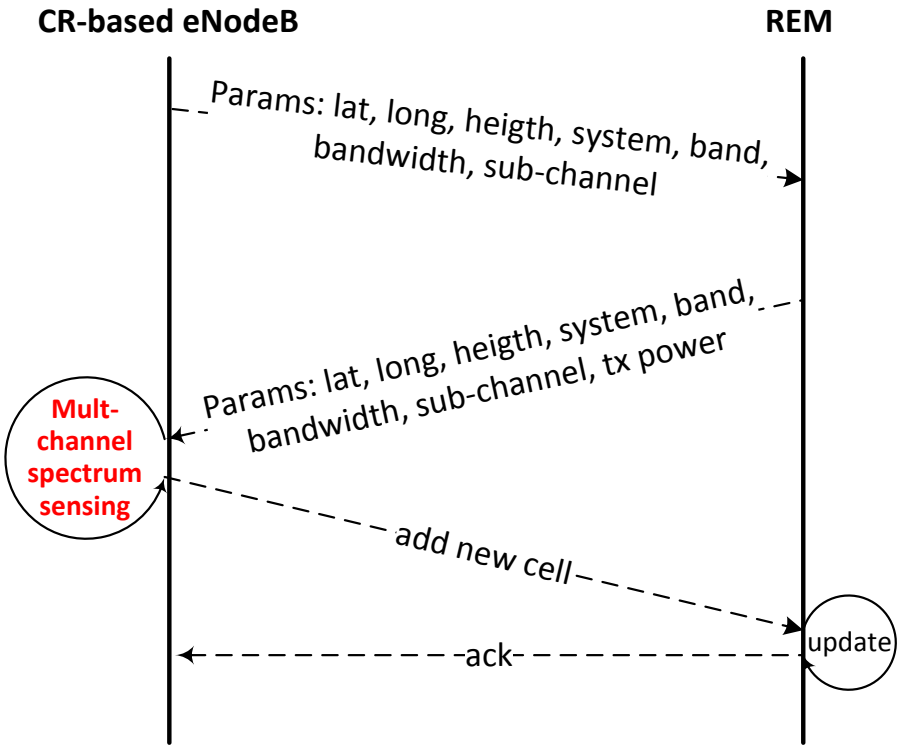

Fig. 7.10: Co-operation between CR-based eNodeB and REM.

- The proposed scheme is assessed with OTA signals in a real environment. A testbed for CR-based eNodeBs has been developed and described in [123] for spectrum sensing single channels.

- For multiband spectrum sensing, OTA signals are captured by a signal analyzer named MXA (as a step to deploy the scheme in testbeds). The captured signals are fed onto the SSM to be processed by the SDR platform. The MXA can operate with a span of multiple channels. In the frequency range, some channels are occupied, and the others are unoccupied.

- With occupied channels at high SNRs (e.g., 25 dB), embedded noise can be ignored. Noise is generated and added to the occupied channels with certain SNR values. It aims at controlling SNR values to compute the detection and classification performances (Pd and PCC) of the proposed scheme.

- The scheme is assessed in a procedure of emergency scenarios when the CR-based eNodeBs are launched to replace the destroyed eNodeBs. As described in Fig. 7.10, the SSM

queries information from the REM. In the design of CR-based LTE systems, additional information is provided from the REM to support the sensing tasks of the SSM. The results from the SSM will update information for the REM. This procedure yields reliable results for the systems and keeps the REM updated with the changes of environments. For example, the REM provides information about the bands to the SSM, in which there are most likely empty channels with some supported parameters.

In the experiments, the REM provides a list of bands to the SSM, which is sorted into a defined priority order with supported information such as center frequency, bandwidth, and operators/Cell-ID (if available). The SSM performs sensing tasks (detection and Cell-ID classification) for the bands and updates the information about current parameters of the channels in the bands.

7.3.5 Experimental Results and Analysis

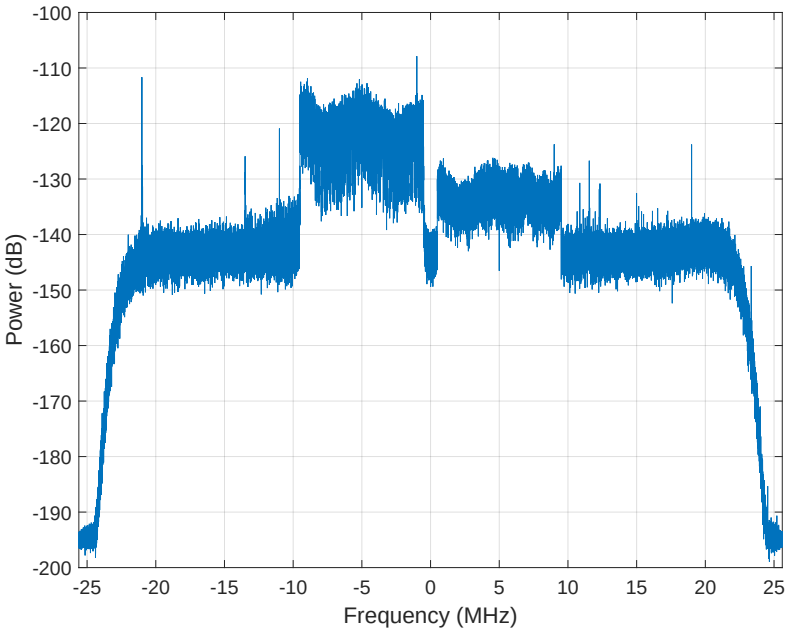

Fig. 7.11: PSD of multiband LTE signals with a bandwidth of 40 MHz, a carrier frequency of 801 MHz, and a sampling rate of 51.2 Msa/s.

Multiband signals are captured, as shown in Fig. 7.11, with four channels of the 10 MHz bandwidth for downlinks at the LTE band 20, in which three channels are assigned for LTE

signals [126]. With a high SNR value, channel occupancy can be visually observed in the frequency range. As shown in the PSD, two channels are occupied by LTE signals, and the other channels are unused. The spectrum shape of occupied channels are not flat due to selective frequency fading. At the center of the spectrum, the PSD is high because the PSS and SSS are boosted and allocated with 1.08 MHz bandwidth.

The multiband signals, as graphically shown in Fig. 7.11, are analyzed by the proposed scheme to detect LTE signals and classify the Cell-ID. At $f_c = 796MHz$, for example, the PSS/SSS-based peaks are plotted in Fig. 7.12. The PSS-based peaks appear in 5 ms, as in Fig. 7.12a. The highest peak will be selected first, corresponding to each NID2 value. The peaks, which are in multiple periodicals of 5 ms, are selected. The summation of the peaks is computed to construct a test statistic for each NID2 value. The maximum of these test statistics is equivalent to the PSS-based test statistic. Under hypothesis H_1, the presence of desired signals, the NID2 value of the maximum statistic is the Sector-Group of the detected LTE signals. For example, the PSS-based test statistic is maximum with NID2=0, as shown in Fig. 7.12a. With the identified Sector-Group, there are 168 choices for PSS when the first PSS-based peak equivalent to the symbol order $0th$ or $10th$. Fig. 7.12b shows 168 SSS-based peaks for each order. The highest peak will determine the NID1 value and the order. In this figure, the SSS-based PSS is maximum at $NID1 = 122$ and the order ($0th$, $10th$). Therefore, Cell-ID is classified with the NID2 and NID1. The Cell-ID is 366, for example, with the peaks shown in Fig. 7.12. The identified Cell-ID can be visually cross-checked with that analyzed by MXA for signals in the single channel, as in Fig. 7.13.

Fig. 7.14 and Fig. 7.15 show Pd (with the false alarm of 1%) and PCC when detected, respectively, of the proposed scheme and single channels. These performances of the proposed scheme are approximated with those of single channels. Therefore, these experimental results and the simulation results in Chapter 6 agree with each other. Besides, the proposed scheme works well in real environments: multipath and frequency-selective fading.

7.3.6 Concluding Remarks

To assess the multiband spectrum sensing scheme, experiments were carried out with the testbed of CCSs, which are CR-based eNodeBs. The experimental results show a high reliability of the

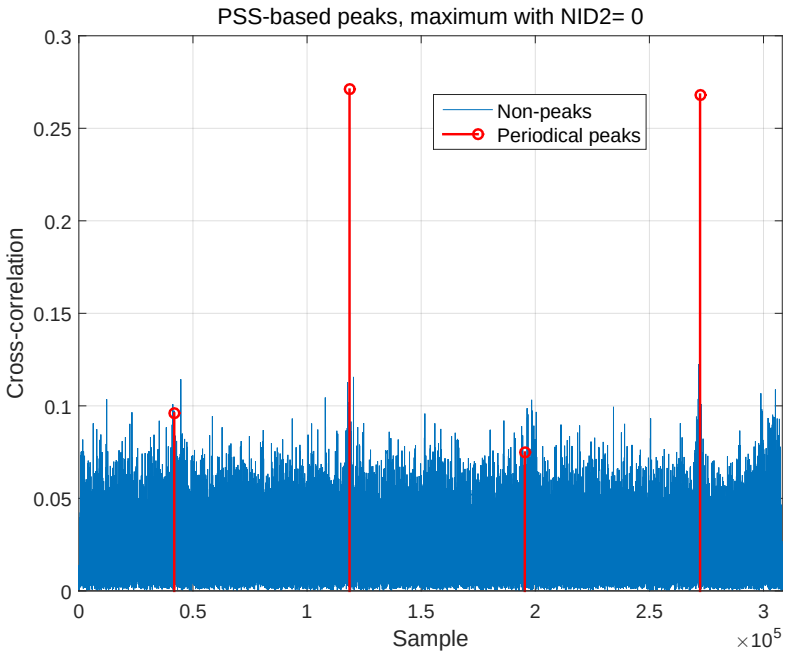

(a) Sector-ID identification

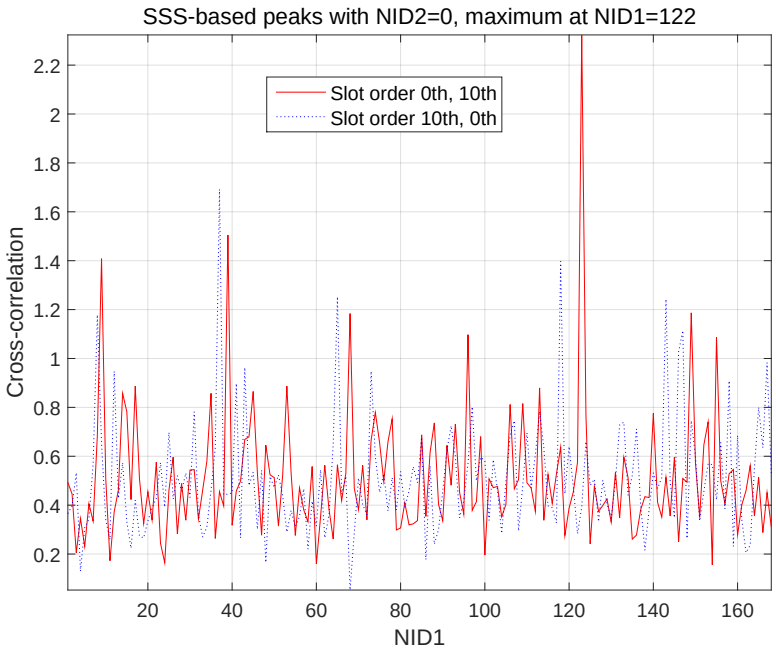

(b) Sector-Group identification

Fig. 7.12: Peaks of cross-correlation at $f_c = 796MHz$.

scheme in practice. Besides, the experiments yield the insights to develop the CCSs, which will be launched in emergency scenarios. Based on the evaluation and the insights, the CCSs can be

Fig. 7.13: LTE signals in a single channel with $f_c = 796MHz$ are captured by MXA and analyzed by a vector-signal-analysis software.

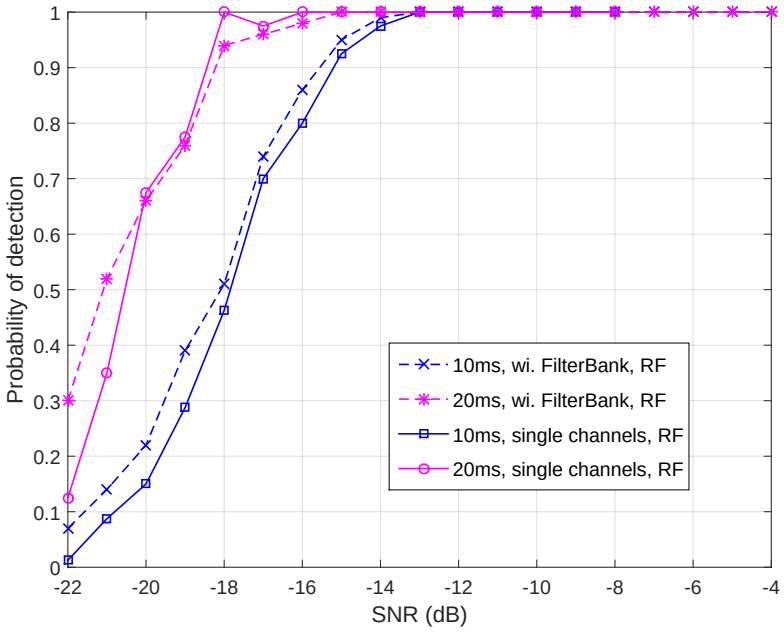

Fig. 7.14: The detection performance of the proposed scheme with OTA signals.

developed to serve the public-safety cellular-communications for our society.

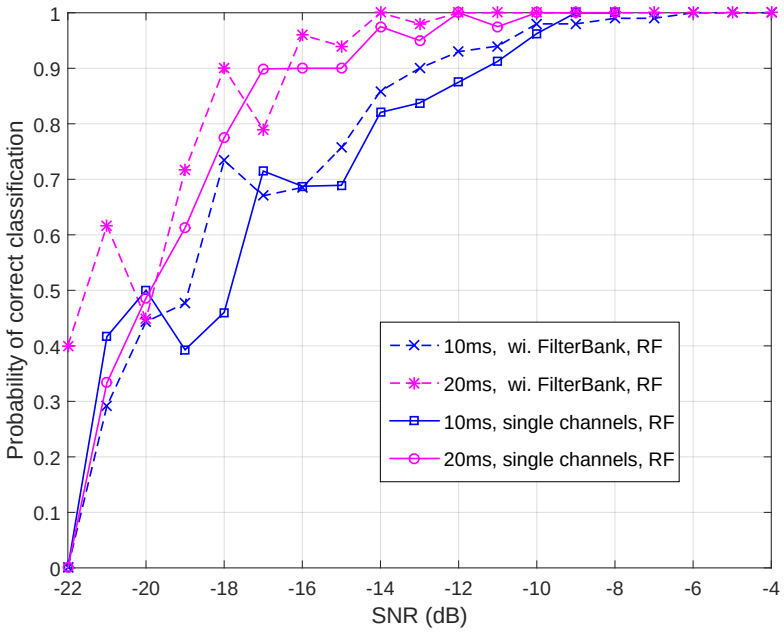

Fig. 7.15: The classification performance of the proposed scheme with respect to Cell-ID.

7.4 Summary

Based on the testbeds for CCSs, the experiments were carried out for the evaluation of the PPA algorithms and multiband spectrum sensing scheme. Experimental results agree with the simulation results, which were presented in previous parts in this dissertation. In Section 7.2, PPA algorithms were evaluated with DVB-T signals, which are the primary signals in unlicensed spectrums. The experimental results show that the PPA algorithms work well in real environments and outperform the existing algorithms. Additionally, PPA algorithms are suitable for short observations, with which the existing algorithm cannot work. The experimental results give clues to apply suitable algorithms for different operations, such as in-band and out-band sensing modes, in CCSs. Similarly, the multiband spectrum sensing scheme was evaluated in Section 7.3 with LTE downlink signals in emergency situations when the CR-based eNodeBs are deployed to replace destroyed eNodeBs. The experimental results approve the reliability of the scheme in a reality. Besides, the experiments show a successful integration approach of the scheme in CCSs.

8 CONCLUSIONS AND FUTURE WORK

8.1 Conclusions

In this dissertation, statistical characteristics of the pilot patterns in pilot-added OFDM signals are exploited with respect to subcarriers and symbols. By utilizing the characteristics, the PPA algorithms are proposed to improve the existing algorithms. The performance gains in the experiments and the simulations agree with each other. Taking into account the observation durations as the system constraint, the experimental results show that PPA algorithms can work with a short observation in which the existing algorithm are disable. Based on these advantages, CCSs can employ the PPA algorithms for sensing tasks (e.g., in the in-band mode), which have a short interval to capture the signals. The PPA algorithms can be widely applied since pilot-added OFDM signals are popular types of signals. In addition, by taking advantage of the preamble P1 in DVB-T2 signals, the P1-based algorithm is proposed for a fast sensing, which has an observation interval equal to the length of the preamble P1. Hence, the P1-based algorithm can be applied in the in-band sensing mode, which needs an extremely short observation to detect the primary signals. Therefore, the PPA and P1-based algorithms can be deployed in CCSs to find WSs in unlicensed spectrum TV bands.

Moreover, the new sensing algorithm based on cyclostationary signatures is proposed in this dissertation when considering the position and amplitude of the peaks in the cyclic and spectral frequency αf profile. The algorithm significantly outperforms the previous algorithms. The performance gains are verified with different formulas of the test statistics and modulation schemes. The algorithm is able to detect the signal in low SNR regimes due to the statistical characteristics of the cyclostationary signatures. Besides, the new algorithm can be developed for a spectrum sensing scheme to detect SC-FDMA signals in resource blocks in the uplink of cellular systems and in D2D communications.

This dissertation proposes the multiband spectrum sensing scheme to detect and classify LTE signals into multiple channels. Based on the scheme, CCSs can find unoccupied channels in multiband spectrums and co-operate effectively with each other to use the channels. The flexible design of the scheme is introduced to employ in CCSs. The experiments are carried out with a testbed of CCSs in a realistic scenario. The experimental results approve the reliability of the scheme with OTA signals in real environments. The experiments also provide the insights of multiband spectrum sensing for CCSs.

In this dissertation, the enhanced spectrum sensing techniques focus on CCSs and are proposed in terms of multiplexing techniques and the kind of spectrums (licensed and unlicensed). The testbeds of CCSs, which are CR-based LTE-Advanced systems, are used to assess the reliability of the spectrum sensing techniques. The experiments are those of pioneering works on spectrum sensing in real CCSs. The spectrum sensing techniques proposed in this dissertation can facilitate CR capabilities for CCSs.

8.2 Future Work

This section mentions some promising research directions on spectrum sensing, as follows:

- The proposed algorithm in this dissertation, which is based on cyclostationary signatures, needs to be evaluated with a spectrum sensing scheme, as proposed in [106, 108], to detect SC-FDMA signals in each resource block. Besides, the cyclostationary signatures need to be examined in multipath fading environments when exploiting the peaks of spectral correlation in the planes of cyclic and spectral frequencies.

- In next generations of cellular systems, the spectrum bands will be much larger than the current spectrum bands to contain many channels. The spectrum bands can be wide as 3 GHz [88]. In this case, the sampling rate for the multiband signal is extremely high. Processing spectrum sensing tasks with the sampling rate will be a burden computation for CCSs. Compressive sensing [127, 128] is a prominent approach to significantly reduce the sampling rate when detecting multiple channels in such multiband spectrums. Therefore, a multiband spectrum sensing with compressive sensing is a promising research for CCSs.

- New multiplexing techniques (e.g., FBMC, as mentioned in [65, 72, 94, 129, 130]) will be

discovered to apply for the signals in the uplink and the downlink into next generations of cellular networks. The signals could have new statistic features which can be exploited for spectrum sensing. Nevertheless, spectrum sensing will meet new challenges to utilize statistic features from the uplink and downlink signals. The algorithms proposed in this dissertation for pilot-added OFDM signals provide clues to apply for FBMC signals. However, statistical features from pilot patterns could not be exploited when pilot patterns are changed.

- Spectrum sensing has a space dimension (or angle directions). This dimension will be promising for research when the primary transmissions are steered by beam-forming techniques. In the future, massive MIMO will be an enabler to increase system capacities. Massive MIMO can form a beam in three-dimensional channels to maximize energy efficiency. With massive MIMO, the beam width will be significantly narrowed, along with the primary transmission direction. Hence, the spectrum frequency can be potentially reused in other directions. Meanwhile, it introduces challenging issues for spatial spectrum sensing to detect the beam with respect to azimuth and elevation angles [131–135].

BIBLIOGRAPHY

[1] 5G-PPP, "5G Vision – The 5G Infrastructure Public Private Partnership: the next generation of communication networks and services," [Online]. Available: https://5g-ppp.eu/, 2015.

[2] W. Jiang, H. Cao, T.T. Nguyen, A.B. Guven, Y. Wang, Y. Gao, A. Kabbani, M. Wiemeler, T. Kreul, Feng Zheng, and T. Kaiser, "Key issues towards beyond LTE-Advanced systems with cognitive radio," in *Signal Processing Advances in Wireless Communications (SPAWC), 2013 IEEE 14th Workshop on*, June 2013, pp. 510–514.

[3] P. Popovski, G. Mange, D. Gozalvez-Serrano, T. Rosowski, G. Zimmermann, P. Agyapong, M. Fallgren, A. Höglund, O. Queseth, H. Tullberg, J. Eichinger, Ö. Bulakci, Z. Li, K. Pawlak, M. Boldi, G. Romano, and J. F. Monserrat, "Final report on the METIS 5G system concept and technology roadmap," Tech. Rep. ICT-317669-METIS/D6.6, Mobile and wireless communications Enablers for the Twenty-twenty Information Society, Apr. 2015.

[4] T.T. Nguyen, H. Cao, T. Kreul, and T. Kaiser, "A multi-channel spectrum sensing scheme with filter bank realization for LTE signals," in *World of Wireless, Mobile and Multimedia Networks (WoWMoM), 2015 IEEE 16th International Symposium on a*, June 2015, pp. 1–5.

[5] T. Taher, R. Attard, A. Riaz, D. Roberson, J. Taylor, K. Zdunek, J. Hallio, R. Ekman, J. Paavola, J. Suutala, J. Roning, M. Matinmikko, M. Hoyhtya, and A. MacKenzie, "Global spectrum observatory network setup and initial findings," in *Cognitive Radio Oriented Wireless Networks and Communications (CROWNCOM), 2014 9th International Conference on*, June 2014, pp. 79–88.

[6] L. Bedogni, M. Di Felice, F. Malabocchia, and L. Bononi, "Indoor communication over TV gray spaces based on spectrum measurements," in *Wireless Communications and Networking Conference (WCNC), 2014 IEEE*, Apr. 2014, pp. 3218–3223.

[7] P. Kumar, N. Rakheja, A. Sarswat, H. Varshney, P. Bhatia, S.R. Goli, V.J. Ribeiro, and M. Sharma, "White space detection and spectrum characterization in urban and rural India," in *World of Wireless, Mobile and Multimedia Networks (WoWMoM), 2013 IEEE 14th International Symposium and Workshops on a*, June 2013, pp. 1–6.

[8] S. Contreras, G. Villardi, R. Funada, and H. Harada, "An investigation into the spectrum occupancy in Japan in the context of TV White Space systems," in *Cognitive Radio Oriented Wireless Networks and Communications (CROWNCOM), 2011 Sixth International ICST Conference on*, June 2011, pp. 341–345.

[9] T.M. Taher, R.B. Bacchus, K.J. Zdunek, and D.A. Roberson, "Long-term spectral occupancy findings in Chicago," in *New Frontiers in Dynamic Spectrum Access Networks (DySPAN), 2011 IEEE Symposium on*, May 2011, pp. 100–107.

[10] Shared Spectrum Company, "General Survey of Radio Frequency Bands - 30 MHz to 3 GHz," [Online]. Available: http://www.sharedspectrum.com, Sept. 2010.

[11] III Mitola, J. and Jr. Maguire, G.Q., "Cognitive radio: making software radios more personal," *Personal Communications, IEEE*, vol. 6, no. 4, pp. 13 –18, Aug. 1999.

[12] III Mitola, J., *Cognitive Radio — An Integrated Agent Architecture for Software Defined Radio*, Ph.D. thesis, Royal Institute of Technology (KTH), 2000.

[13] T.T. Nguyen, H. Cao, T. Kreul, and T. Kaiser, "Exploiting Periodical Peaks of Autocorrelation of Pilot-Added OFDM Signals for Enhanced Spectrum Sensing Algorithms," in *OFDM 2014; 18th International OFDM Workshop 2014 (InOWo'14); Proceedings of*, Aug. 2014, pp. 79–84.

[14] T.T. Nguyen, H. Cao, A.B. Güven, Y. Gao, A. Kabbani, T. Kreul, and T. Kaiser, "Robust spectrum sensing of DVB-T2 signal using the first preamble symbol," in *Advanced Technologies for Communications (ATC), 2013 International Conference on*, Oct. 2013, pp. 261–265.

[15] T.T. Nguyen, T. Kreul, and T. Kaiser, "An Enhanced Spectrum Sensing Algorithm with Maximum Ratio Combination of Spectral Correlation," in *23rd European Signal Processing Conference (EUSIPCO 2015)*, 31 Aug.–4 Sept. 2015, pp. 1232–1235.

[16] T.T. Nguyen, A. Kabbani, S. Peethala, T. Kreul, and T. Kaiser, "Experiments on Spectrum Sensing Algorithms of Pilot-Added OFDM Signals with a Cognitive LTE-A System," in *20th IEEE International Workshop on Computer Aided Modelling and Design of Communication Links and Networks (IEEE CAMAD 2015)*, Sept. 2015, pp. 303–307.

[17] T.T. Nguyen, M. Hoffmann, T. Kreul, and T. Kaiser, "Experiment on Multi-Channel Spectrum Sensing with Filter Bank Realization for Cognitive LTE-A Systems," in *The 2015 International Conference on Advanced Technologies for Communications (ATC15)*, Oct. 2015, pp. 509–513.

[18] S. Haykin, D.J. Thomson, and J.H. Reed, "Spectrum sensing for cognitive radio," *Proceedings of the IEEE*, vol. 97, no. 5, pp. 849 –877, May 2009.

[19] Simon Haykin, "Cognitive radio: brain-empowered wireless communications," *Selected Areas in Communications, IEEE Journal on*, vol. 23, no. 2, pp. 201–220, Feb. 2005.

[20] T. Yucek and H. Arslan, "A survey of spectrum sensing algorithms for cognitive radio applications," *Communications Surveys Tutorials, IEEE*, vol. 11, no. 1, pp. 116–130, 2009.

[21] H. Cao, W. Jiang, T. Javornik, M. Wiemeler, T.T. Nguyen, and T. Kaiser, "Spectrum awareness scheme of the rapidly deployable eNodeB for unexpected and temporary events," in *Computer Aided Modeling and Design of Communication Links and Networks (CAMAD), 2013 IEEE 18th International Workshop on*, Sept. 2013, pp. 196–200.

[22] ITU-R SM.2152, "Definitions of Software Defined Radio (SDR) and Cognitive Radio System (CRS)," Report ITU-R SM.215, Sept. 2009.

[23] SDR Forum, "SDRF Cognitive Radio Definitions," Working Document SDRF-06-R-0011-V1.0.0, SDR Forum, available online, Nov. 2007.

[24] W.A. Gardner, "Exploitation of spectral redundancy in cyclostationary signals," *Signal Processing Magazine, IEEE*, vol. 8, no. 2, pp. 14 –36, Apr. 1991.

[25] A. Papoulis and S.U. Pillai, *Probability, random variables, and stochastic processes*, Tata McGraw-Hill Education, 2002.

[26] W.A. Gardner, "The spectral correlation theory of cyclostationary time-series," *Signal Processing*, vol. 11, no. 1, pp. 13 – 36, 1986.

[27] W.A. Gardner, "Signal interception: a unifying theoretical framework for feature detection," *Communications, IEEE Transactions on*, vol. 36, no. 8, pp. 897–906, Aug. 1988.

[28] S.M. Kay, *Fundamentals of Statistical Signal Processing: Detection Theory*, Prentice Hall, 1998.

[29] John Aldrich, "R.A. Fisher and the making of maximum likelihood 1912-1922," *Statist. Sci.*, vol. 12, no. 3, pp. 162–176, Dec. 1997.

[30] Teng Joon Lim, Rui Zhang, Ying Chang Liang, and Yonghong Zeng, "GLRT-Based Spectrum Sensing for Cognitive Radio," in *Global Telecommunications Conference*, Nov. 2008, pp. 1 –5.

[31] Rui Zhang, Teng Lim, Ying-Chang Liang, and Yonghong Zeng, "Multi-antenna based spectrum sensing for cognitive radios: A GLRT approach," *Communications, IEEE Transactions on*, vol. 58, no. 1, pp. 84 –88, Jan. 2010.

[32] E. Axell, G. Leus, and E.G. Larsson, "Overview of spectrum sensing for cognitive radio," in *Cognitive Information Processing (CIP), 2010 2nd International Workshop on*, June 2010, pp. 322 –327.

[33] E. Axell, G. Leus, E.G. Larsson, and H.V. Poor, "Spectrum Sensing for Cognitive Radio : State-of-the-Art and Recent Advances," *Signal Processing Magazine, IEEE*, vol. 29, no. 3, pp. 101 –116, May 2012.

[34] D. Tse and P. Viswanath, *Fundamentals of Wireless Communication*, Cambridge University Press, 2005.

[35] F.C. Robey, D.R. Fuhrmann, E.J. Kelly, and R. Nitzberg, "A CFAR adaptive matched filter detector," *Aerospace and Electronic Systems, IEEE Transactions on*, vol. 28, no. 1, pp. 208–216, Jan. 1992.

[36] Yuanwei Jin and Benjamin Friedlander, "A CFAR adaptive subspace detector for second-order Gaussian signals," *Signal Processing, IEEE Transactions on*, vol. 53, no. 3, pp. 871–884, Mar. 2005.

[37] J. Liu, Zi-Jing Zhang, and Yun Yang, "Performance Enhancement of Subspace Detection With a Diversely Polarized Antenna," *Signal Processing Letters, IEEE*, vol. 19, no. 1, pp. 4–7, Jan. 2012.

[38] J. Liu, W. Liu, B. Chen, H. Liu, and H. Li, "Detection Probability of a CFAR Matched Filter with Signal Steering Vector Errors," *Signal Processing Letters, IEEE*, vol. 22, no. 12, pp. 2474–2478, Dec. 2015.

[39] H. Cao, W. Jiang, T.T. Nguyen, A.B. Guven, Y. Wang, Y. Gao, A. Rabbani, M. Wiemeler, T. Kreul, Feng Zheng, and T. Kaiser, "The design of an LTE-A system enhanced with cognitive radio," in *Signal Processing Conference (EUSIPCO), 2013 Proceedings of the 21st European*, Sept. 2013, pp. 1–5.

[40] H. Urkowitz, "Energy detection of unknown deterministic signals," *Proceedings of the IEEE*, vol. 55, no. 4, pp. 523 – 531, april 1967.

[41] Anant Sahai, Niels Hoven, and Rahul Tandra, "Some Fundamental Limits on Cognitive Radio," in *in Forty-second Allerton Conference on Communication, Control, and Computing*, 2004.

[42] R. Tandra and A. Sahai, "Fundamental limits on detection in low SNR under noise uncertainty," in *Wireless Networks, Communications and Mobile Computing, 2005 International Conference on*, Jun. 2005, vol. 1, pp. 464 –469.

[43] R. Tandra and A. Sahai, "SNR Walls for Signal Detection," *Selected Topics in Signal Processing, IEEE Journal of*, vol. 2, no. 1, pp. 4–17, Feb. 2008.

[44] A. Sahai and D. Cabric, "Spectrum Sensing: Fundamental Limits and Practical Challenges," in *in Tutorials of IEEE International Symp. New Frontiers Dynamic Spectrum Access Networks (DySPAN)*, Nov. 2005.

[45] Stephen J. Shellhammer, Sai Shankar N, Rahul Tandra, and James Tomcik, "Performance of Power Detector Sensors of DTV Signals in IEEE 802.22 WRANs," in *Proceedings of the First International Workshop on Technology and Policy for Accessing Spectrum*, New York, NY, USA, 2006, TAPAS '06, ACM.

[46] Steve Shellhammer and Rahul Tandra, "Performance of the Power Detector with Noise Uncertainty," Tech. Rep., IEEE P802.22, available online, July 2006.

[47] Pu Wang, Jun Fang, Ning Han, and Hongbin Li, "Multiantenna-assisted spectrum sensing for cognitive radio," *Vehicular Technology, IEEE Transactions on*, vol. 59, no. 4, pp. 1791 –1800, May 2010.

[48] A. Taherpour, M. Nasiri-Kenari, and S. Gazor, "Multiple antenna spectrum sensing in cognitive radios," *Wireless Communications, IEEE Transactions on*, vol. 9, no. 2, pp. 814 –823, Feb. 2010.

[49] Yonghong Zeng and Ying chang Liang, "Eigenvalue-based spectrum sensing algorithms for cognitive radio," *Communications, IEEE Transactions on*, vol. 57, no. 6, pp. 1784 –1793, June 2009.

[50] A. Kortun, T. Ratnarajah, M. Sellathurai, Ying chang Liang, and Yonghong Zeng, "On the Eigenvalue-Based Spectrum Sensing and Secondary User Throughput," *Vehicular Technology, IEEE Transactions on*, vol. 63, no. 3, pp. 1480–1486, March 2014.

[51] Zhongding Lei and F. Chin, "Sensing OFDM systems under frequency-selective fading channels," *Vehicular Technology, IEEE Transactions on*, vol. 59, no. 4, pp. 1960–1968, 2010.

[52] S. Chaudhari, V. Koivunen, and H.V. Poor, "Autocorrelation-based decentralized sequential detection of ofdm signals in cognitive radios," *Signal Processing, IEEE Transactions on*, vol. 57, no. 7, pp. 2690–2700, 2009.

[53] Hou-Shin Chen, Wen Gao, and D. Daut, "Spectrum sensing for OFDM systems employing pilot tones," *Wireless Communications, IEEE Transactions on*, vol. 8, no. 12, pp. 5862 –5870, Dec. 2009.

[54] Yang Wen, Wei Huang, and Zhongpei Zhang, "Cazac sequence and its application in LTE random access," in *Information Theory Workshop, 2006. ITW '06 Punta del Este. IEEE*, 2006, pp. 544–547.

[55] W.A. Gardner, "Identification of systems with cyclostationary input and correlated input/output measurement noise," *Automatic Control, IEEE Transactions on*, vol. 35, no. 4, pp. 449–452, 1990.

[56] B.J. Skinner, F.M. Ingels, and J.P. Donohoe, "Stationary and cyclostationary random process models," in *Southeastcon '94. Creative Technology Transfer - A Global Affair., Proceedings of the 1994 IEEE*, 1994, pp. 450–454.

[57] Paul Sutton, *Rendezvous and Coordination in OFDM-based Dynamic Spectrum Access Networks*, Ph.D. thesis, University of Dublin, Trinity College, Irland, 2008.

[58] Hanwen Cao, Qipeng Cai, J.P. Miranda, and T. Kaiser, "Cyclostationary multitone beacon signal for opportunistic spectrum access," in *Cognitive Radio Oriented Wireless Networks and Communications, 2009. CROWNCOM '09. 4th International Conference on*, June 2009, pp. 1 –6.

[59] Hanwen Cao, Qipeng Cai, João Paulo Miranda, and Thomas Kaiser, "Cyclostationary beacon for assisting spectrum sensing in opportunistic spectrum access," *Majlesi Journal of Electrical Engineering*, vol. 5, no. 1, 2011.

[60] H. Tang, "Some physical layer issues of wide-band cognitive radio systems," in *New Frontiers in Dynamic Spectrum Access Networks, 2005. DySPAN 2005. 2005 First IEEE International Symposium on*, Nov. 2005, pp. 151 –159.

[61] M. Iqbal and A. Ghafoor, "Analysis of Multiband Joint Detection Framework for Waveform-Based Sensing in Cognitive Radios," in *Vehicular Technology Conference (VTC Fall), 2012 IEEE*, Sept. 2012, pp. 1–5.

[62] Cisco, "Cisco visual networking index: Global mobile data traffic forecast update, 2014-2019," *White Paper*, Feb. 2015.

[63] EPSRC, "National strategy for quantum technologies: A NEW ERA FOR THE UK," *Innovate UK and the Engineering and Physical Sciences Research Council*, vol. T15/080, 2015.

[64] Anthony Cuthbertson, "Quantum revolution: UK strategy outlines research into 6G smartphones and quantum computers," *Ibtimes news*, Mar. 2015.

[65] T. Wild, M. Kasparick, G. Wunder, Y. Chen, F. Schaich, V. Berg, N. Cassiau, J.-B. Doré, D. Kténas, M. Dryjanski, S. Pietrzyk, I. S. Gaspar, and N. Michailow, "5G Waveform Candidate Selection," Tech. Rep. D3.1, 5GNOW Project, Nov. 2013.

[66] European Union, "Why the eu is betting big on 5G," *in researcheu - Focus magazine - WHY THE EU IS BETTING BIG ON 5G*, , no. 15, pp. pp.1–36., 2015.

[67] A. Bleicher, "The 5G phone future [News]," *Spectrum, IEEE*, vol. 50, no. 7, pp. 15–16, July 2013.

[68] T.S. Rappaport, Shu Sun, R. Mayzus, Hang Zhao, Y. Azar, K. Wang, G.N. Wong, J.K. Schulz, M. Samimi, and F. Gutierrez, "Millimeter Wave Mobile Communications for 5G Cellular: It Will Work!," *Access, IEEE*, vol. 1, pp. 335–349, 2013.

[69] W. Roh, Ji-Yun Seol, Jeongho Park, Byunghwan Lee, Jaekon Lee, Yungsoo Kim, Jaeweon Cho, Kyungwhoon Cheun, and F. Aryanfar, "Millimeter-wave beamforming as an enabling technology for 5G cellular communications: Theoretical feasibility and prototype results," *Communications Magazine, IEEE*, vol. 52, no. 2, pp. 106–113, Feb. 2014.

[70] European Union, "METIS defines the future of wireless technologies," *in researcheu - Focus magazine - why the EU is betting big on 5G*, 2015.

[71] Nokia Siemens Networks, "2020: Beyond 4G Radio Evolution for the Gigabit Experience," *White paper*, 2011.

[72] Q.C. Li, Huaning Niu, A.T. Papathanassiou, and Geng Wu, "5G Network Capacity: Key Elements and Technologies," *Vehicular Technology Magazine, IEEE*, vol. 9, no. 1, pp. 71–78, Mar. 2014.

[73] GSMA Intelligence, "ANALYSIS – Understanding 5G: Perspectives on future technological advancements in mobile," *Report*, Dec. 2014.

[74] T.S. Rappaport, Shu Sun, R. Mayzus, Hang Zhao, Y. Azar, K. Wang, G.N. Wong, J.K. Schulz, M. Samimi, and F. Gutierrez, "Millimeter wave mobile communications for 5G cellular: It will work!," *Access, IEEE*, vol. 1, pp. 335–349, 2013.

[75] Cheng-Xiang Wang, F. Haider, Xiqi Gao, Xiao-Hu You, Yang Yang, Dongfeng Yuan, H. Aggoune, H. Haas, S. Fletcher, and E. Hepsaydir, "Cellular architecture and key technologies for 5G wireless communication networks," *Communications Magazine, IEEE*, vol. 52, no. 2, pp. 122–130, Feb. 2014.

[76] F Boccardi, R.W. Heath, A. Lozano, T.L. Marzetta, and P. Popovski, "Five disruptive technology directions for 5G," *Communications Magazine, IEEE*, vol. 52, no. 2, pp. 74–80, Feb. 2014.

[77] M.D. Mueck, I. Karls, R. Arefi, T. Haustein, R.J. Weiler, and K. Sakaguchi, "Global standards enabling a 5th generation communications system architecture vision," in *Globecom Workshops (GC Wkshps), 2014*, Dec. 2014, pp. 571–576.

[78] Zhouyue Pi and F. Khan, "An introduction to millimeter-wave mobile broadband systems," *Communications Magazine, IEEE*, vol. 49, no. 6, pp. 101–107, June 2011.

[79] Tugba Erpek, Karl Steadman, and David Jones, "Dublin Ireland, spectrum occupancy measurements," Tech. Rep., Shared Spectrum Company, Nov. 2007.

[80] ITU-R M.2225, "Introduction to cognitive radio systems in the land mobile service," Tech. Rep., ITU-R, 2011.

[81] ITU-R M.2242, "Cognitive radio systems specific for International Mobile Telecommunications systems," Tech. Rep., ITU-R, 2011.

[82] kogLTE, *Project of Federal Ministry of Education and Research (BMBF) of Germany*, [Online]. Available: http://www.vdivde-it.de/KIS/vernetzt-leben/kognitive-drahtlose-kommunikationssysteme/koglte.

[83] ABSOLUTE, *EU FP7 ABSOLUTE Project*, [Online]. Available: http://www.absolute-project.eu/.

[84] FCC, "Second report and order and memorandum opinion and order," [Online]. Available: http://transition.fcc.gov, Nov. 2008.

[85] ETSI-TR103067, "Reconfigurable Radio Systems (RRS); Feasibility study on Radio Frequency (RF) performance for Cognitive Radio Systems operating in UHF TV band White Spaces ," Tech. Rep. V1.1.1, ETSI, available online, May 2013.

[86] A. Apostolidis, L. Campoy, K. Chatzikokolakis, K. J. Friederichs, T. Irnich, K. Koufos, J. Kronander, J. Luo, E. Mohyeldin, P. Olmos, T. Rosowski, H. Schotten, B. Singh, M. Tercero, O. Tirkkonen, and M. A. Uusitalo, "Intermediate description of the spectrum needs and usage principles," Tech. Rep. ICT-317669-METIS/D5.1, Mobile and wireless communications Enablers for the Twenty-twenty Information Society, Aug. 2013.

[87] J.-J. van de Beek, M. Sandell, and P.O. Borjesson, "Ml estimation of time and frequency offset in ofdm systems," *Signal Processing, IEEE Transactions on*, vol. 45, no. 7, pp. 1800–1805, 1997.

[88] G. Hattab and M. Ibnkahla, "Multiband spectrum access: Great promises for future cognitive radio networks," *Proceedings of the IEEE*, vol. 102, no. 3, pp. 282–306, Mar. 2014.

[89] Hanwen Cao, S. Daoud, A. Wilzeck, and T. Kaiser, "Practical issues in spectrum sensing for multi-carrier system employing pilot tones," in *Applied Sciences in Biomedical and Communication Technologies (ISABEL), 2010 3rd International Symposium on*, Nov. 2010, pp. 1 –5.

[90] Z. Chen, T. Luan, and X. D Zhang, "Sensing orthogonal frequency division multiplexing systems for cognitive radio with cyclic prefix and pilot tones," *Communications, IET*, vol. 6, no. 1, pp. 97–106, 2012.

[91] ETSI, "Digital video broadcasting (DVB); framing structure, channel coding and modulation for digital terrestrial television," European Telecommun. Standard EN300744, Jan. 2009.

[92] Zhengwei Lu, Yi Ma, P. Cheraghi, and R. Tafazolli, "Novel pilot-assisted spectrum sensing for ofdm systems by exploiting statistical difference between subcarriers," *Communications, IEEE Transactions on*, vol. 61, no. 4, pp. 1264–1276, 2013.

[93] Ji-Woong Choi and Yong-Hwan Lee, "Optimum pilot pattern for channel estimation in OFDM systems," *Wireless Communications, IEEE Transactions on*, vol. 4, no. 5, pp. 2083–2088, Sept. 2005.

[94] Wei Jiang and M. Schellmann, "Suppressing the out-of-band power radiation in multicarrier systems: A comparative study," in *Global Communications Conference (GLOBECOM), 2012 IEEE*, Dec 2012, pp. 1477–1482.

[95] IEEE-802.22, "WRAN channel modeling," Tech. Rep., IEEE, 2005.

[96] M. Failli, "Digital land mobile radio communications COST 207," Tech. rep., European Commission, 1989.

[97] ETSI, "Digital video broadcasting (DVB); frame structure channel coding and modulation for a second generation digital terrestrial television broadcasting system (DVB-T2)," European Telecommun. Standard EN302755, Apr. 2012.

[98] IEEE P802.22, "Sensing scheme for DVB-T," Tech. Rep., IEEE 802.22, available online, July 2006.

[99] D. Danev, E. Axell, and E.G. Larsson, "Spectrum sensing methods for detection of DVB-T signals in AWGN and fading channels," in *Personal Indoor and Mobile Radio Communications (PIMRC), 2010 IEEE 21st International Symposium on*, Sept. 2010, pp. 2721 –2726.

[100] FCC, "Federal communications commission spectrum policy task force," [Online]. Available: http://transition.fcc.gov, 2002.

[101] Wenshan Yin, Pinyi Ren, Jun Cai, and Zhou Su, "A pilot-aided detector for spectrum sensing of digital video broadcasting-terrestrial signals in cognitive radio networks," *Wireless Communications and Mobile Computing*, vol. 13, no. 13, pp. 1177–1191, 2013.

[102] A. Fehske, J. Gaeddert, and J. Reed, "A new approach to signal classification using spectral correlation and neural networks," in *New Frontiers in Dynamic Spectrum Access Networks, 2005. DySPAN 2005. 2005 First IEEE International Symposium on*, Nov. 2005, pp. 144–150.

[103] Zhiqiang Wu, E. Like, and V. Chakravarthy, "Reliable modulation classification at low SNR using spectral correlation," in *Consumer Communications and Networking Conference, 2007. CCNC 2007. 4th IEEE*, Jan. 2007, pp. 1134–1138.

[104] E. Like, V. Chakravarthy, R. Husnay, and Zhiqiang Wu, "Modulation recognition in multipath fading channels using cyclic spectral analysis," in *Global Telecommunications Conference, 2008. IEEE GLOBECOM 2008. IEEE*, Nov. 2008, pp. 1–6.

[105] Zhiqiang Wu, E. Like, and V. Chakravarthy, "Reliable modulation classification at low SNR using spectral correlation," in *Consumer Communications and Networking Conference, 2007. CCNC 2007. 4th IEEE*, Jan. 2007, pp. 1134–1138.

[106] Wensheng Zhang and Y. Sanada, "Low-complexity cyclostationarity feature detection scheme of localized SC-FDMA uplink system for application to detect and avoid," in *Communications and Information Technologies (ISCIT), 2010 International Symposium on*, Oct. 2010, pp. 962–967.

[107] A Mirdamadi and M. Sabbaghian, "Spectrum sensing of interleaved SC-FDMA signals in cognitive radio networks," *Vehicular Technology, IEEE Transactions on*, vol. PP, no. 99, pp. 1–1, 2014.

[108] A. Mirdamadi and M. Sabbaghian, "Spectrum sensing of interleaved SC-FDMA signals in cognitive radio networks," *Vehicular Technology, IEEE Transactions on*, vol. 64, no. 4, pp. 1633–1637, Apr. 2015.

[109] W.A. Jerjawi, Y.A. Eldemerdash, and O.A. Dobre, "Second-order cyclostationarity-based detection of LTE SC-FDMA signals for cognitive radio systems," *Instrumentation and Measurement, IEEE Transactions on*, vol. 64, no. 3, pp. 823–833, March 2015.

[110] 3GPP-TS36211, "LTE; Evolved Universal Terrestrial Radio Access (E-UTRA); physical channels and modulation," Tech. Rep. V10.4.0, 3GPP, available online, Jan. 2012.

[111] P. Phunchongharn, E. Hossain, and D.I. Kim, "Resource allocation for device-to-device communications underlaying LTE-advanced networks," *Wireless Communications, IEEE*, vol. 20, no. 4, pp. 91–100, Aug. 2013.

[112] K. Gomez, L. Goratti, T. Rasheed, and L. Reynaud, "Enabling disaster-resilient 4G mobile communication networks," *Communications Magazine, IEEE*, vol. 52, no. 12, pp. 66–73, Dec. 2014.

[113] A.H. Sakr and E. Hossain, "Cognitive and energy harvesting-based D2D communication in cellular networks: Stochastic geometry modeling and analysis," *Communications, IEEE Transactions on*, vol. 63, no. 5, pp. 1867–1880, May 2015.

[114] Lili Wei, R.Q. Hu, Yi Qian, and Geng Wu, "Enable device-to-device communications underlaying cellular networks: challenges and research aspects," *Communications Magazine, IEEE*, vol. 52, no. 6, pp. 90–96, June 2014.

[115] B. Farhang-Boroujeny, "Filter bank spectrum sensing for cognitive radios," *Signal Processing, IEEE Transactions on*, vol. 56, no. 5, pp. 1801 –1811, May 2008.

[116] Hanwen Cao, Wei Jiang, and T. Kaiser, "Multi-channel robust spectrum sensing with low-complexity filter bank realization," in *Personal Indoor and Mobile Radio Communications (PIMRC), 2013 IEEE 24th International Symposium on*, Sept. 2013, pp. 861–865.

[117] Hanwen Cao and J. Peissig, "Practical spectrum sensing with frequency-domain processing in cognitive radio," in *Signal Processing Conference (EUSIPCO), 2012 Proceedings of the 20th European*, Aug. 2012, pp. 435–439.

[118] C. Mehlführer, J. Colom Ikuno, M. Simko, S. Schwarz, M. Wrulich, and M. Rupp, "The Vienna LTE simulators - enabling reproducibility in wireless communications research," *EURASIP Journal on Advances in Signal Processing*, vol. 2011, pp. 1–13, 2011.

[119] S.J. Shellhammer, A.K. Sadek, and Wenyi Zhang, "Technical challenges for cognitive radio in the TV white space spectrum," in *Information Theory and Applications Workshop, 2009*, Feb. 2009, pp. 323 –333.

[120] Hou-Shin Chen, Wen Gao, and D.G. Daut, "Spectrum sensing for OFDM systems employing pilot tones and application to DVB-T OFDM," in *Communications, 2008. ICC '08. IEEE International Conference on*, May 2008, pp. 3421 –3426.

[121] DVBT Report, "Abschlussbericht DVB-T Deutschland," Tech. Rep., Task Force DVB-T Deutschland von ARD und ZDF, Institut für Rundfunktechnik München, www.ueberallfernsehen.de, Aug. 2014.

[122] IEEE-802.22, "IEEE Standard for Information Technology- Telecommunications and information exchange between systems- Wireless Regional Area Networks (WRAN)- Specific requirements- Part 22: Cognitive Wireless RAN Medium Access Control (MAC) and Physical Layer (PHY) specifications: Policies and procedures for operation in the TV Bands," IEEE Standard, IEEE, July 2011.

[123] Kabbani Ammar, Ramadan Ali Ali, Hanwen Cao, Asim Burak Güven, Yuan Gao, Sundar Peethala, and Thomas Kaiser, "Implementation Aspects of a DSP-Based LTE Cognitive Radio Testbed," in *10th International Conference on Cognitive Radio Oriented Wireless Networks*, Doha, Qatar, Apr. 2015, pp. 261–265.

[124] Albert H. Nuttall, "Some windows with very good sidelobe behavior," *Acoustics, Speech and Signal Processing, IEEE Transactions on*, vol. 29, no. 1, pp. 84–91, Feb. 1981.

[125] GRASS Development Team, *Geographic Resources Analysis Support System (GRASS GIS) Software*, Open Source Geospatial Foundation, 2015.

[126] 3GPP-TS36.101, "LTE; Evolved Universal Terrestrial Radio Access (E-UTRA); User Equipment (UE) radio transmission and reception," Tech. Spec. V12.7.0, 3GPP, available online, May 2015.

[127] R.G. Baraniuk, "Compressive Sensing [Lecture Notes]," *Signal Processing Magazine, IEEE*, vol. 24, no. 4, pp. 118–121, July 2007.

[128] R.G. Baraniuk, V. Cevher, M.F. Duarte, and C. Hegde, "Model-Based Compressive Sensing," *Information Theory, IEEE Transactions on*, vol. 56, no. 4, pp. 1982–2001, Apr. 2010.

[129] F. Schaich, V. Ringset, M. Bellanger, H. Zhang, and D. L. Ruyet, "Compatibility of OFDM and FBMC systems and reconfigurability of terminals," Tech. Rep. D7.1, PHYDYAS - PHYsical layer for DYnamic AccesS and cognitive radio, July 2009.

[130] H. Zhang, D. L. Ruyet, M. Terré, D. Roviras, M. Renfors, T. Ihalainen, C. Bader, M. Shaat, A. Merentitis, D. Triantafyllopoulou, M. Huchard, and A. Kuzminskiy, "Application of the FBMC physical layer in a cognitive radio scenario," Tech. Rep. D8.1, PHYDYAS - PHYsical layer for DYnamic AccesS and cognitive radio, July 2009.

[131] Anding Wang, Lingjia Liu, and Jianzhong Zhang, "Low complexity direction of arrival (DoA) estimation for 2D massive MIMO systems," in *Globecom Workshops (GC Wkshps), 2012 IEEE*, Dec. 2012, pp. 703–707.

[132] Yi Zhu, Lingjia Liu, Anding Wang, K. Sayana, and J.C. Zhang, "DoA estimation and capacity analysis for 2D active massive MIMO systems," in *Communications (ICC), 2013 IEEE International Conference on*, June 2013, pp. 4630–4634.

[133] Yi Zhu, Lingjia Liu, and Jianzhong Zhang, "Joint angle and delay estimation for 2D active broadband MIMO-OFDM systems," in *Global Communications Conference (GLOBECOM), 2013 IEEE*, Dec. 2013, pp. 3300–3305.

[134] Dawei Ying, F.W. Vook, T.A. Thomas, D.J. Love, and A. Ghosh, "Kronecker product correlation model and limited feedback codebook design in a 3D channel model," in *Communications (ICC), 2014 IEEE International Conference on*, June 2014, pp. 5865–5870.

[135] Kai-Yu Yang, Jwo-Yuh Wu, and Wen-Hsuan Li, "A low-complexity direction-of-arrival estimation algorithm for full-dimension massive MIMO systems," in *Communication Systems (ICCS), 2014 IEEE International Conference on*, Nov. 2014, pp. 472–476.